Clinical and Molecular Characterization of Human Hereditary Skeletal Disorders in Consanguineous Families

by

Abdul Aziz

Department of Biochemistry
Faculty of Biological Sciences
Quaid-i-Azam University
Islamabad, Pakistan
2015

Clinical and Molecular Characterization of Human Hereditary Skeletal Disorders in Consanguineous Families

A thesis submitted in the partial fulfillment of the requirements for the degree of Doctor of Philosophy

in

Biochemistry

by

Abdul Aziz

Department of Biochemistry
Faculty of Biological Sciences
Quaid-i-Azam University
Islamabad, Pakistan
2015

Declaration

I hereby declared that the work presented in this thesis is my own effort and hard work and it is written and composed by me. No part of this thesis has been previously published or presented for any other degree or certificate.

Abdul Aziz

Dedicated

to

My loving parents
Whose prayers, love and affections are source of strength for me in
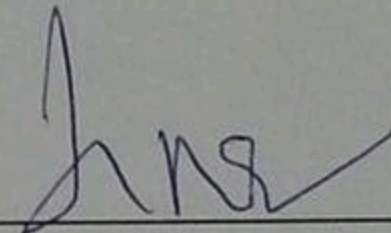*every step of my life.*

CERTIFICATE

This thesis, titled "Clinical and Molecular Characterization of Human Hereditary Skeletal Disorders in Consanguineous Families" submitted by **Mr. Abdul Aziz** to the Department of Biochemistry, Faculty of Biological Sciences, Quaid-i-Azam University, Islamabad, Pakistan, is accepted in its present form as satisfying the thesis requirement for the Degree of Doctor of Philosophy in Biochemistry/Molecular Biology.
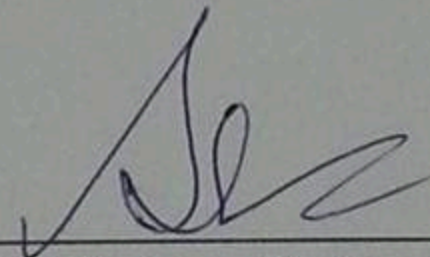
Supervisor: _____

Dr. Wasim Ahmad
Professor

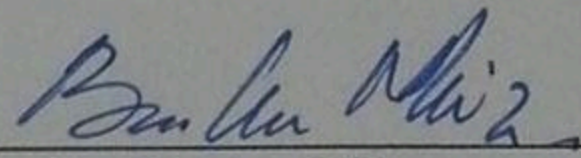External Examiner: _____

Dr. Allah Nawaz
Principal Biochemist
(CDA) Capital Hospital, Islamabad.

External Examiner: _____

Dr. Shaheen Shahzad
Assistant Professor
Department of Environmental Sciences
International Islamic University, Islamabad

Chairperson: _____

Dr. Bushra Mirza
Professor

Dated: _____May 15, 2015_____

ACKNOWLEDGEMENTS

First of all I would like to thank the one above all of us, the omnipresent Allah, for his blessings and mighty grace over me. It would not have been possible to write this doctoral thesis without the help and support of the kind people around me. It is a pleasure to thank all those who made this possible.

I feel proud to be associated with Quaid-i-Azam University, Islamabad, Pakistan since M.Sc. It gave me knowledge, hardworking able teachers, loving and caring friends. I will always remember the time I spent here as golden time of my life.

I feel proud to pay deep gratitude to my most experienced, perfectionist and considerate supervisor, Dr. Wasim Ahmad, Professor, Department of Biochemistry, Quaid-i-Azam University, Islamabad, under whose inspiring guidance, valuable suggestions, caring attitude, immense endurance and encouragements, this research work was carried out.

Special thanks to Dr. Bushra Mirza, Chairperson, Department of Biochemistry, Quaid-i-Azam University, Islamabad, for her cooperation. Thanks to the biochemistry office staff for managing my documents file from the beginning of my PhD.

I acknowledge Higher Education Commission (HEC), Islamabad, Pakistan, for supporting my research work presented in the dissertation.

I am deeply grateful to Prof. Dr. Suzanne M Leal, Baylor College of Medicine Texas USA for her help in human genome scan and exome sequencing.

It gives me great pleasure in acknowledging the help and support of my lab seniors and colleagues Dr. Abdul Wali, Dr. Jawad Hassan, Dr. Salman Chisti, Dr. Umme Kalsoom, Dr. Bushra Khan, Dr. Sulman Basit, Dr. Saadullah Khan, Dost Muhammad, Abid Jan, Irfan Raza, Muhammad Umair, Raja Hussain, Irfanullah Farhad, Sabba Mehmood, Farooq Ahmad, Khadim Shah, Muhammad Ikram and Asmat Ullah.

My heartfelt thanks to my friends Dr. Muhammad Ajmal, Dr. Khalid Ahmad, Dr. Mubarak Ali Khan, Dr. Zulqarnain, Sardar Ali Khan, Amjad Shahzad, Shams Uz Zaman, and Muhammad Shakil Khan for their company and prayers.

I wish to express sincere thanks to my juniors for their cooperation and pleasant company. I really have a good time with them.

LIST OF FIGURES

Continued…..

Continued from the previous page

Continued…..

Continued from the previous page

Continued from the previous page

Continued from the previous page

Continued…..

Continued from the previous page

*Clinical and Molecular Characterization of Human Hereditary Skeletal Disorders
in Consanguineous Families*

Continued from the previous page

Continued from the previous page

Continued from the previous page

Continued…..

Continued from the previous page

Continued from the previous page

LIST OF TABLES

ABSTRACT

Human skeletal dysplasias are genetically heterogeneous group of disorders that results from errors in bone, cartilage and joint development. They are characterized by abnormalities in patterning, differentiation, linear growth and maintenance of the human skeleton. A complex series of signaling cascades, including FGF, BMP, TGF β, WNT, Notch, Hedgehog, are essential for proper development of skeleton.

The study presented in the dissertation describes clinical and molecular analysis often consanguineous families (A-J) showing different types of skeletal disorders. These families were collected from different remote regions of Pakistan. Individuals with diseased phenotype in each family were clinically examined by expert medical officers at government hospitals. Subsequently the disorders were characterized at molecular level by testing linkage to known genes, human genome scan and DNA sequencing using both exome and cycle sequencing methods.

In two families (A, B) after failing to establish linkage to known genes responsible for causing postaxial polydactyly, human genome scan using SNP markers was performed to map the causative genes. In family A, the locus was mapped to a 37.0 Mb region on chromosome 8q21.13-q24.12. Further, whole exome sequencing (WES) identified the first disease causing sequence varient (c.478C>T, p.Arg160*) in the gene *FAM92A1*, mapped on chromosome 8q21.13-q24.12. In the other family, B, genome scan revealed two regions of 37.0 Mb and 22.3 Mb on chromosome 2p14-q12.1, and 6p22.3-p21.1, respectively. Maximum possible multiple LOD score of 1.92 was obtained with SNP markers on both the chromosomes.

In family C, segregating syndactyly, human genome scan mapped a disease locus, flanked by SNP rs2829950 and rs566038, on chromosome 21q21.3-q22.3. Maximum multipoint LOD score of 2.52 was obtained with the SNP rs761372.

Using polymorphic microsatellite markers, linkage in three families (D, E, F), segregating split hand and foot malformation in autosomal recessive manner, was established to SHFM-6 on chromosome 12q11-q13. Subsequently sequence analysis of the *WNT10B* gene led to the identification of two novel sequence varients 4-bp deletion (c.1165_1168delAAGT) in family D and 7-bp duplication (c.300_306dupAGGGCGG) in family E.

Three other families (G, H, I), segregating Ellis–van Creveld syndrome, were clinically characterized to record range of features observed in the affected members.

Abstract

Genotyping using microsatellite markers established linkage in two families (G, H) on chromosome 4p16. DNA sequence analysis revealed two novel sequence varients, one each in *EVC* and *EVC2* gene. A nonsense sequence varient (p.Trp234*) was detected in *EVC2* in the family G and 15-bp duplication (c.1932_1946dupAGCCCTCCGGAGGCT) in the *EVC* gene in the other family H. Affected individuals in the family J showed clinical features of acromesomelic dysplasia type Maroteaux (AMDM), segregated in an autosomal recessive manner. Genotyping using microsatellite markers established linkage in the family to *NPR2* gene on chromosome 9p13-q12. However, DNA sequence analysis of the gene failed to identify any potential sequence variant, which could be responsible for generating AMDM phenotype in the family.

Work presented in the dissertation resulted in publications of the following articles.

1. **Aziz A,** Muhammad Ansar, Regie Lyn P. Santos-Cortez,Kwanghyuk Lee, University of Washington Center for Mendelian Genomics, Deborah A Nickerson, Jay Shendure, Michael Bamshad, Wasim Ahmad, Suzanne M Leal (2014). Exome sequencing identified a non-sense mutation in the gene *FAM92A1*. **(In Preparation)**

2. **Aziz A**, Raza SI, Ali S, Ahmad W **(2014).** Novel homozygous mutations in the *EVC* and *EVC2* genes in two consanguineous families segregating autosomal recessive Ellis–van Creveld syndrome. **Clinical Dysmorphology (Submitted)**

3. **Aziz A** , Irfanullah, Khan S, Zimri FK, Muhammad N, Rashid S, Ahmad W **(2014)**. Novel homozygous mutations in the *WNT10B* gene underlying autosomal recessive split hand/foot malformation in three consanguineous families. **Gene 534: 265–271**

Chapter 1

Introduction

Clinical and Molecular Characterization of Human Hereditary Skeletal Disorders in Consanguineous Families

INTRODUCTION

Bones, constituting part of vertebrate's endoskeleton, are rigid organs with complex external and internal structure and function to support and protect the body, and produce white and red blood cells.

In the vertebrate embryo, skeletogenesis begins when ectoderm and mesoderm give rise to multipotent mesenchymal cells, which migrate to specific locations in the body, and commit to skeleton formation. The embryonic cells further differentiate into three types of cells including chondrocytes, osteoclasts and osteoblasts. Chondrocytes finally differentiate into cartilage while osteoclasts and osteoblasts in to bone. The skeletogenic cells then starts osteogenesis (formation of bones) by two processes: intramembranous ossification (direct conversion of osteoblasts to bone matrix) and endochondral ossification (formation of cartilage template by chondrocytes that is subsequently replaced by bone). Bones of craniofacial skeleton and parts of clavicle are formed by intramembranous ossification while endochondral bone formation accounts for the development of long bones and all the other bones in the skeleton. Finally, a process of growth and remodeling after birth (in a growth and maintenance phase) results in formation of a skeleton (Zelzer and Olsen, 2003). These processes of development, differentiation and organ formation are governed by various transcription factors, growth factors, hormones and their intercellular signals (Karsenty and Wagner, 2002; Tuan, 2003). Defects in any of the step of skeletal development or growth can give rise to skeletal anomalies.

During the development of embryonic skeleton, complex interaction between skeletogenic gene networks determines the fate of aggregating mesenchymal cells. For instance, Wnt pathway regulates skeletogenic cell fate determination by inducing osteoblast differentiation and repressing chondrocytes differentiation (Hill *et al*., 2005; Rodda and McMahon, 2006). *Sox9* is the earliest marker of chondrogenesis and proliferation/differentiation of chondrocytes is tightly regulated by a negative feedback loop between Indian hedgehog (Ihh) and parathyroid hormone-related protein (PTHrP) differentiation and is required for chondrocytes hypertrophy (Otto *et al*., 1997; Takeda *et al*., 2001). Similarly, fibroblast growth factors (FGFs) and their receptors, bone morphogenetic proteins (BMPs) and their receptors are also critical

regulators of proliferation and differentiation of chondrocytes (Li and Cao, 2006; Hung *et al*., 2007). BMP3, a novel member of the BMP family, can block signaling through the type II BMP receptor, activin receptor, type 2b (Kokabu *et al*., 2012). In human skeletal dysplasia, FGF pathway found to be directly involved, mediate their cellular responses by activating receptor tyrosine kinases. FGF Binds to FGFR induces phosphorylation of tyrosine residues and receptor dimerization in the FGFR cytoplasmic domains. The transforming growth factor β (TGFβ) superfamily comprised of several secreted signaling molecules playing important role in normal growth and development, i.e cell proliferation, cell differentiation, cell cycle arrest, and programmed cell death (Massague *et al*., 1994; Kingsley, 1994a). It is mostly found in bone, and is necessary for the proper coupling of osteoblastic and osteoclastic activity (Bonewald, 1999). BMPs and BMP-like genes are highly conserved members of the TGFβ superfamily, and are critical for skeletal patterning and bone formation (Serra and Chang, 2003; Hartung *et al*., 2006; Wu *et al*., 2007). Notch signaling pathway acts as a negative regulator of both osteoblasts and osteoclasts and play an important role to maintain the homeostatic balance between bone formation and bone resorption. It is essential for promoting immature osteoblast formation while inhibiting terminal osteoblast maturation (Bai *et al*., 2008; Engin *et al*., 2008; Hilton *et al*., 2008). The hedgehog signaling pathway also playing crucial role in establishment and maintenance of left-right asymmetry, neural tube formation, and patterning of several skeletal elements (Ehlen *et al*., 2006).

Skeletal development

a. Skeletal Patterning

In higher organisms the skeleton is one of the most highly patterned structures. The adult human skeletal system consists of 206 bones vary greatly in size, shape and functions. The patterning is a process during which the number, size, and shape of the individual skeletal elements are delineated and factors involved in this specification are called patterning factors. Once the pattern is set, mesenchyme precursor cells (skeletogenic cells) move to the site of skeletogenesis, where these cells condense and differentiate. During this process cells from three distinct embryonic lineages, ectoderm derived neural crest, mesoderm derived paraxial and lateral plate mesoderm. The majority of the flat bones of the body are formed from neural crest through

intramembranous ossification where by mesenchymal condensations differentiate directly into bones without cartilage intermediate (de Crombrugghe *et al.*, 2001). Paraxial mesoderm gives rise to somites which develop into progenitors sclerotome cells which then form axial skeleton (ribs and vertebrae). Lateral plate mesoderm forms the appendicular skeleton of the limbs through endochondral ossification, a process during which chondrogenic aggregates change into bones (de Crombrugghe *et al.*, 2000).

- **Craniofacial Skeleton**

The Craniofacial skeletal bones have both an ectodermal and mesodermal origin. Neural crest (NC) cells give rise to most of the cranial skeleton (Kuratani, 2005; Creuzet *et al.,* 2005; Helms *et al.*, 2005), which have an ectodermal origin. Neural crest cell is a pluripotent cell population derived from lateral ridges of the neural plate. After formation they disperse from the dorsal surface of the neural tube and undergo epithelial–mesenchymal transition (EMT), become ectomesenchyme and migrate extensively through the embryo, giving rise to a wide variety of differentiated cell types (Chai and Maxson, 2006). Commitment of neural crest cells to skeletal fates depends on their interaction with epithelial cells (Langille, 1994).

The Craniofacial skeleton is formed of two main components; the neurocranium, bones surrounding brain and sense organs and the viscerocranium, consisting of facial bones and the pharyngeal, temporal, palatal, and auditory bones. The complete viscerocranium and part of the neurocranium are formed from the neural crest cells (Wilkie and Morriss-kay, 2001). Several genes have been identified involved in neural crest patterning. *PAX3* gene involved in neural crest patterning belongs to a highly conserved family of transcription factors, paired box genes, containing two DNA binding domains, a paired domain and a homeodomain (Tassabehji *et al.*, 1992). Mutations in *PAX3* causes Waardenberg syndrome type 1 (WS1; MIM 193500) and type 3 (WS3; MIM 148820), an auditory-pigmentary syndrome characterized by abnormal pigmentation of hair, eyes, and skin, deafness and dystopia canthorum (Tekin *et al.*, 2001; Wollnik *et al.*, 2003; Tamayo *et al.*, 2008; Pingault *et al.*, 2010).

- **Axial Skeleton**

The axial skeleton consisting of the vertebrae and the dorsal part of the ribs is entirely derived from the somites, transient organizational structures of development derived from paraxial mesoderm and added on both sides of the neural tube in a restro-caudal sequence. Studies have shown the synthesis, segmentation and polarity of newly formed somites are driven by a somite segmentation clock that involves oscillation of hairy 1 expression. This in turn derives the expression of lunatic fringe (Lfng) and other components of Notch-Delta pathway (palmeirim *et al*., 1997; McGrew *et al*., 1998). Formation of defective somites causes many developmental disorders of axial skeleton for example Alagille syndrome (AGS; MIM 118450) and Spondylocostal dysostosis (SCDO; MIM 277300).

Alagille syndrome is an autosomal dominant disorder caused by heterozygous deletion or loss-of-function mutations in Notch ligand JAGGED1 or Notch receptor NOTCH2. The clinical features include skeletal defects like butterfly vertebrae, craniofacial and digit abnormalities as well as defects in liver, heart, and kidney (Li *et al*., 1997; Oda *et al*., 1997; McDaniell *et al*., 2006).

The SCDO are group of similar phenotypes characterized by trunk dwarfism, vertebral and rib defects including multiple hemivertebrae, butterfly vertebrae, rib fusion, deletions and misalignment (Turnpenny *et al*., 2007). To date four different subtypes of SCDO have been described, each caused by mutations in different genes of somite segmentation clock. Loss of function mutations in the Notch ligand, DLL3 causes SCDO type 1 (Bulman *et al*., 2000), while type 2, 3 and 4 are caused by mutations in downstream targets of Notch pathway, MESP2, LFNG and HES7 respectively (Whittock *et al*., 2004; Sparrow *et al*., 2006, 2008).

Spatial coordination is conveyed by a gradient of FGF8 expression. As the somite moves rostrally it matures and differentiates into dermatomyotome and the sclerotome, the primary origin of the axial skeleton. This process is regulated by SHH secreted by notochord (Kornak and Mundlos, 2003).

- **Appendicular Skeleton**

The limb skeleton arising from the lateral plate mesoderm, which forms the limb bud as the result of a series of interactions with overlying ectoderm (Ng *et al*., 1999). Differentiation of mesenchyme cells in the limb bud occurs in proximodistal sequence to form various tissues of the limb. The differentiation and positional identity of each cell is controlled by three signaling regions: the apical ectodermal ridge (AER), the zone of polarizing activity (ZPA), and the non-ridge ectoderm, each one being responsible for directing growth and patterning along the three axis; proximodistal, anteroposterior and dorsoventral, respectively (Mariani and Martin, 2003; Niswander, 2003; Tickle, 2003).

AER, an anatomical structure consisting of densely packed ectodermal cells is located at the tip of the limb bud. Several members of the fibroblast growth factors (Fgfs) family; Fgf8, Fgf4, Fgf2, Fgf9, and Fgf17 are secreted by AER cells (Niswander *et al*., 1993; Fallon *et al*., 1994; Crossley *et al*., 1996; Martin, 1998), most important being Fgf8 and have been shown to be essential and sufficient to initiate and outgrowth of the control of the limb (Mariani *et al*., 2008). In the dorsal ectoderm WNT7a is highly expressed in the underlying mesenchyme induces the expression of LMX1 transcription factor which has a key role in dorsoventral patterning (Riddle *et al*., 1995).

ZPA is a region of mesenchyme located at the posterior limb bud margin. SHH is expressed in this region and is the main mediator in anteroposterior patterning (Chiang *et al*., 1996). Mutations in the regulatory region (ZRS) of *SHH* gene causes triphalangeal thumb polysyndactyly (TPTPS; MIM 174500) (Klopocki *et al*., 2008; Sun *et al*., 2008), preaxial polydactyly type II (PPD2; MIM 174500) (Lettice *et al*., 2002, 2003; Li *et al*., 2009), and syndactyly type IV (SD4, Haas type polysyndactyly; MIM 186200) (Sun *et al*., 2008; Wu *et al*., 2009).

b. **Condensation and Differentiation of Mesenchymal Cells**

Once the skeletogenic cells have entered into the chondrogenic lineage, they condense and then differentiate into cartilage forming chondrocytes or bone forming osteoblast. These cells eventually exit the cell cycle and become bonafide hypertrophic chondrocytes and start producing type X collagen. The SOX9 is an important

regulator of condensed cells differentiation into chondrocytes (Bi *et al*., 1999). SOX9 alone is incapable of inducing chondrogenesis, as in vitro experiments have shown that cells expressing only SOX9 can commit to other cell fates (Akiyama *et al*., 2005). SOX9 along with SOX5 and SOX6 have been shown to transcriptionally control expression of the other proteins (Akiyama, 2008). These three proteins together induce the chondrocytes differentiation (Ikeda *et al*., 2004). Heterozygous mutations in SOX9 cause a severe form of chondrodysplasia, Campomelic dysplasia (CD; MIM 114290) (Wagner *et al*., 1994). Recently, Kurth *et al*. (2009) identified that non coding elements located upstream of *SOX9*, have a role in regulating SOX9 expression and duplications of this region affects SOX9 expression, causing brachydactyly–anonychia in families with Cooks syndrome.

The Osteoblasts of cortical bone are originated from the mesenchymal cells of perichardium through blood vessels into the developing marrow (Maes *et al.,* 2010) and form the precursors of trabecular bone, the relation of osteoblast precursor to skeletal progenitor is unknown, but these progenitors lie near capillaries and show similarities with pericytes (Sacchetti *et al.,* 2007; Mendez-Ferrer *et al.,* 2010; Grcevic *et al.,* 2012).

They differentiate from skeletogenic cells in two main steps; they first build an organic non-mineralized (osteoid) matrix, strongly upregulate collagen-1 expression and express alkaline phosphatase, an important enzyme in matrix mineralization. As they mature, they produce bone-specific proteins, such as osteocalcin (BGP) and bone sialoprotein (BSP), and mineralize the osteoid matrix. These differentiation steps are governed by three specific transcription factors: RUNX2, OSX (osterix), and ATF4 (activating transcription factor-4, or cyclic AMP-responsive element-binding protein 2, CREB2) (Karsenty *et al*., 2009; Hartmann, 2009; Jensen *et al*., 2010).

RUNX2 is a master osteogenic factor being expressed by skeletogenic cells, growth plate chondrocytes, and by differentiating osteoblasts until maturation (Schroeder *et al*., 2005). OSX, a Kruppel-like zinc finger domain-containing transcription factor expressed exclusively in osteoblasts is required for the differentiation of RUNX2 expressing skeletogenic cells into osteoblasts in both endochondral and intramembranous bones. Both RUNX2 and OSX can also directly bind and activate

COL1A1, BSP and BGP (Ducy *et al*., 1997; Nakashima *et al*., 2002; Sinha *et al*., 2010). Transcription factor ATF4 controls osteoblast maturation. ATF4 is also needed for synthesis of collagen, the main protein in bone. Its deficiency results in delayed bone formation during mouse embryonic development (Yang and Karsenty, 2004).

c. Bone Ossification and Growth

During embryonic development bone can ossify into two ways, endochondral ossification and intramembranous ossification that govern bone development (Olsen *et al*., 2000; Kronenberg, 2003; Karsenty *et al*., 2009). Intramembranous ossification is the one in which the bony tissue replaced the sheet-like connective tissue membranes and results in the formation of intramembranous bones. They consist of some flat bones of the skull and some of the irregular bones. The major part of the skeleton is formed by endochondral ossification, in which cartilage anlagen is formed first and further replaced by bone (Erlebacher *et al*., 1995). The cartilage is thought to simply be a "model" the shape the bone should take on, and often referred to as a "cartilaginous model". One of the important steps in formation of growth plate is endochondral ossification. It is required for the bone synthesis during early development as well as essential for the postnatal development until the end of puberty. In a long bone, epiphyseal plate play a role in separation of the diaphysis from the epiphysis The chondrocytes of the epiphyseal plateare arranged in four layers through a series of maturation steps; resting chondrocytes, proliferating chondrocytes, prehypertrophic chondrocytes, and hypertrophic chondrocytes. Resting chondrocytes is closest to the epiphysis which does not participate actively in growth. The second layer or proliferating chondrocytes, includes string of many young cells go through mitosis. Hypertrophic chondrocytes synthesizes an extracellular matrix rich in collagen X (Iyama *et al*., 1991) where it deposits the angiogenic factor, vascular endothelial growth factor (VEGF). The VEGF promotes the formation of blood vessels from the perichondrium (Gerber *et al*., 1999). Soon after perichondrial angiogenesis, the blood vessels invade the cartilage matrix; osteoblasts, osteoclasts and hematopoietic cells migrate to the diaphysis and form the primary ossification center. Within these centers the hypertrophic chondrocytes undergo apoptosis, osteoclasts degrade the cartilage matrix, osteoblasts lay down bone matrix, hematopoietic cells generate bone marrow and perichondrium differentiates into a

bone collar. Secondary ossification centers develop in the epiphysis postnatally leaving a cartilage plate between epiphysis and diaphysis that close in early adulthood (Lefebvre and Bhattaram, 2010).

d. Bone Remodeling

Bone remodeling involves the removal of mineralized bone by osteoclasts followed by the formation of bone matrix through the osteoblasts that subsequently become mineralized. After a bone is formed, it has to preserve the overall mass and undergo constant restructuring when exposed to mechanical stresses or changing metabolic needs. Disturbance in remodeling either causes bone loss (osteoporosis) or excess bone accumulation (osteopetrosis). Factors essential for proper coupling of osteoblastic and osteoclastic activity includes TGFβ and members of canonical Wnt signaling pathway. Several skeletal dysplasias highlight the importance of these pathways in bone mass regulation. Throughout life, homeostatic mechanisms in the skeleton control bone density, maintenance and cartilage integrity. Dysregulation in these processes can result in skeletal disorders.

Human Skeletal Disorders

Human skeletal dysplasias are genetically heterogeneous group of disorders that results from errors in bone, cartilage and joint development. They are characterized by abnormalities in patterning, differentiation, linear growth and maintenance of the human skeleton. A complex series of signaling cascades, including the FGF, BMP, TGF β, WNT, Notch, Hedgehog pathways, are essential for proper skeletogenesis. Human skeletal dysplasias are often a consequence of a primary or secondary dysregulation of these pathways. Although individually rare, the overall birth incidence is estimated to be 1/5000 live births (Orioli *et al*., 1986). Skeletal disorders can be broadly divided into three main subgroups; osteodysplasias, chondrodysplasias, and dysostoses. The first two are generalized skeletal malformations affecting bone and cartilage, respectively while the malformation of individual bones or a group of bones has been defined as dysostoses. Though this classification of skeletal dysplasias can sometimes be useful, due to the overlap in the developmental processes that regulate skeletogenesis, firm delineation is generally not possible. On the basis of radiographic, clinical and molecular criteria, there are more

than 450 well-characterized skeletal dysplasias. According to the latest 2010 revision of the Nosology and Classification of Genetic Skeletal Disorders, 456 skeletal malformations were included and placed in 40 groups. Of these conditions, 316 are associated with one or more of 226 different genes (Warman *et al.*, 2011).

Most of the skeletal disorders have been associated with excessive and decreased FGF signaling. These disorders have been linked to *FGFR1* (MIM 136350), *FGFR2* (MIM 176943)*,* and *FGFR3* (MIM 134934) gene mutations. Mutations in *FGFR1* or *FGFR2* cause craniosynostosis (Wilkie, 2005). Craniosynostosis is due to gain of function mutation in *FGFR2* resulting in excess FGFR2 signaling which is linked to an increased in the rate of osteoblast proliferation or differentiation or to increased mineralization function of osteoblast which lead to premature suture closure (Ornitz and Marie, 2002; Marie *et al.*, 2008). Mutation in *FGFR3* gene lead to activation of the receptor which results in increased FGF signaling where excess FGF signaling can cause decrease growth plate proliferation and is the primary cause of a chondroplasia (Rousseau *et al.*, 1994; Shiang *et al.*, 1994; Naski *et al.*, 1996). Defects in the ligands of FGF pathway have also been linked to human skeletal disorders. Mutation in *FGF10* (MIM 602115) cause lacrimoauriculodentodigital syndrome (LADD, MIM 149730) and is seem to be due to decreased FGF signaling (Rohmann *et al.*, 2006). Similarly a missense mutation in *FGF9* (MIM 600921) has been found to be associated with multiple synostosis syndrome characterized by fusion of joints in both the hands and the feet (Wu *et al.*, 2009). This mutation leads to decreased FGF signaling and decreased chondrocytes proliferation and differentiation (Harada *et al.*, 2009). Camurati-Engelmann disease (CED, MIM 131300), cause by TGFβ1 activating mutations, a rare autosomal dominant disorder characterized bycortical thickening of the long bones and increased bone formation (Kinoshita *et al.*, 2000; Janssens *et al.*, 2006). CED mutation produces excessive TGFβ in the bone marrow resulting in increased bone formation. Another human skeletal dysplasia caused by disruption and activation of TGFβ signaling pathway is Loeys-Dietz syndrome. Geleophysic dysplasia (MIM 231050) is an additional link between TGFβ signaling and human skeletal dysplasia. Geleophysic dysplasia is characterized by premature ossification of the cranium and obliteration of the sutures and is caused by homozygous mutation in the gene ADAMTS-like protein- 2 (*ADAMTSL2,* MIM

612277) (Le Goff *et al*., 2008). Mutation in *GDF5* (MIM 601146) gene cause wide variety of skeletal anomalies in humans including brachydactyly type A2 (BDA2; MIM 112600), brachydactyly type C (BDC; MIM 113100) (Yang *et al*., 2008), fibular hypoplasia and complex brachydactyly (Du Pan syndrome) (MIM 228900), Grebe type chondrodysplasia (MIM 200700), Hunter-Thompson type acromesomelic dysplasia (MIM 201250), multiple synostosis syndrome type 1 (MIM 186500) and proximal symphalangism (SYM1; MIM 185800) (Yang *et al*., 2008, Seemann *et al*., 2005; Polinkovsky *et al*., 1997; Faiyaz-ul-Haque *et al*., 2002; Thomas *et al*., 1996, 1997; Dawson *et al*., 2006). *Gdf5* absence leads to brachypodism in mice (Storm *et al*., 1994).

Genetic defects in Notch signaling cascade result in two types of human skeletal disorders; Spondylocostaldysostosis (SCDO) and Alagille syndrome (Dequeant and Pourquie, 2008). Homozygous loss of function mutations in delta-like 3 (*DLL3,* MIM 602768), mesoderm posterior 2 (*MESP2*, MIM 605195)*,* lunatic fringe (*LFNG,* MIM 602576) and hairy/enhancer of split 7 (*HES7,* MIM 608059) genes cause different types of SCDO disease (Bulman *et al*., 2000; Whittock *et al*., 2004; Sparrow *et al*., 2006, 2008).

Appendicular Patterning Defect

Many limb skeleton disorders include abnormalities of patterning of hands and feet.

Polydactyly

The term Polydactyly, "poly- many and dactylos- digits" is acknowledged to Theodor Kerckring, a Dutch physician in the 17th century (Kerchring *et al*., 1988). Polydactyly or polydactylism is referring to the occurrence of supernumerary digits, toes or duplication of digital parts. This situation was described as 'superfluous fingers in the 16th century by Ambrose Parey (Bell *et al*., 1953). It is among the most common congenital limb anomaly observed immediately at birth, manifesting in a variety of forms, ranging from complete duplication of a limb or limb part to a complete duplication of a digit. Its occurrence is estimated to be 1.6–10.7/1,000 in general population and 0.3–3.6/1,000 in live-births. Males are often affected twice as females (Mellin 1963; Castilla *et al.,* 1973). Phenotypically, polydactyly is an extremely

heterogeneous deformity (TemtamyandMcKusick, 1978). Usually, there is high tendency for the involvement of right hand than the left, upper limbs than the lower and left foot than the right (Castilla *et al.*, 1973; Malik *et al.*, 2014). It occurs both in isolated and syndromic forms. Two most common types are pre-axial polydactyly (PPD) having superfluous digit attached on the thumb side or great toe and postaxial polydactyly (PAP) with extra digits at the side of the 5th finger or toe (Temtamy and McKusick, 1978; Wassel, 1969; Winter and Tickle, 1993). Meso-axial polydactyly is a very rare form involving second, third, or fourth digits has been described in the literature as well.

Polydactyly classification

In the classifications of polydactyly, the Temtamy and McKusick (1978) scheme is the most widely used among dysmorphologists geneticists and genetic counselors. In this system, the three mainpolydactylies with sub-types are

    a. pre-axialpolydactyly

    b. post-axialpolydactyly

    c. complex types

    a. Preaxialpolydactylies (PPD)

Temtamy and McKusick (1978) identified four types of preaxial polydactylies: polydactyly of thumb/hallux (type 1), triphalangeal thumb polydactyly (TPT, type 2), polydactyly of pointer finger (type 3), and crossed polydactylyor polysyndactyly (CP, type 4)

- **Thumb polydactyly (Preaxial type 1)**

This is the most common type of polydactyly representing a duplication of one or more than one components of a biphalangeal thumb (MIM 174400). In bilateral cases only hands are affected preferentially and the right hand is mostly involved than the left (Malik *et al.*, 2014). There is low occurrence of familial reappearance and high prevalence of affected males (Orioli and Castilla, 1999). Their severity may be from milder to high as follow; the distal phalanx is broad or the duplication of distal phalanx; base of the distal two third of phalanx is common but with distinct bifurcation; undeveloped extra thumb with no tendinous attachment and showing

hypoplasia of the thumb muscles structure; two supernumerary phalanges with undeveloped thumb which fix close to the base of the proximal phalanx, articulating with the metacarpal head; replication of complete thumb, including two phalanges and a metacarpal (Temtamy and McKusick, 1978). Septodactyly or heptadactyly is also a type of thumb polydactyly in which triplication of thumb occurred resulting in seven digits (Zuidam *et al*., 2008). Familial preaxial polydactyly type 1 shows autosomal dominant inheritance pattern with reduced penetrance (Castilla *et al.,* 1973: Orioli and Castilla, 1999). *SHH/ZRS* mutations are known to cause one subtype of preaxial type 1 polydactyly (Wieczorek *et al.,* 2010; Lettice *et al.,* 2002).

Another type of thumb polydactyly is hallux polydactyly (MIM 601759). It is known to exist as a predominant presentation or an isolated entity in families (Castilla *et al.,* 1973). The incidence is 2.4/100,000 and 16.5/100,000of hallux duplication vs thumb polydactyly in South America, respectively. In hallux duplication, females are less affected as compared to males, mostly unilateral and predominantly involved the right foot (Orioli and Castilla, 1999). Up to date the molecular base of non-syndromic hallucal polydactyly remains unknown. It has been suggested that there is a possible relationship between hallucal polydactyly and maternal diabetes with a very extraordinary proximal placement of the extra digit (Carey *et al.,* 1990). The association of hallux Duplication with clinodactyly has been shown to segregate with microdeletion at chromosome 2q31.1- q31.2 (Tsai *et al*., 2009).

- **Triphalangeal thumb polydactyly (TPT) (Preaxial type 2)**

Preaxial polydactyly type 2 (MIM 174500) is also known as triphalangeal thumb polydactyly replaced biphalangeal thumb. The thumb has an extra middle phalanx with abnormally long and thin first metacarpal containing epiphyses at both ends On the other hand; phenotype of TPT is usually associated with polydactyly of the thumb with normal first metacarpal. The TPT is frequently opposable, and there may be duplication in the feet of great toe (Temtamy and McKusick, 1978). TPT is usually symmetrical and bilateral (Swanson and Brown, 1962). Its inheritance pattern is autosomal dominant with incomplete penetrance (Temtamy and McKusick, 1978). Preaxial polydactyly type 2 was mapped by Tsukurov *et al*. (1994) on chromosome 7q36. Normal *SHH* expression occurs in the zone of polarizing activity (ZPA)

posteriorly in the limb bud, and is regulated by ZPA regulatory sequence (ZRS). Point mutation in *ZRS* which lies within intron 5 of the *LMBR1* gene segregates with PPD type 2 (Lettice *et al*., 2003)

- **Polydactyly of index fingers (Preaxial type 3)**

Preaxial polydactyly type 3 (MIM 174600) is very rare and segregated as autosomal dominant trait. In this type of polydactyly usually the index finger is duplicated. One or two triphalangeal digits replaced the thumb. The metacarpal of the accessory digit showing distal epiphysis, due to this reason type 3 is separated from preaxial polydactyly type 2 or TPT (Temtamy and McKusick, 1978; Swanson and Brown, 1962). Sometimes there is preaxial polydactyly of first or second toes. The 'central polydactyly' and 'Index polydactyly' are sometimes lumped together and considered as a variant of thumb duplication (Wood, 1970). Duplication at the radial side normally is smaller and the duplication level may be more distal or at the metacarpal. The extra digit normally is in major angulations or radial deviation, and the normal digit may be deviated toward the ulnar side into a varying degree (Graham and Ress, 1998).

- **Polysyndactyly, CP (Preaxial type 4)**

In this type of polydactyly the thumb is duplicated mildly, the distal phalanx shows radial deviation or with broad and bifid thumb (MIM 174700). Syndactyly of third-and-fourth fingers is rarely present (Temtamy and McKusick, 1978). In the feet first toe shows polydactyly, and the first metacarpal is tibially deviated and short. There is syndactyly of all toes or second and third toe. It is noted that this entity is different from synpolydactyly, in which syndactyly with in the web is associated with additional digit (Malik, 2012). The word 'crossed polydactyly' is typically used for the presence of post-axial and pre-axial polydactyly, only there is a difference between the hands and feet in axis of the additional digits. In CP type 1, there is postaxial polydactyly in hands and preaxial polydactyly in feet. CP type 2 shows post-axial polydactyly of feet combined with preaxial polydactyly of hands (Temtamy and McKusick, 1978). Mutations in *GLI3* and *ZRS/SHH* have been reported for the appearance of CP type 1 which is allelic to postaxial polydactyly A/B (Radhakrishna *et al*., 1999).

b. Postaxial polydactyly (PAP)

In postaxial polydactyly (MIM 174200), there is one or more than one extra ulnar or fibular digit or part of it. Specifically for the postaxial polydactyly, two distinct catagories have been recognized, i.e postaxial type A and postaxial type B, which differ in severity, penetrance estimates and inheritance pattern (Temtamy and McKusick, 1978).

- **Postaxial type A**

In type A, extra digit is fully developed articulating with either the fifth metacarpal or metatarsal, or with a duplicated metacarpal or metatarsal (Temtamy and McKusick 1978). The duplicated digit, depending upon its size may harbour one to three bony elements, which result in flexion wrinkle and a well-developed nail. Postaxial digit and the fifth ray shows a high variable angle-of-articulation (i.e. $<30\circ -180\circ$). In most cases, the extra digit is non-functional and may create problems in daily-life activities. Type A is segregated as an autosomal dominant trait with clear penetrance (Castilla *et al*., 1997; Kucheria *et al*., 1981). Recently two autosomal recessive PAP type A in two Pakistani families have been mapped on chromosomes 4p16.3 (*ZNF141*) and 13q13.3-q21.2, (Kalsoom *et al.,* 2012, 2013).

- **Postaxial type B**

In PAP type B, the richest type of polydactyly in a variety of populations, the extra digit is not well formed and frequently occurs in the form of a skin tag ranging from a negligible sign of small protuberance to spine-like outgrowth on the ulnar side of fifth finger, to a two to three cm long nubbin-like 'pedunculated postminimus' which usually having bony element and a nail (Castilla *et al.,* 1973). The articulation site of the fifth digit along this nubbin is variable and frequently through a small cutaneous bridge. Preferentially the left hand and the upper limbs are affected. This type showing more complicated genetics and the estimated penetrance is 43% (Castilla *et al.,* 1973). Both PAP types A and B have been suggested two separate and genetically heterogeneous groups due to their different segregation patterns and independent occurrences (Castilla *et al.,* 1973; Temtamy and McKusick 1978).

Up to date several autosomal dominant loci for postaxial polydactyly have been reported including PAP1 mapped on chromosome 7p13 with mutations in the *GLI3* gene (Radhakrishna *et al*., 1997a,b), PAP2 having chromosomal address of 13q21-q32 (Akarsu *et al*., 1997) and PAPA3 with characteristics of PAP-A/B mapped on chromosome 19p13.1-13.2 (Zhao *et al*., 2002). Galjaard *et al*. (2003) have reported another autosomal dominant PAP with PAP-A/B phenotypes and partial cutaneous syndactyly on chromosome 7q21-q34.

c. Complex types of polydactyly

This type of polydactyly is not fit into familiar phenotype of postaxial or preaxial polydactyly that is why it is placed into complex type categories.

- **Mirror-image polydactyly: (MIP)**

In MIP (MIM 135750) there is a duplication of posterior digits while the anterior digits are completely replaced in reverse order by the posterior digits i.e. the arrangement of supernumerary digits in descending order from a single central digit e.g. little finger, ring finger, middle finger, index finger and then middle finger, ring finger, little finger with the absence of a thumb/hallux (Temtamy and McKusick, 1978). Another family described by Martin *et al*. (1993), in which the affected individuals showing complete duplication of all fingers with 10 digits on the left and 9 digits on the right, forming bilaterally a complicated type of configuration. Isolated Mirror-image polydactyly (MIP) is very rare and inherited as an autosomal dominant entity, while it is usually described as a part of Laurin-Sandrow syndrome, which is characterized by agenesis of tibia and/or radius, duplication of fibula and/or ulna, duplication of little, ring and middle fingers, and absence of thumbs. The tubular bones of lower and upper limbs has direct to a suggestion of three heritable types of Mirror-image polydactyly (MIP): (a) PPD with tibial defect is a rare, autosomal dominant trait with expressivity and variable penetrance; (b) agenesis of the tibia and mirror foot; and (c) dimelia of fibula and ulnar (Temtamy and McKusick, 1978). Mutation in *MIPOL1* cause one of the phenotype of MIP localized at chromosome 14q13 (Kondoh *et al*., 2002). Another gene *PITX1* mutation causes MIP with lower-limb malformations (Klopocki *et al*., 2012).

- **Mesoaxial /Central polydactyly**

Mesoaxial or Central polydactyly, is a 'hidden' duplications with apparent syndactyly and even synonychia, may be present as a mass of tissue in the middle part of the hand, though, not all mesoaxial types are hidden. Mesoaxial polydactyly like duplications of second finger frequently is inherited autosomal dominantly (Graham and Ress, 1998). The deformity is usually bilateral, although different type's contra lateral hand deformities of central cleft or complex syndactyly also present. The fourth digit is most frequently duplicated, followed by the long radial ray; these two are more common than the duplications of index digit (Temtamy and McKusick, 1978).

- **Palmer and dorsal polydactyly**

This is very rare and unusual type of polydactyly in which extra digit arising from the ventrum or dorsum of the autopod. It may be shown as a minor skin tag or a poorly developed digit ray, or an entirely developed digit with or without nail and inserted into the autopod or palm as a hook. Depending upon the articulation, level of growth, and musculature, the duplicated digit could be active and mobile. The mobile duplicated digit in the hand, a ventral or palmer origin of a mobile duplicated digit is reported (Nair *et al*., 2001). Similarly, it has been described that duplicated digit arising from the dorsam of foot (Hussain *et al*., 2007).

- **Haas type polysyndactyly**

In Haas type polysyndactyly (OMIM-186200), all the fingers are fused cutaneously, and there is an extra preaxial or postaxial ray in the web (Haas 1940). Owing to a complete syndactyly the movement of fingers is limited and the fusion of adjacent fingers gives the hand a cup-shaped like appearance. Haas type deformity is generally classified as type 5 syndactyly (Malik, 2012). On the bases of evidences, it has been observed that haas type polysyndactyly is genetically heterogenous. *GLI3* and *ZRS /SHH* mutations are known to cause this deformity (Radhakrishna *et al*., 1999; Wieczorek *et al*., 2010).

Syndactyly

The term syndactyly is originated from Greek 'Syn' means together and 'Dactylos' means digits, is a digital abnormality in which contiguous fingers and/or toes are webbed because there is embryological failure of fingers separation during limb development. It is common in several species, including kangaroos and birds. Syndactyly is one of the most frequent hereditary limb malformations showing an incidence of 3–10 in 10000 births, although higher estimates ranging from 10–40/10000 have been reported (Hay, 1971; Castilla *et al*., 1980). Clinically syndactyly are a genetically heterogeneous group of disorders of hands and feet, may be symmetrical or asymmetrical, unilateral or bilateral and the fusion may be cutaneous or bony. In addition there is common inter- and intra-familial phenotypic variability is present. The condition is so unpredictable that the same affected individual can exhibit asymmetrical phenotypes in the right and left and upper and lower limbs. Syndactyly may be described as cutaneous or bony, partial or complete, and involving the phalanges or can be extending up to carpal/tarsal or metacarpal/metatarsal levels, sometimes proximating the distal end of foreleg/forearm (Temtamy and McKusick, 1978). On the basis of phenotype and genotype, the recent classification scheme describes nine types syndactyly with subdivisions, which is useful in the understanding of syndactyly deformity and in showing its affinity with other digit abnormality, including oligodactyly, polydactyly, and brachydactyly (Malik, 2012). The majority of which are isolated syndactyly. Most of these are thought to be inherited as autosomal dominant fashion. Though, two autosomal recessive and an X-linked recessive type have also been described. Normally, autosomal dominant phenotypes are rather less severe and show broadly incomplete penetrances and variable expressivity. Similarly, autosomal recessive syndactylies are clinically more severe with rather consistent phenotypes. The isolated forms of syndactyly are most easily evaluated in their subgroups, rather than as single entity. Temtamy and McKusick (1978) divided isolated syndactyly into five types. On the basis of genotype and phenotype the recent classification scheme describes nine types syndactyly.

- **Syndactyly type I (SD1)**

Syndactyly type 1 (SD1; MIM 185900) having autosomal dominant inheritance fashion, accounts for the majority of isolated syndactylies (Castilla *et al*., 1980). Phenotypically SD1 is characterized by complete or partial webbing of third and fourth fingers and second and third toes, while sometime finger are associated with bony fusion. Based on current classification and clinical observations, Syndactyly type 1 can be subdivided into four types (a, b, c, d).

SD1-a also known as Weidenreich type (OMIM 609815) is characterized by bilateral fusion of 2nd and 3rd toes, not including hand abnormalities. Malik *et al*. (2005), mapped this subtype to chromosome 3p21.31 by predicting genetic heterogeneity in zygodactyly and propose to designate the 3p21.31 locus as ZD1.

SD1-b, also known as Lueken type (OMIM 185900). The features are bilateral Cutaneous 3rd and 4th fingers and fusion of 2nd and 3rd toes. Bosse *et al*. (2000) mapped a large German Syndactyly type 1b family on chromosome 2q34-q36. This locus was known as SD1 locus (Ghadami *et al*., 2001)

SD1-c, also known as Montagu type or 3rd and 4th fingers syndactyly, is characterized by bilateral or unilateral cutaneous or bony webbing of 3rd and 4th fingers and occasionally of 4th and 5th fingers. It is described that the feet are not included in this subtype (Hsu, 1965; Montagu, 1953).

SD1-d also named as Castilla type syndactyly and has been shown in an epidemiological study (Castilla *et al*., 1980). It is characterized by webbing of 4th and 5th toes. These four subtypes are very rare and little is known about the gene locus, for the rare SD1-c and SD1-d subtypes have not been identified.

- **Syndactyly type 2 (SD2)**

Syndactyly type 2 (MIM 185900), also called as synpolydactyly or Vordingborg type, a well-characterized type, is genetically and clinically one of the most heterogeneous groups involves third web spaces of the hands and bilateral synpolydactyly of the fourth web spaces of the feet with partial or complete digit duplication within the syndactylous web. Syndactyly type 2 is the only syndactyly type with a mesoaxial extra finger. Up to date synpolydactyly have been localized on three different

chromosome (SPD1-3) with a genetic address of SPD1 located at 2q31 (Sarfarazi *et al*., 1995) with mutations in *HOXD13* gene (Muragaki *et al*., 1996; Goodman *et al*., 1997; Gong *et al*., 2011, Kurban *et al*., 2011), SPD2 is located at 22q13.31 (Debeer *et al*., 2002b) caused by disruption in gene *FBLN1* (Debeer *et al*., 2002a). SPD2 is usually thought to include synostosis of the metatarsal and metacarpal bones. SPD3 is localized at 14q11.2-q12 (Malik *et al*., 2006) with causative gene not yet reported.

- **Syndactyly type 3 (SD3)**

Syndactyly type 3 (SD3, MIM 186100), also named as Johnston–Kirby type, a ring-small syndactyly, is fusion of bilateral and distal phalanges usually. It may be only a rudimentary middle phalanx in the small finger (Johnston and Kirby, 1955). In order to accommodate the webbing with small finger, the fourth finger shows valgus deviation when the fusion is complete (Temtamy and McKusick 1978). The feet are usually unaffected, the fused fingers are adducted and the nails are medially fused of the syndactylous fingers. Gladwin *et al*. (1997) mapped oculodentodigitaldysplasia (ODDD) with characteristic SD3 phenotypes on human chromosome 6q22-q23, with causative mutations in connexin 43 gene (*GJA1*) (Paznekas *et al*., 2003).

- **Syndactyly type 4 (SD4)**

Syndactyly type 4 (SD4, MIM 186200), Haas-type synpolydactyly is rare, described by Haas in 1940, has an occurrence of 1 in 300 000, having autosomal dominant inheritance pattern, described as complete syndactyly (Castilla *et al*., 1980). In this type, all the digits of both hands are affected, with associated polydactyly, usually involving 6 digits and 6 metacarpals, with completely fused nails or may be separated by a groove only. There is limited flexion of fingers and the fusion of adjacent fingers gives a cup-shaped appearance to the hands. Sato *et al*. (2007) mapped SD4 with tibial hypoplasia on the long arm of chromosome 7 with a genetic address of 7q36. Duplications in long-range sonic hedgehog (SHH) regulator (ZRS) have been reported as a causative agent for SD4 along with associated digit phenotypes (Klopocki *et al*., 2008; Sun *et al*., 2008; Wu *et al*., 2009). Wang *et al.* (2007) identified *LMBR1* gene mutation in Chinese family being causative agent in SD4 development.

- **Syndactyly Type 5 (SD5)**

Syndactyly type 5(MIM 186300) is rare type, also known as Dowd type syndactyly, transmitted in autosomal dominant fashion. It is characterized by webbing of long and ring fingers along with second and third toes with metacarpals 4 and 5 as the hallmark. Syndactyly is frequently extra-ordinary extensive and complete (Robinow *et al*., 1982). Some other symptoms including deviation of ulnar fingers from 2nd to 5th, shortening of fused 4th and 5th metacarpals, inter-digital cleft between 3rd and 4th fingers, absent distal inter-phalangeal creases of the affected fingers and short distal phalanges are also present (Dowd, 1896). Zhao *et al*. (2007) reported *HOXD13* gene to be a causative agent for SD5 in two large Han Chinese families. This anomaly was described in five generations family from the island of Sesland by Kemp and Ravn (1932). Some cases without fusion of metatarsal also exists, but normally seen with other foot deformities (Robinow *et al.,* 1982).

- **Syndactyly Type 6 (SD6)**

Syndactyly type 6 also known as Mitten type, is unilateral syndactyly, in which all the fingers are webbed except the thumb in a hand and fused 2nd and 3rd toes (Temtamy and McKusick 1978). It is described that in most cases distal and terminal phalanges are merged in a knot-like structure. SD6 is inherited as an autosomal dominant pattern with incomplete penetrance and variable expressivity has been recommended for this rare type. Due to its rarity this non-syndromic phenotype is least researched, although Tentamy and McKusick placed this type of syndactyly in their preliminary classification.

- **Syndactyly Type 7 (SD7)**

Syndactyly type 7 (MIM 212780) also known as Cenani–Lenz type syndactyly (CLS) segregating in autosomal recessive manner, manifest severe abnormalities of hands and all digital elements. It is described by the disorganization of bones of hand in such a way that there is no identification of phalangeal element (Cenani and Lenz, 1967). The phalanges, carpals and metacarpals show asymmetrical synostosis giving cup-shaped hands. The abnormality can involve ulna and radius that are either short, fused, or rudimentary may resulting in dislocation of the radial head and shortening of

the central portion of forearm (Temtamy and McKusick, 1978). In Cenani–Lenz type there are two grossly variant clinical features including an oligodactyly type and a spoon hand type (Harpf *et al*., 2005)

Li *et al*. (2010) reported that CLS, both oligodactyly and spoon-head types, with limb and kidney malformations are caused by multiple mutations in *LRP4*, mapped on chromosome 11p11.2. It is thought to be causative agent in SD7, play a major role in Wnt/b-Catenin signaling.

- **Syndactyly Type 8 (SD8)**

Syndactyly Type 8 also named as Orel-Holmes type, in which there are fusion of 4th and 5th metacarpals with a clear ulnar deviation of the 5th finger having no other abnormality. The 4th and 5th metacarpals are shortened with significant separation between their distal ends (Orel, 1928; Holmes *et al*., 1972). Initially it was thought to be X-linked recessive trait, however one report showing autosomal dominant inheritance for this phenotype (Lerch, 1948).

- **Syndactyly Type 9 (SD9)**

Type 9, Mesoaxial synostotic syndactyly (MSSD, MIM 609432), is reported in two consanguineous pedigrees from Turkish and Pakistan (Percin *et al*., 1998; Malik *et al*., 2004) in which the affected individuals showed mesoaxial shortening of fingers, malformed thumbs, 3rd and 4th metacarpals showed osseous synostosis resulting into a single digit and the 5th finger is hypoplastic and clinodactyly. Additional features include preaxial webbing with hypoplasia of terminal phalangeal of all the toes. SD type 9 was mapped to chromosome 17p13.3 and inherited in autosomal recessive manner (Malik *et al*., 2005).

Ectrodactyly/Split Hand-Foot Malformation (SHFM)

Split-hand/foot malformation (SHFM) is a rare congenital limb malformation involving the central rays of the autopods, presenting with syndactyly, median clefts of hands and feet, and aplasia and/or hypoplasia of phalangeal, metacarpal and metatarsal bones. The clinical picture of SHFM varies in severity from patient to patient as well between the limbs in the same individual (Duijf *et al.,* 2003; Elliott and Evans, 2008). SHFM exists both in isolated or part of a complex syndrome. Isolated

SHFM have six different forms, behaves as an autosomal dominant, autosomal recessive and X-linked fashion. To date seven types of SHFM have been mapped on different human chromosomes. However, only 3 genes (*TP63*, *WNT10B*, *DLX5*) for the seven loci have been identified.

SHFM1 characterized by deep median clefts, the absence of the central digital rays, and syndactyly of the remaining digits. This disorder transmitted as an autosomal dominant trait, has been mapped to chromosome 7q21.3-q22 (Scherer *et al*., 1994), harbour translocations, deletions, and inversions in this chromosomal region.

SHFM2 is characterized by involvement of all four limbs with monodactyly or bidactyly of both hands and lobster-claw deformities of both feet. Mode of inheritance of SHFM2 is X-linked trait (Ahmad *et al*., 1987). Faiyaz-Ul-Haque *et al*. (2005) narrowed the previously linked 22-Mb genetic interval on Xq24–q26 to a 5.1-Mb region.

SHFM3 transmitted as autosomal dominant trait and characterized by aplasia and/or hypoplasia of the phalanges, metacarpals and metatarsals, was initially mapped to a large interval of human chromosome 10q24-25 (Nunes *et al*., 1995; Ozen *et al*., 1999). De Mollerat *et al*. (2003) reported that complex rearrangement on chromosome 10q24-q25 around the Dactylyn locus, possibly associated with gene inactivation, however no demonstration that Dactylyn is the disease gene for SHFM3.

SHFM4 showing variable phenotypes of split hands and feet with aplasia of phalangeal, metacarpal and metatarsal bones, with or without syndactyly and webbing, has been mapped on human chromosome 3q27 (Ianakiev *et al*., 2000). It is caused by pathogenic sequence variants in *p63* gene, coding for a transcription factor homologous to p53 and p73 (Ianakiev *et al*., 2000; van Bokhoven and Brunner, 2002; Berdon-Zapata *et al*., 2004).

SHFM5 having autosomal dominant inheritance fashion has been mapped on chromosome 2q31 (Boles *et al*., 1995). It includes closely related genes *DLX1* and *DLX2* in this region with no pathogenic variants yet reported. The double knockout of *Dlx5* and *Dlx6* (Dlx5/6 D-KO) in the mouse causes ectrodactyly in the hind limbs with defective development of the middle portion of the apical ectoderm ridge (AER) (Merlo *et al*., 2002; Robledo *et al*., 2002). Goodman *et al*. (2002) proposed that

haploinsufficiency of the 5' *HOXD, EVX2*, or *DLX1* and *DLX2* genes may lead to SHFM5 and other digit defects.

SHFM6 having autosomal recessive inheritance fashion, has been mapped on chromosome 12q13.11-q13, with mutations in *WNT10B* as a causative gene (Ugur and Tolun, 2008; Blattner *et al*., 2010; Khan *et al*., 2012; Aziz *et al.,* 2014). The gene *WNT10B* is one of the members of WNT gene family, which contains at least 18 other genes. Proteins encoded by these genes bind cell surface frizzled (FZD) and low-density lipoprotein receptor related proteins resulting in activation of a conserved "canonical" signaling pathway (Peifer and Polakis, 2000). The Wnt signaling through proteins such as Wnt6, Wnt10a and Wnt10b plays an important role in development and maintenance of many organs and tissues including bones (Cadigan and Nusse, 1997; Cawthorn *et al*., 2012). The role of Wnt signaling pathway has been investigated in the developing limb bud that controls multiple processes such as limb patterning and limb morphogenesis. Another locus for SHFM was identified by Gurnett *et al*. (2006) on chromosome 8q21.11–q22.3. It includes closely related genes *FZD6* and *GDF6* in this region with no pathogenic variants yet reported.

Ellis-Van Creveld Syndrome

Ellis–van Creveld (EVC, MIM 225500) syndrome is an autosomal recessive skeletal dysplasia, first described by Richard Ellis and Simon Van Creveld in 1940. Skeletal defects, oral and dental anomalies, nail dystrophies and cardiac abnormalities are the identifying features of EVC syndrome. To date several cases have been reported in different ethnic groups with parental consanguinity in about 30% of cases (Gorlin *et al*., 2001). EVC syndrome is commonly observed in Amish community of Lancaster, Pennsylvania, where the incidence is estimated to be 5/1000 live births as compared to 7/10,00,000 in non-Amish population (Stoll *et al*., 1989; Dugoff *et al*., 2001). Since 1940 about 300 cases of the syndrome have been reported in different ethnic groups (Zangwill *et al*., 1998).

Major skeletal abnormalities reported in cases of EVC syndrome included distal shortening of upper and lower limbs, disproportionate dwarfism with short ribs and exceptionally long and narrow trunk, short broad hands with bilateral postaxial polydactyly type A, partial cutaneous syndactyly and genu velgum. Radiological

study showed short middle and distal phalanges, hamate and capitate bone fusion, coned shaped epiphysis, mild bowing of humerus, complete or partial fusion of metacarpal and metatarsal bones, fusion of proximal tibia and fibula (Ulucan *et al.*, 2008; Vinay *et al.*, 2009). Oral and dental anomalies associated with EvC are maxillary and mandibular submucosal clefts, labiogingival adherences causing a lip to present a V shaped notch in the mid line, dystrophic philtrum, multiple frenula, hypodontia, natal and neonatal teeth, conical and microdontic teeth, malocclusion, delayed teeth eruption and enamel hypoplasia (Sarnat *et al.*, 1980; Deborah *et al.*, 1988; Hunter and Roberts, 1998; Atasu and Biren, 2000; Cahuana *et al.*, 2004). Nearly nails in all the EVC patients are short, thin, hypoplastic and often spoon shaped (Al-khenaizan *et al.*, 2001; Gorlin *et al.*, 2001). Congenital heart defects occur in 50–60% of EVC cases, and are a major cause of reduced life expectancy (Digilio *et al.*, 1999). AVCD (Atrioventricular Canal Defect), CA (Common Atrium), LSVC (Left Superior Vena Cava) and pulmonary venous abnormalities are most commonly heart defects reported in EVC patients (Digilio *et al.*, 1999; Hills *et al.*, 2011).

Ellis-van Creveld syndrome is caused by mutations in two genes, *EVC* (MIM 604831) and *EVC2* (MIM 607261), arranged in head to head configuration and separated by 2.6 kb genomic sequence on chromosome 4p16 (Ruiz-Perez *et al.*, 2003). The EVC and EVC2 express in the heart, kidney, lungs and developing bones. In bones, the expression was observed in the developing vertebral bodies, ribs and both upper and lower limbs being higher in the distal limbs compared with the proximal limbs (Ruiz-Perez *et al.*, 2000). The EVC phenotype caused by mutations in either of the two genes is indistinguishable, which indicates that both the genes are involved in common signaling pathway (Tompson *et al.*, 2007; Valencia *et al.*, 2009).

Both EVC and EVC2 act as positive regulators of hedgehog (hh) signal transduction pathway by localizing at the basal body and membrane of chondrocyte cilia, in a co-dependent manner. Their co-localization requires the interaction between the intracellular C-terminus portions of EVC and EVC2 (Ruiz-Perez *et al.*, 2007; Blair *et al.*, 2011). EVC is also expressed in the primary cilia of osteoblasts thus transducing the hh signals in osteoblast. Pacheco *et al.* (2012) have reported that EVC is involved in promoting chondrocyte proliferation and hypertrophy, and differentiation of osteoblasts in the perichondrium. These authors have further shown normal Indian

hedgehog (Ihh) expression in EVC knockout mice but reduced expression of Ihh downstream targets Ptch1, Gli1 and Pthrp in chondrocytes.

Mapping of Skeletal Disorders Genes

Linkage analysis and association studies are currently used techniques for genetic mapping. Linkage analysis is used to identify a wide genomic region that might contain a disease gene, while an association study is designed to identify the causal gene (s) within the linkage region (Ferreira, 2004). The basic principle of linkage analysis is that alleles at two nearby loci on the chromosome will segregate together more often during meiosis.

Linkage analysis is based on two main approaches, parametric (model-based) and nonparametric (model-free). Parametric linkage analysis is most suitable for monogenic disorders showing Mendelian inheritance pattern and requires a specific genetic model for which parameters like gene frequencies, mode of inheritance, and penetrance have been estimated.

Once a chromosomal location (candidate region) for a disease phenotype has been established by linkage analysis all genes in the candidate region are analyzed for mutations. Different types of marker are used to track a gene within a family which may consists of all types of genetic variations like single nucleotide polymorphism (SNPs), microsatellite repeats number variations and copy number variations (CNVs). The microsatellites are highly polymorphic and informative for recovering maximum information from a pedigree. SNPs markers on the other hand are biallelic and abundant throughout the human genome, and can be easily genotyped with reduced time and cost in high throughput formats such as SNP microarrays (Gibbs and Singleton, 2006; Wang *et al.*, 2009).

Linkage study design is unsuitable for extremely rare Mendelian disorders because of the difficulty in collection of an adequate number of affected individuals (of multigenerational pedigree) and families for a statistically powerful study. This approach is also not applicable for sporadic cases. Furthermore, the linkage study design is also not robust enough for Mendelian disorders with genetic heterogeneity and phenotypic heterogeneity.

Up to 1 million SNPs throughout the genome can now be assayed by commercially available genotyping microarray products. CNVs are used in array comparative genomic hybridization (aCGH), that scan the entire genome and readily identifies pathogenic chromosomal duplications or deletions responsible for disease phenotype.

The identification of gene underlying Mendelian disorders has been accelerated recently by the introduction of novel genetic technique, whole exome sequencing (WES). The basic principal of WES is to selectively amplify or capture coding regions which harbors 85% of disease mutations (Choi *et al*., 2009), from a DNA sample followed by massively parallel next generation sequencing (NGS) (Biesecker, 2010). It is an effective technique to study the extremely rare Mendelian disorders for which only small numbers of samples are available, sporadic cases and complex diseases that are otherwise not possible by conventional linkage studies. Other applications includes detection of population genetic variation e.g for genetic-association studies, molecular diagnosis of Charcot– Marie–Tooth neuropathy and autosomal recessive Emery-Dreifuss muscular dystrophy (Lupski *et al*., 2010; Montenegro *et al*., 2011; Jimenez-Escrig *et al*., 2012). The cost of exome sequencing studies is now more affordable.

Objective of the study, presented in the thesis, was to identify the genetic defects underlying skeletal dysplasias in Pakistan. The localization of genetic defect was detected using a panel of microsatellite markers spaced at approximately 3 cM and high density genome wide SNP arrays. This was followed by DNA sequencing of the candidate genes to identify potential sequence variants. Following this strategy ten families with various disorders of skeleton were collected from different parts of Pakistan. Two of these families showed autosomal recessive form of polydactyly, one syndactyly, three split-hands and foot malformation, three Ellis-Van creveled Syndrome, and one Acromesomelic dysplasia. Human genome scan mapped three novel loci and exome sequencing identified a disease causing mutation in a novel gene. In addition, four novel mutations have been identified in *EVC, EVC2* and *WNT10B* genes in families linked to previously reported loci.

Chapter 2

Materials & Methods

Clinical and Molecular Characterization of Human Hereditary Skeletal Disorders in Consanguineous Families

MATERIALS and METHODS

Subjects Recruited for the Study

For the study, presented in the present dissertation, ten consanguineous families exhibiting various forms of inherited skeletal dysplasias were recruited from different remote regions of three provinces Punjab, Sindh and Khyber Pakhtunkhwa (KPK) of the country. Approval of the study was obtained from the Institutional Review Board (IRB), Quaid-i-Azam University (QAU), Islamabad, Pakistan. All the ten families were informed about purpose of the study, and accordingly written consents were provided by affected members/parents/guardians for clinical and genetic analyses of the condition diagnosed in the family.

Depending upon the information provided by elders of the families, pedigrees were constructed following the procedure described by Bennett *et al.* (2008). Pattern of inheritance of the disease in each pedigree was deduced by observing mode of transmission of the phenotype within the family. Males and females were symbolized by squares and circles, respectively. Unfilled and blackened squares and circles represent unaffected and affected individuals, respectively. Crossed symbols indicate deceased individuals. Each generation was denoted by Roman numerals (I, II, III, IV, V, VI) while individuals within a generation were denoted by Arabic numerals (1, 2, 3, 4). Double marriage lines indicate consanguineous unions.

Affected individuals of the families were clinically investigated by Medical Officers/Incharge of Health Services at National Institute of Rehabilitation Medicine, Islamabad and Pakistan Institute of Medical Sciences (PIMS), Islamabad. In few cases, investigation was performed at local government hospitals. Medical Officers at the hospital provided information about the type of bones involved in the skeletal dysplasia and status of dentition, sweating, nails, heart, eyes, chest, brain etc in the affected members. Bone X rays of the patients, diagnosed with skeletal deformities, were provided by Department of Radiology at the respective hospital.

Blood Sampling

Peripheral blood samples, 5-10 ml, were collected from those affected and unaffected individuals who were available at the time of the study, in 10 ml vacutainer tubes (BD vacutainer K2 EDTA 18 mg) by venipuncture with the help of 5 ml (BD 0.60 mm X 25 mm, 23 G X 1 TW) and 10 ml (BD 0.8 mm X 38 mm 21 G X 1 ½ TW) syringes, attached usually with a butterfly (BD Vacutainer, Ecllipse[TM]Blood collection needle with pre-attached holder). Blood samples were stored at 4°C.

Extraction of Human Genomic DNA

From peripheral blood samples, genomic DNA was extracted following standard phenol-chloroform method (Sambrook*et al.,* 1989) and commercially available extraction kits.

a. Phenol-Chloroform Method

In organic (Phenol-Chloroform) method, 0.75 ml of blood and equal volume of solution A (0.32 M Sucrose, 10 mM Tris pH 7.5, 5 mM $MgCl_2$, 1% v/v Triton X-100) was mixed in a 1.5 ml microcentrifuge tube (Axygen, Union City, California, USA) and kept at room temperature for 10-15 minutes. The centrifugation was then performed at 13,000 rpm for 1min, supernatant was discarded and pellet was suspended in 400 μl of solution A. Centrifugation was repeated and the nuclear pellet was resuspended in 400 μl of solution B (10 mM Tris pH 7.5, 400 mMNaCl, 2 mM EDTA pH 8.0), 12 μl of 20% SDS and 6μl of proteinase K and incubated at 37°C overnight or at 65°C for 3 hours. Following the pellet was dissolved, 500 μl of fresh mixture of equal volumes of Phenol and Chloroform: Isoamyl alcohol (24:1 volumes) was added to the microcentrifuge tube, mixed thoroughly and centrifuged for 10 minutes at 13,000 rpm. The upper aqueous phase was then transferred to a new microcentrifuge tube and 500 μl of Chloroform: Isoamyl alcohol mixture was added and recentrifuged for 10 minutes at 13000 rpm. The aqueous phase was again placed in a new microcentrifuge tube and DNA was precipitated by adding 55 μl of sodium acetate (3M, pH 6) and 500 μl of ice cold isopropanol, followed by centrifugation at 13,000 rpm for 10 minutes. The supernatant was discarded and DNA pellet was washed with ice cold 70% ethanol and dried in vacuum concentrator 5301 (Eppendorf, Hamburg, Germany) at 30°C for 7-10 minutes. Dried DNA pellet was dissolved in 150 μl of Tris-EDTA buffer (10 mM Tris-HCl, 0.2 mM Na_2EDTA, pH

7.5) and then quantified by Nanodrop-1000 spectrometer (Thermo Scientific, Wilmington, USA).

b. DNA Extraction using Commercially Available Kits

GenElute^{TM} Blood Genomic DNA Kit (SIGMA ALDRICH, Germany) was used for isolating DNA from blood. Prior to DNA extraction, the blood collected in the EDTA tubes was equilibrated to room temperature. Extraction was performed according to manufacturer's protocol beginning by mixing 200 µl of blood and 25 µl of proteinase K solution in a1.5 ml micocentrifuge tube. 200 µl of lysis Solution C was then added to the tube. The mixture was vortexed thoroughly for 10-15 seconds and incubated at 65ºC for 10-15 minutes for lysis. After incubation, 200µl of ethanol (99-100%) was added to the lysate, mixed thoroughly and transferred to the prepared GenElute Miniprep Binding Column (prepared by adding 500µl of Column Preparation Solution to GenElute Miniprep Binding Column, and centrifuged at 13,000×g for 1min). Centrifugation was then performed at 6500×g for 1 min, followed by addition of 500 ul of wash solution (ethanol added) and centrifugation was repeated again at 6500×g for 1 min. The column was transferred into new collection tube and 500µl of wash solution (ethanol added) was added and centrifugation was carried out for 3minutes at maximum speed to dry the column. Finally 200 µl of the elution solution was added to the column and centrifugation at 6500×g for 1minute was performed twice. The eluted DNA was stored in a microcentrifuge tube at 4°C.

RNA Isolation and cDNA Preparation

For RNA isolation, 3 ml of the peripheral blood was collected in Tempus™ Blood RNA Tubes (AB, Foster City CA, USA). Total RNA from the whole blood was isolated using Tempus™ Spin RNA Isolation kit (AB, Foster City CA, USA) according to the manufacturer's protocol. RNA was further purified by treatment with 10X DNase (Massachusetts, USA), containing 100 mM Tris–HCl (pH 7.5), 25 mM MgCl2 and 1 mM CaCl$_2$, to remove traces of genomic DNA present in RNA preparation. The purified RNA was stored at −20°C. The cDNA was prepared using total RNA as template by RT-PCR reaction using TaqMan® PreAmp Master Mix Kit (AB, Foster City CA, USA).

Polymerase Chain Reaction

The DNA was quantified by NanoDrop spectrophotometer (NanoDrop Technologies, Inc., USA), measuring optical density at 260 nm and diluted to 40 ng/µl. Polymerase chain reaction (PCR) was carried out in 25 µl reaction volumes containing 40 ng human genomic DNA, 10-20 pmol of each primer, 200 µM of each deoxynucleoside triphosphate (dNTP), 2.5 µl reaction buffer (KCl 50 mM, Tris-HCl pH 8.3, 1.5 mM $MgCl_2$) and 1 unit of Taq DNA polymerase (MBI Fermentas, Life Sciences, UK). The thermal cycling conditions used included 95°C for 10 min, followed by 40 cycles of 94°C for 45 seconds, 55-57°C for 1 min, 72°C for 1 min and a final extension at 72°C for 10 min. Amplification of GC rich sequences and other such targets was achieved using GC-rich PCR system (Roche Applied Science, Indianapolis, USA), capable of amplifying sequences up to 5 kb. PCR was performed using GeneAmp® PCR system 9700 obtained from Applied Biosystems (Applera Corp, Foster City, CA, USA).

Mapping Known Genes

The families, recruited for the present study, were initially tested for linkage using highly polymorphic microsatellite markers linked to the previously known causative genes. The microsatellite markers with an average heterozygosity of > 70% were selected from second-generation combined linkage physical map of the human genome build 36.2 (Matise *et al*., 2007). Chromosomal location of the genes, considered for analysis, was according to National Center for Biotechnology Information (NCBI). Positive and convincing linkage to a gene in the family was followed by sequencing the corresponding gene to identify a functional pathogenic variant causing a particular disease phenotype. Polymerase chain reaction (PCR) was performed as: 1 µl of genomic DNA (40 ng), 0.3 µl of each primer (20 pmol/µl), 0.5 µl of deoxyribonucleotide (dNTPs) mix (20mM), 1 unit of Taq DNA polymerase, 2.5 µl of 10x reaction buffer and 1.5 µl of 25mM $MgCl_2$ (MBI Fermentas, Life Sciences, UK) in a final volume of 25 µl. The thermal cycling conditions used included 95°C for 1 min, followed by 39 cycles of 95°C for 1 min, 57°C for 1 min, 72°C for 1 min, and final extension at 72°C for 10 min. PCR amplified products were resolved on 8% non-denaturing polyacrylamide gel, stained with ethidium bromide and genotypes were assigned by visual inspection. The microsatellite markers used for mapping known genes in the families are listed in Table 2.1.

Human Genome Scan

In case of those families which failed to show linkage to the previously reported genes, human genome scan was carried out at Center for Mendelian Genomics, Washington USA. The genome scan was performed using Infinium® Human core exome chip (Illumina, USA), which consists of more than 500,000 SNP markers. The genotype data was analyzed by Homozygositymapper to find common homozygous by descent regions (Seelow *et al*., 2009, ttp://www.homozygositymapper.org/) and linkage analysis was performed on Superlink-Online (Silberstein *et al*., 2006). These analyses were performed by assuming the disease frequency 0.001 and complete recessive inheritance model. Allele frequencies for SNP markers were estimated using founders and reconstructed founders from additional Pakistani families genotyped along with families presented in the dissertation. The genetic map positions were based on the Rutgers combined linkage-physical maps (build 37) (Matise *et al*., 2007).

Array Comparative Genomic Hybridization (Array CGH)

Array CGH is an advance technique based on the co-hybridization of control genomic and sample DNAs. High resolution array comparative genomic hybridization (aCGH) (1M oligo array, Agilent Technologies, Santa Clara, California, USA) was performed to screen for pathogenic copy number variation (CNV), in an affected member of the family under observation. DNA's from both the test and control individuals were subjected to restriction digestion. 5.8 µl of Digestion Master Mix [2.6 µl 10X buffer C, 0.20 µl of BSA (10 µg/µl), 0.50 µl each of Alu I (10 u/µl, promega, Madison, Wisconsin, USA) and Rsa I (10u/µl, promega, Madison, Wisconsin, USA)] was added to reaction tube containing 1.5 µg/20.2 µl of DNA to make a total volume of 26 µl. To inactivate the enzymes after mixing the samples were placed in thermocycler for incubation at 37°C for 2 hours and then at 65°C for 20 minutes. 2 µl of the digested genomic DNA was run on 0.8% agarose gel to check the completeness of the digestion. According to Agilent's protocol for enzymatic labeling, digested test and control DNA was labeled with CY3-dUTP and CY5-dUTP, respectively using random primers and the exo-Klenow fragment (Supplied with Agilent Genomic DNA Labeling Kit PLUS). For labeling, 5 µl of random primers were added to each reaction tube containing 26 µl of digested genomic DNA, mixed well and placed in

thermocycler for incubation at 95°C for 3min. The samples were allowed to cool down at 4°C for at least 5 min before adding 19 µl of labeling master mix (10 µl 5X buffer, 5 µl 10X dNTP-Mix, 3 µl CY3 or CY5 and 1 µl Klenow fragment) and then the cycler program continues for 2hr at 37°C and finally for 10min at 65°C for enzyme inactivation. The fluorescently labeled DNA's were purified with Microcon YM-30 filter (Millipore, Billerica, MA, USA) and efficiency of labeling was measured using a Nanophotometer® P-Class (Implen, GmbH, München, Germany). The appropriate CY5-labeled sample and CY3-labeled sample were combined in a new 1.5-ml microfuge tube and nuclease free water was added to bring volume to 158 µl. 362 µl of the hybridization master mix containing 50 µl Cot1-DNA human (Invitrogen Co, San Diego, CA, USA), 52 µl 10x Blocking Agent (supplied by Agilent, Santa Clara, California, USA) 260 µl 2x Hi-RPM-Hyb-buffer (supplied by Agilent, Santa Clara, California, USA) was added to the labeled sample mixture. The tubes were then shifted to preheated water bath set at 95°C and allowed to incubate for 3 min, and then immediately transferred to thermomixer at 37°C for 30 min. The samples were loaded on to 1M Array (Agilent Technologies, Santa Clara, California, USA) and hybridized for 40hr at 65°C and 20 rpm in the Hyb-Oven from Agilent (Santa Clara, California, USA).

Washing was performed after hybridization, according to manufacturer's instructions (Agilent Technologies, Santa Clara, California, USA) and array was scanned with GenePix 4000B scanner at 3 µm resolution. Analysis of the files prepared after scanning was performed with Feature Extraction 9.5.3.1 and CGH Analytics 3.4.40 software (Agilent Technologies, Santa Clara, CA), with the following settings used: Aberration Algorithm: ADM-2; Threshold: 6.0; Window Size: 0.2 Mb; Filter: 5 probes, log2 ratio ¼ 0.29, based on NCBI Build 36 of the human genome and UCSC version hg18 released on March, 2006. The genomic profile was visualized with Signal Map software (Signal Map v1.9.0.03, Nimble Gen).

Candidate Genes Sequencing

Candidate genes in linkage interval were prioritized with GeneDistiller-2 (http://www.genedistiller.org/) by selecting the physical position of the markers at start and end of the interval. GeneDistiller-2 software search for a gene of interest in the linkage interval on the basis of information available about human disease

phenotype, animal model, molecular function, tissue specific expression and subcellular localization. In the present study, five candidate genes were sequenced to search for the pathogenic sequence variant. These included *FAM92A1* (NM_145269), *WNT10B* (MIM 601906), *NPR2* (MIM 108961), *EVC* (MIM 604831), and *EVC2* (MIM 607261). Primers to amplify the exons and splice junctions of the candidate genes were designed from intronic regions of the genes using primer3 software (Rozen and Skaletsky, 2000). Primer sequences, melting temperature (Tm) and size of the amplified products of various exons of each gene are listed in Tables 2.2-2.6. Reaction mixture containing 1µl DNA (50ng), 1µl primer (10pmol/µl), 1µl dNTPs mix (20mM), 1µl Taq (5u/µl), 5 µl of 10x buffer, 3 µl $MgCl_2$ (25mM) in a total volume of 50 µl was subjected to thermocycling conditions as described above. The amplified PCR products were analyzed on 2% agarose gel, purified by commercially available kit, Fermentas GeneJET^{TM} PCR Purification Kit (MBI Fermentas, Life Sciences, UK), reanalyzed on 2% agarose gel and were sequenced in sense and antisense direction by dye termination cycle sequencing chemistry on ABI 310 genetic analyzer (Applied Biosystems, Inc., Foster City, CA, USA). Sequenced data was aligned to reference genomic sequence from Ensemble Genome Browser (http://www.ensemble.org) via BIOEDIT sequence alignment editor version 6.0.7 (http://www.mbio.ncsu.edu/BioEdit/bioedit.html) for the identification of pathogenic sequence variant. Ethnically matched control individuals were screened for newly identified mutations. Segregation analysis of the mutations in all family members was performed by sequencing. Homology searches were carried out to check the evolutionary conservation of substituted residues. Restriction fragment length polymorphism (RFLP) analysis was carried out in cases where mutations created or abolished the restriction enzyme site. Pathological characteristics of the mutation were analyzed using protein prediction tools, PolyPhen-2 (http://genetics.bwh.harvard.edu/pph/) and SIFT http://sift.jcvi.org/www/SIFT_seq_submit2.html).

Whole Exome Sequencing (WES)

Whole exome sequencing was carried out at Center for Mendelian Genomics, Washington USA. Briefly, for whole exome sequencing of the target region of all human Consensus Coding Sequence (CCDS) exons (Pruitt *et al*., 2009), 4 µg of

genomic DNA was enriched with Agilent's Sure Select Human All Exon Kit V2 (Agilent Technologies, Santa Clara, California, USA) followed by sequencing on Illumina Genome Analyzer II with 100 bp single end reads (Illumina, Inc., Allendale, NJ, USA). The raw data of ~5GB per Exome was mapped to the haploid human reference sequence hg 19 (GRCh37) with Novoalign (Hercus, 2011). Single nucleotide variants and short insertions and deletion were identified with SAM tools (Li *et al*., 2010). All variants were annotated with annovar (Wabg *et al*., 2010) and filtered for missense, nonsense, frameshift, and splice site mutations in GeneTalk (Krawitz and Kamphans, 2012). All genotypes that possessed a frequency above 0.001 in dbSNP (http://www.ncbi.nlm.nih.gov/projects/SNP/), the 1000 genomes project or the 5000 exomes project (Altshuler *et al*., 2010; URL:http://evs.gs.washinton.edu/EVS/) were removed. The filtered variants were verified by routine Sanger Sequencing in all family members with ABI Prism BigDye terminator cycle sequencing reaction kit (Applied Biosystems, Foster City, California, USA) on ABI3730 Genetic Analyzer (Applied Biosystems, Foster City, California, USA). Primer sequences, melting temperature (Tm) and size of the amplified products for all variants are presented in Table 2.2-2.6.

Table 2.1: List of microsatellite markers used to test linkage to genes/loci involved in various forms of skeletal deformities

No	Phenotype	Chromosome	Gene	Markers	cM[*]	Mb[+]
1.	PAPA1 (Postaxial Polydactyly Type A and B) Preaxial Polydactyly Type IV	7p13	*GLI3*	D7S2541	60.90	40.11
				D7S2469	61.51	41.08
				D7S3043	62.11	41.55
				D7S691	62.99	41.99
				D7S1526	64.03	42.47
				D7S2428	64.26	43.21
				D7S1488	66.53	44.75
				D7S2427	66.58	44.93
2.	PAP-A2 (Postaxial Polydactyly Type A)	13q21-q32		D13S1318	64.58	71.39
				D13S800	67.39	72.77
				D13S162	71.71	74.87
				D13S1306	73.25	76.54
				D13S921	75.46	79.57
				D13S628	79.02	84.58
				D13S1300	83.9	91.40
				D13S1280	90.12	95.54
3.	PAP-A3 (Postaxial Polydactyly Type A/B)	19p13.1-p13.2		D19S583	29.1	9.91
				D19S584	31.43	11.06
				D19S558	33.62	13.17
				D19S840	34.46	13.70
				D19S226	36.7	14.49
				D19S929	37.65	15.02
4.	PAP-A4 (Postaxial Polydactyly Type A/B and partial cutaneous syndactyly)	7q21-q34		D7S820	98.12	83.62
				D7S2409	103.20	91.13
				D7S2480	110.44	99.89
				D7S2459	118.18	107.11
				D7S655	126.55	118.45
				D7S635	131.29	127.06
				D7S512	138.56	131.51
				D7S2560	146.39	137.84
				D7S2513	151.48	141.05

Continued.....

Continued from the previous page

No	Phenotype	Chromosome	Gene	Markers	cM[*]	Mb[+]
5.	Postaxial Polydactyly PAP-A (Autosomal Recessive)	13q13.3-q21.2		D13S1288	39.13	38.42
				D13S263	43.02	40.97
				D13S1312	54.95	44.83
				D13S1807	55.50	54.00
				D13S233	56.13	58.34
				D13S889	58.52	62.46
6	Syndactyly type 1	2q34-q36		D2S153	208.89	211.4
				D2S1345	213.2	214.9
				D2S164	218.5	217.7
				D2S163	223.9	220.6
				D2S102	227.5	222.8
7	Syndactyly type 2	2q31	HOXD13	D2S148	186.9	177.5
				D2S364	190.1	182.8
				D2S389	194.6	191.4
				D2S117	197.2	195.4
				D2S2392	200.1	199.5
8	Syndactyly type 3	6q22-q23	GJA1	D6S1608	125.2	120.9
				D6S979	127.2	124.0
				D6S1702	130.3	125.4
				D6S407	132.5	128.8
				D6S1572	135.4	131.3
9	Syndactyly type 4	7q36	LMBR1	D7S3058	176.5	154.1
				D7S550	180.6	155.2
				D7S559	183.93	156.1
				D7S22	186.0	157.6
				D7S427	188.0	158.5

Continued from the previous page

N o	Phenotype	Chromosome	Gene	Markers	cM[*]	Mb[+]
10	Synpolydactyly Type 2	22q13.31	*FBLN1*	D22S532	63.07	44.50
				D22S1153	63.22	44.78
				D22S1160	63.55	44.80
				D22S1170	68.37	46.72
				D22S1169	74.77	47.78
11	Split-hand/foot malformation 6	12p11.1-q13.13	*WNT10B*	D12S2080	56.45	33.30
				D12S1668	57.55	39.48
				D12S291	61.09	41.68
				D12S85	63.41	45.62
				D12S339	65.54	46.80
				D12S347	67.30	50.29
				D12S1586	69.56	52.43
12	Acromesomelic Dysplasia, Type Maroteaux	9p21-p12	*NPR2*	D9S1118	57.01	31.82
				D9S1845	58.15	33.05
				D9S1817	59.01	33.75
				D9S50	60.81	36.70
				D9S1874	61.38	37.12
13	Ellis-van Creveld Syndrome (EVC)	4P16	*EVC* *EVC2*	D4S2936	0.61	0.682
				D4S412	3.6	3.350
				D4S2285	7.97	5.154
				D4S3366	12.57	6.535
				D4S3007	13.21	6.833
				D4S394	14.94	7.010
				D4S2983	17.75	7.796

*genetic distance (centiMorgan) and +physical distance (mega base pairs) are according to the second-generation combined linkage physical map of the human genome (Matise *et al.,* 2007).

Table 2.2: Primer sequences used for amplification of the gene *WNT10B*

Exon	Primer	Sequences 5' to 3'	Product Size (bp)	Tm (°C)
2&3	WNT10B-2_3F	CTCAGGGACTCTGGGAATC	769	57.1
	WNT10B-2_3R	AATTCCAGGAGAGGCCCCT		62.2
4	WNT10B-4F	CTTTCTGCCTCCACACTCTC	552	57.6
	WNT10B-4R	GGTGAGTGTCAGTCACTCAT		53.1
5	WNT10B-5F1	GCTAACTGCAATGTCCTTTCTG	575	59.0
	WNT10B-5R1	CATCACACAGCACATAGCAG		56.3
5	WNT10B-5F2	CTCTCAGGAGAGCTGGTCTA	434	54.8
	WNT10B-5R2	AGGCTACACATCCCAGAGTC		56.8

Tm = melting temperature, ^{0}C = degree centigrade, bp = base pair

Table 2.3: Primer sequences used for amplification of the gene *EVC*

Exon	Primer	Sequences 5' to 3'	Product Size (bp)	Tm (°C)
1	EVC-1F	AGTTTTGAGCGGTGATCCAG	611	60.3
	EVC-1R	AACGGAGTGGGATGTAACAG		57.5
2	EVC-2F	CAAGCTTGAGAAGCACAGAG	356	56.5
	EVC-2R	GAGGCTTGTCTACATGACAC		53.0
3	EVC-3F	CCTTTCTGAGGCTGCTATTAC	294	56.0
	EVC-3R	CAGGACCAAACATCACACAG		57.5
4	EVC-4F	CTAGCGTGAATCACTGGTAG	401	53.6
	EVC-4R	CCTCCTCTGACAATGATGTG		56.5
5	EVC-5F	CTGTGGCTTGTACTGATGAG	284	54.3
	EVC-5R	ACTGATGTCTGCCTCTCAAG		55.4

Continued from the previous page

Exon	Primer	Sequences 5' to 3'	Product Size (bp)	Tm (°C)
6	EVC-6F	TCGGAGTTCCTTTCCTTCAG	515	59.4
	EVC-6R	CAGTGACCGTCTTTGAGTAG		53.4
7	EVC-7F	GGTCAAACCTCATGTACAAC	447	52.7
	EVC-7R	TAGCATCAGAAACTGGATCC		55.3
8	EVC-8F	GAACCAGACAATGGAACCAG	571	58.0
	EVC-8R	GATGGATGGAAGGGTCAATG		60.1
9	EVC-9F	AGATCTCGCTCATGAAGGAG	568	57.1
	EVC-9R	GTACAGAGAAGGGAAGAGAG		50.6
10	EVC-10F	ACTACTAGTGGGACCTACAG	529	48.3
	EVC-10R	GCAGCACAACTCTTATCACC		55.9
11	EVC-11F	TGCCTCAGTTTCCTTGTGTG	430	59.9
	EVC-11R	AACTGCCTCGGTTTCTGATG		60.3
12	EVC-12F	CTTGAGAGTTCCTGTCTGTG	469	53.2
	EVC-12R	CAACAGTCATCTCCGTAGAG		53.3
13	EVC-13F	ATCCCTTCCTTACTCCACAG	460	55.7
	EVC-13R	CACTGTACAGATGAGGACAC		50.9
14	EVC-14F	AATAGACAAGCAGATGGCGG	583	60.2
	EVC-14R	ATGTGTGCAGTGTAAGCTGC		57.5
15	EVC-15F	CACAGACACCTAACAGACAC	535	51.1
	EVC-15R	AAGTCATGGAGAAGTCAGGC		56.9

Continued from the previous page

Exon	Primer	Sequences 5' to 3'	Product Size (bp)	Tm(℃)
16	EVC-16F	TGGTGAGTAGGTGGAAGATC	467	55.0
	EVC-16R	CACTGGATGTGTGCTTATGC		57.7
17	EVC-17F	GGTGGAAGGATACACTCTTG	438	54.6
	EVC-17R	TCACTCATTTGTGCCAGGTG		60.7
18	EVC-18F	CTCTCTAAACTCCCGTGTTG	631	55.0
	EVC-18R	TGTCAGCTCCATAGATGAGG		56.3
19	EVC-19F	CTCTCTGGGATGTATGTTGG	493	55.5
	EVC-19R	AGTCAGTTAGGAGACACAGC		51.8
20	EVC-20F	AGTTGAGTGGCTGCAATAGC	472	58.1
	EVC-20R	AAACAGGAAGGGTAACAGCC		58.2
21	EVC-21F	CACTTGGATGACCTCCTACC	409	57.0
	EVC-21R	TTCTCTGTCCCTCTCAGAAG		54.6

Tm = melting temperature, ^{0}C = degree centigrade, bp = base pair

Table 2.4: Primer sequences used for amplification of the gene *EVC2*

Exon	Primer	Sequences 5' to 3'	Product Size (bp)	Tm (°C)
2	EVC2-2F	TCCATGTACCCTGTAGTCTG	479	53.4
	EVC2-2R	AGTCAAACCTCCTCTCCATC		55.7
3	EVC2-3F	TGGTGTAAGCTCATGTCCAC	398	57.1
	EVC2-3R	AGACTTGTGTAGGTAAGCCC		53.5
4	EVC2-4F	TTCCTGGATGCCTAATGTGC	367	61.0
	EVC2-4R	CTGACCCAGAACACATTCAC		56.4
5	EVC2-5F	TACAAAGGGCTTCCTTGCTG	391	60.4
	EVC2-5R	CTTATCTGCTAGGTGGCATC		55.1

Continued…..

Continued from the previous page

Exon	Primer	Sequences 5' to 3'	Product Size (bp)	Tm (°C)
6	EVC2-6F	TTCACAAGCTCTGACCTGTG	318	57.5
	EVC2-6R	CCAGTCTCAACGCATAACTG		56.9
7	EVC2-7F	GACTCAAATGCAAGCGAGTC	519	58.6
	EVC2-7R	GTTCTGTGATTGTGCCTAGG		55.8
8	EVC2-8F	TTACTGTGGTCACAGTGGTG	476	55.3
	EVC2-8R	GACTTCCTTAGAGCAGGAAG		53.5
9	EVC2-9F	TGGATGAAGCAGAAGTGAGC	610	59.1
	EVC2-9R	AATGAGTGGGTGGTTGGATG		60.6
10	EVC2-10F	GCCTGTACACATTGCATTGC	405	60.2
	EVC2-10R	AGGACTGAACTCTGAGAGAG		50.8
11	EVC2-11F	CATCTGGGTCTAGAATGCAC	476	55.7
	EVC2-11R	CCAGTCTGTGGTATTCTGTC		52.9
12	EVC2-12F	GGAGATGAATGTTCAGGCAC	384	58.1
	EVC2-12R	TAGATGGCACATCATGGTGC		60.5
13	EVC2-13F	TCTGCCCTTACTCTGCTAG	503	53.3
	EVC2-13R	AAGTCGCTACCAATCAACAG		55.5
14	EVC2-14F	TGCATCTCTGGCTTCTTCAC	435	59.1
	EVC2-14R	GAATAGCTGGACACCAATGC		58.2
15	EVC2-15F	AACTGAGCTCCTTCCAGAAG	365	56.3
	EVC2-15R	TGTGTCAGCTATCAGAGCAG		55.1
16	EVC2-16F	ATGGAATGAAGGATGGCTGG	620	62.1
	EVC2-16R	GTTGAGAGAGTGCCAAGTAC		52.3
17	EVC2-17F	ATCGTGGTGCACTCACATTG	521	60.6
	EVC2-17R	AGCTCGTGTTGGAGCAATG		60.0

Continued….

Continued from the previous page

Exon	Primer	Sequences 5' to 3'	Product Size (bp)	Tm (°C)
18	EVC2-18F	ATGGCTGAGATGTGTGCTTC	334	58.8
	EVC2-18R	TAGAGCTTCGCACACATCTG		57.7
19	EVC2-19F	TCACTCCAGGACAGAATGTC	657	56.0
	EVC2-19R	AACACATGCTCCCACACTTG		59.6
20	EVC2-20F	TCACTCCAGGACAGAATGTC	657	56.0
	EVC2-20R	AACACATGCTCCCACACTTG		59.6
21A	EVC2-21-1F	ACAGCAATCTGGTGACCAAG	549	58.7
	EVC2-21-1R	TCTGTGCCTTCTGCATGTGC		63.6
21B	EVC2-21-2F	GGAGCATCTGAAGAGAGAAG	554	54.2
	EVC2-21-2R	TTGAACTGGTGACGGTAGAC		56.1
22	EVC2-22F	TGTTTATGGAGTGCTCCTGC	268	58.9
	EVC2-22R	ATTACGCAAACAGAGGCTCC		59.3

Tm = melting temperature, ^{0}C = degree centigrade, bp = base pair

Table 2.5: Primer sequences used for amplification of the gene *NPR2*

Exon	Primer	Sequences 5' to 3'	Product Size (bp)	Tm (°C)
1	NPR2-1F1	CTAGCCTACTCCTCCTCTTC	640	52.6
	NPR2-1R1	CATCCAGGTACAGCAAGG		54.9
1	NPR2-1F2	CCAGAACACAACCTGAGCTA	684	56.5
	NPR2-1R2	CCACATACAGCTGCTCAATG		57.9
2	NPR2-2F	GTTGATAGGTTAGGGCACTC	399	53.9
	NPR2-2R	GTCTTGTGAGAGAGAATTTCC		53.1
3&4	NPR2-3_4F	TAGTAGCCCTTTCAAAGC	768	50.6
	NPR2-1F1	TGGTGATCCTGACATCTGT		52.6
5&6	NPR2-5_6F	ACAGATGTCAGGATCACCAC	716	50.6
	NPR2-5_6R	GCAGAAGCACAGTTAAGAGTG		54.5

Continued…..

Continued from the previous page

Exon	Primer	Sequences 5' to 3'	Product Size (bp)	Tm (°C)
7	NPR2-7F	CACTCTTAACTGTGCTTCTG	401	51.0
	NPR2-7R	CTAAAGAGAAAGGCTAGAGA		48.5
8	NPR2-8F	CTGTCTCTCAGGTGTAACAG	343	50.5
	NPR2-8R	CAGGGGCTATCATTACAAG		53.2
9&10	NPR2-9_10F	GCTTGTAATGATAGCCCCTGC	534	60.1
	NPR2-9_10R	ATCAACCCCTTGCCCATCTA		61.6
11&12	NPR2-11_12F	TAGATGGGCAAGGGGTTGAT	564	61.6
	NPR2-11_12F	GGAATAAGGGGAGATGAGAG		55.3
13	NPR2-13F	CTGTAGACAGCTAGCCAGTG	338	53.8
	NPR2-13R	TATTACTGTCACTCCACCTC		49.8
14&15	NPR2-14_15F	GAGGTGGAGTGACAGTAATA	561	49.8
	NPR2-14_15F	TTCATGCACTAGGACTAATG		51.3
16	NPR2-16F	CATTAGTCCTAGTGCATGAA	395	51.3
	NPR2-16R	ATCTATAAGCAGGGGTGCT		54.0
17	NPR2-17F	TACAGCTCATCTCTGCTGC	324	55.1
	NPR2-17R	GATGTGGGAACTCTAGAACA		52.5
18	NPR2-18F	TGTTCTAGAGTTCCCACATC	331	52.5
	NPR2-18R	GAGCTACATCTGTCTACGAA		50.4
19&20	NPR2-19_20F	TCATTCCGCAAATGTTTACT	672	55.4
	NPR2-19_20R	CTCAGATTAAGAAATTGGAGG		53.8
21&22	NPR2-21_22F	CGGTGCTATACAGTATCACC	707	53.2
	NPR2-21_22R	GTGCATACCCCATAACCTTT		56.4

F = forward primer, R = reverse primer, bp = base pairs, Tm = melting temperature, ^{0}C = degree centigrade

Table 2.6: Primer sequences used for amplification of the gene *FAM92A1*

Exon	Primer	Sequences 5' to 3'	Product Size (bp)	Tm (°C)
11	FAM92a1-6-1F	CCAGTACTGCAATGGTAGAA	231	53.8
	FAM92a1-6-1R	CATGTTTTGAACCCTAACAGT		54.3
11	FAM92a1-6-2F	AGCCAGTACTGCAATGGTAG	374	55.5
	FAM92a1-6-2R	CCTCCCAAAGTGCTAGGATT		58.3

F = forward primer, R = reverse primer, bp = base pairs, Tm = melting temperature, ^{0}C = degree centigrade

Chapter 3

Human Limb Abnormalities

Clinical and Molecular Characterization of Human Hereditary Skeletal Disorders in Consanguineous Families

HUMAN LIMB ABNORMALITIES

Congenital limb malformations particularly those involving numbers of the digits are one of the most frequent forms of human disorders. Digital abnormalities with variable number of digits or webbed digits include; polydactyly, occurrence of extra fingers and/or toes, oligodactyly, digits number less than five and syndactyly in which two or more than two digits are fused. Polydactyly may be classified into three categories. The preaxial polydactyly characterized by an extra thumb or large toe deformity, central polydactyly in which the three central digits are affected, and postaxial polydactyly (PAP) with an extra little finger or toe (Swanson, 1976; Blauth and Olason, 1988; Buck-Gramcko, 1998).

Polydactyly and syndactyly are relatively common phenotype observed in various populations. Specifically for the postaxial polydactyly (PAP), two distinct categories have been recognized, i.e postaxial type A and postaxial type B, which differ in severity, penetrance estimates and inheritance pattern (Temtamy and McKusick, 1978). In type A a well-formed extra digit articulates with fifth or sixth metacarpal while in type B a rudimentary poorly developed extra digit in the form of extra skin tag is present (Temtamy and Mckusick, 1978). The occurrence of PAP in the general population varies among different racial groups and is about ten times more frequent in Africans than in European ancestries; with an incidence rate of 1/300 to 1/100 and 1/3,300 to 1/630 live births, respectively (Frazier, 1960; Temtamy, 1990). Recently, Malik *et al*. (2014) has reported 48.24% cases of preaxial polydactyly and 51.8% postaxial polydactyly in a study of 313 Pakistani families with polydactyly.

Both syndromic and non-syndromic (isolated) forms of PAP have been reported in the literature. Isolated (non-syndromic) forms of PAP in which polydactyly is the only clinical condition usually segregates as an autosomal dominant trait mostly with variable expression. To date, four autosomal dominant loci for PAP have been mapped on different human chromosomes. These include PAPA1 (MIM 174200) with PAPA features on chromosome 7p13 and caused by mutations in gene *GLI3* (Radhakrishna *et al*., 1997a, b), PAPA2 (MIM 602085) on chromosome 13q21-q32 with features of PAP-A (Akarsu *et al*., 1997), PAPA3 (MIM 607324) with features of PAP-A/B on chromosome 19p13.1–13.2 (Zhao *et al*., 2002) and the fourth locus on chromosome

7q21–q34 in a Dutch family (Galjaard *et al*., 2003). Several isolated autosomal recessive cases of PAP have also been described in the literature (Mohan 1969; Mollica *et al*., 1978; Malik *et al*., 2014). Recently two autosomal recessive forms of PAP type A in two Pakistani families have been mapped on chromosomes 4p16.3 (*ZNF141*) and 13q13.3-q21.2, (Kalsoom *et al.,* 2012, 2013).

Syndactyly is a digital abnormality in which contiguous fingers and/or toes are webbed because there is embryological failure of fingers separation during limb development. Clinically syndactyly are a genetically heterogeneous group of disorders of hands and feet, may be symmetrical or asymmetrical, unilateral or bilateral and the fusion may be cutaneous or bony. On the basis of phenotype and genotype, the recent classification scheme describes nine types of syndactyly with subdivisions, which is useful in the understanding of syndactyly deformity and in showing its affinity with other digit abnormality, including oligodactyly, polydactyly, and brachydactyly (Malik, 2012). Most of these are thought to be inherited as autosomal dominant fashion.

The present chapter describes autosomal recessive forms of Polydactyly and Syndactyly in three consanguineous families. Genetic linkage study led to the identification of three novel loci including two for polydactyly and one for syndactyly. Further exome sequencing led to the identification of a nonsense mutation in *FAM92A1* gene.

Consanguineous Families Segregating Polydactyly

Family A

Family A (Figure 3.1) with autosomal recessive form of postaxial polydactyly type A was sampled from a remote area in district Dera Ismail Khan of Khyber Pakhtunkhwa (KPK) province of the country. The blood samples were obtained from three affected (V-1, V-2, V-3) and three unaffected individuals (III-3, IV-1, V-4) of the family.

Clinical Features

Clinical features of the affected individuals were carefully noted. The expression of postaxial polydactyly phenotype was highly variable among affected individuals of the family as well between the limbs in the same individual (Figure 3.2). Bilateral

postaxial polydactyly of hands and feet was observed in the affected individual V-1. However, slightly altered phenotype was observed in the two limbs of the same individual (Figure 3.2 a, b). Another affected Individual (V-2) had postaxial polydactyly only in the left hand while right hand and both feet were normal (Figure 3.2c). In an affected individual V-3, postaxial polydactyly was found in both hands, however variable status of this condition was observed between the two hands of the affected individual. The extra finger was deviated to ulnar side in the right hand while it was straight in the left hand (Figure 3.2d). Both feet were normal in this affected individual (V-3).

Teeth, nails, sweating and hearing were normal in all the three affected individuals. Neurological problems and facial dysmorphism were not observed in any of the affected individuals. Heterozygous carrier individuals had normal hands and feet, and were clinically indistinguishable from genotypically normal individuals.

Family B

Family B (Figure 3.3) with autosomal recessive form of postaxial polydactyly type A was sampled from Murree in Rawalpindi district of the Punjab province of the country. The blood samples were obtained from total eight individuals including three affected (V-1, V-2, V-5) and five unaffected (IV-3, IV-6, IV-7, V-3, V-7) of the family.

Clinical Features

All the three affected individuals (V-1, V-2, V-5), displaying PAP-A, were investigated at the local government hospital. Medical staff at the hospital provided clinical information about bone, skin, dentition, sweating, nails, cardiological and neurological abnormalities. Age of the affected individuals ranged from 5 to 40 years at the time of the study. They had normal teeth, nail and facial features. Skin, sweating, hearing and height (167-172 cm) were also normal in the affected individuals. Neurological and cardiological problems were not observed. Bilateral postaxial polydactyly of hands and feet was present in two affected (V-1, V-2) and unilateral polydactyly of the feet in an individual (V-5). In an affected individual (V-2), extra fingers and toes were amputated on both hands and feet, respectively (Figure 3.4).

Homozygosity Mapping in two Families (A, B)

Linkage in the two families (A, B) was initially tested by typing microsatellite markers mapped in the intervals of previously reported four autosomal dominant and two autosomal recessive postaxial polydactyly loci. This included PAP-A1 on chromosome 7p13 (D7S2541, D7S2469, D7S3043, D7S691, D7S1526, D7S2428, D7S1488, D7S2427) harboring *GLI3* gene, PAP-A2 on 13q21-q32 (D13S1318, D13S800, D13S162, D13S1306, D13S921, D13S628, D13S1300, D13S1280), PAP-A3 on 19p13.1-p13.2 (D19S583, D19S584, D19S558, D19S840, D19S226, D19S929), PAP-A4 on 7q21-q34 (D7S820, D7S2409, D7S2480, D7S2459, D7S655), PAP-A on 4p16.1-p16.3 (D4S2936, D4S412, D4S2285, D4S3366, D4S3007, D4S394, D4S2983) harboring *ZNF141* gene, and PAP-A on 13q13.3-q21.2 (D13S1288, D13S263, D13S1312, D13S1807, D13S233, D13S889). PCR amplification of the microsatellite markers was performed as described in Chapter 2. Haplotype analysis (not shown) failed to detect linkage to any of the genes tested here.

After failing to detect linkage in the two families, human genome scan using SNP markers was performed to map the causative genes. DNA of eleven individuals including three affected (V-1, V-2, V-3) and three unaffected (IV-1, IV-2, V-4) of the family A and two affected (IV-1, IV-2) and three unaffected (III-1, III-2, IV-3) of the family B was used for genome wide homozygosity mapping. Genotyping was performed using the Affymetrix GeneChip Human Mapping 250K Nsp array (Affymetrix, Santa Clara, CA, USA). The genotype of each SNP was determined by the BRLMM algorithm incorporated in Affymetrix Genotyping Console. A call rate (percentage of SNPs genotyped by sample) of 98% was obtained across the entire sample. Mapping order, and physical and genetic distances of SNPs were obtained from Affymetrix (Santa Clara, CA, USA). Analysis of SNP data of three affected and equal number of unaffected individuals with HomozygosityMapper (http://www.homozygositymapper.org) identified a 37.0 Mb single long stretch (Figure 3.5) of consecutive homozygous SNPs on chromosome 8q21.13-q24.12 flanked by rs2053962 and rs2514582 present in all affected persons (Figure 3.6) in family A. In the other family, B, genome scan revealed two regions showing homozygous pattern of alleles in affected members. This included 37.0 Mb flanked by SNPs rs6755128 and rs10177144 on chromosome 2p14-q12.1 (Figure 3.7), and 22.3

Clinical and Molecular Characterization of Human Hereditary Skeletal Disorders in Consanguineous Families

Mb flanked by rs6459448 and rs6904723 on 6p22.3-p21.1 (Figure 3.8). Physical and genetic distances of SNPs were obtained from UCSC Genome browser Build 39 (February 2009, http://genome.ucsc.edu/cgi-bin/hgGateway).

Parametric two-point LOD scores were calculated using online version of superlink software (http://bioinfo.cs.technion.ac.il/superlink-online/) while Allegro was used for multipoint analysis. LOD scores were calculated using a fully penetrant autosomal recessive model with a disease allele frequency of 0.001. In family A, maximum two-point LOD score of 2.43 was obtained with SNP rs2300490. Multipoint LOD score of 2.82 was obtained with the same SNP rs2300490, reaching the maximum possible score for the pedigree structure (Table 3.1). In family B maximum two-point LOD score of 1.65 and multipoint score of 1.91 were obtained with SNP rs3771188 and SNP rs6740317on chromosome 2p14-q12.1, respectively (Table 3.2). In the same family, linkage was established on chromosome 6p22.3-p21.1 as well. At this chromosomal region, maximum two-point LOD score of 1.46 was obtained with SNP rs9466754 and multipoint score of 1.92 with SNP rs9348410. This was the maximum possible LOD score achievable for the pedigree structure (Table 3.3).

Exome Sequencing

In family A, linked to 37.0 MB region on chromosome 8q21.13-q24.12, potential sequence variants carrying genes were searched using whole exome sequencing in an affected individual (V-3) performed at the University of Washington, Center for Mendelian Genomics. After the library construction sequence capture was performed in solution with the Roche NimbleGen SeqCap EZ Human Exome Library v2.0 to target approximately 36.6 Mb of coding exons, by following manufacturer's protocols. Sequencing was carried out on Illumina HiSeq and Fastq files were aligned to human reference sequence (hg19) by using Burrows-Wheeler Aligner (BWA) (http://bio-bwa.sourceforge.net/ (Li and Durbin, 2009). The aligned data was further subjected to analysis with Genome Analysis Toolkit (GATK) (http://www.broadinstitute.org/gatk/) (McKeena *et al*., 2010). Annotation of variant sites was performed using Seattle Seq 137 (http://snp.gs.washington.edu/SeattleSeqAnnotation137). The pathogenicity of the potential variant was predicted by Mutation Taster (Schwarz *et al*., 2010).

Finally, the filtered exome data was analyzed to find homozygous coding or splice variants within the HBD region identified in this family. Presence/absence of the homozygous variants were further checked in the public SNP databases, 1000 genomes data and in-house exome sequencing data of 133 individuals. Sanger cycle sequencing was used to verify the segregation of a homozygous variant using primers listed in the Table 2.6 (Materials and Methods: Chapter 2). The only variant that cosegregated with the phenotype was a nonsense mutation involving transition of C to T at nucleotide position 478 (c.478C>T) identified in exon 6 of the *FAM92A1* gene, on chromosome 8q21.13-q24.12, in all the affected individuals. The variant resulted in substitution of a codon for amino acid arginine with a premature stop codon (p.Arg160*) (Figure 3.9). To exclude the possibility of the variant **(**c.478C>T, p.Arg160***)** representing a non-pathogenic polymorphism, a panel of 283 unrelated ethnically matched control individuals were screened and this mutation was not identified outside the family.

Family C

Family C with syndactyly type 1(SD1) resides in Lahore, district of Punjab province of Pakistan. Analysis of the family pedigree drawing (Figure 3.10) provided convincing evidence of an autosomal recessive mode of inheritance of the phenotype. For genetic analysis, blood samples were obtained from six affected (IV-6, IV-8, V-1, V-2, V-3, VI-2) and seven unaffected individuals (III-7, IV-1, IV-2, IV-7, V-4, V-13, VI-1) of the family.

Clinical Features

Clinical features of the affected individuals were carefully recorded. All the six affected members of the family presented simple, bilateral, symmetrical and complete type of syndactyly. It involved complete fusion of middle and ring finger in both hands. Both the fingers were fused by skin or soft tissues. The fused fingers had distinct nails. The abnormalities were found only in the hands, and the feet were normal (Figure 3.11). Additionally, clinodactyly of the middle finger was observed in the two affected individuals (V-2, V-3) of the family. Affected members did not provide consent for radiograph analysis of the hands. There was no other apparent congenital malformation, and systematic examination revealed no other abnormality.

Homozygosity Mapping in Family C

Family C, segregating syndactyly, was first tested for linkage to previously described autosomal dominant genes by genotyping highly polymorphic microsatellite markers listed in the Table 2.1 (Materials and Methods: Chapter 2). This included Syndactyly type 1 (SD1) mapped on chromosome 2q34-q36 (D2S153, D2S1345, D2S164, D2S163, D2S102), SD type 2 on 2q31 harboring *HOXD13* gene (D2S148, D2S364, D2S389, D2S117, D2S2392), SD type 3 on 6q22-q23 harboring *GJA1* gene (D6S1608, D6S979, D6S1702, D6S407, D6S1572), SD type 4 on 7q36 harboring *LMBR1* gene (D7S3058, D7S550, D7S559, D7S22, D7S427), and SPD type 2 on 22q13.31 harboring *FBLN1* gene (D22S532, D22S1153, D22S1160, D22S1170, D5S1169). Haplotype analysis (not shown) excluded linkage to the aforementioned genes in the family.

After excluding linkage to the previously reported genes, the family was subjected to genome-wide scan. DNA from seven members of the family including three affected (IV-1, IV-2, IV-4) and three normal (III-1, III-2, IV-3) was subjected to genome scan using Affymetrix GeneChip Human Mapping 250K Nsp array. The genotypes of each SNP were determined by the Affymetrix GTC (genotyping console) software having BRLMM algorithm incorporated. A call rate (percentage of SNPs genotyped by sample) of 97% was obtained across the entire sample. Mapping order, and physical and genetic distances of SNPs were obtained from Affymetrix. Analysis of SNP data of three affected and three unaffected members of the family with HomozygosityMapper (http://www.homozygositymapper.org) identified a 16.3 Mb single long stretch of consecutive SNPs segregating with the disease phenotype on chromosome 21q21.3-q22.3 flanked by rs2829950 (27.22 Mb) and rs566038 (44.74 Mb) present in all affected persons (Figure 3.12). Maximum two-point LOD score of 2.09 was obtained with SNP rs727957. Multipoint LOD score of 2.52 was obtained with SNP rs761372 for this region reaching the maximum possible score for the pedigree structure (Table 3.4).

Discussion

This chapter describes clinical and genetic investigation of three consanguineous families segregating either postaxial polydactyly type A or syndactyly in an autosomal recessive manners.

Postaxial Polydactyly (PAP), characterized by fifth digit duplication in hands and/or feet, is a rare anomaly of hand and foot and often segregates in autosomal dominant manner. Previously, only two families segregating PAP in autosomal recessive manner were reported (Mollica *et al.*, 1978; Kalsoom *et al.*, 2011). Kalsoom *et al.* (2011) further reported mapping of the PAP on chromosome 13q13.3-q21.2 in a family of Pakistani origin. In the two families, A and B, investigated in the present study, affected individuals showed well developed supernumerary digits. In addition, intra-familial variation of polydactyly was observed in affected members of the family A. A bone deformity, hallux valgus, reported by Kalsoom *et al.* (2011), was not observed in any affected member of the two families. Similarly, features associated with PAP type B and reported in families with autosomal dominant form (Radhakrishna *et al.*, 1996; Akarsu *et al.*, 1997; Zhao *et al.*, 2002) were missing in affected members of the family A and B.

In the other family (C) cutaneous syndactyly was observed in the affected members. Intra-familial variation of the phenotype exists in the affected individuals. The affected individuals showed bilateral fusion of middle and ring fingers in hands, with unaffected feet. Clinodactyly of middle and little fingers was also observed. To date, several cases of syndactyly ranging from partial to complete cutaneous syndactyly of digits have been reported (Temtamy and Mckusick, 1978). Most of these cases showed autosomal dominant pattern of inheritance. However, three other cases showing inheritance in autosomal recessive and X-linked have been reported as well (Malik, 2012). This included type-9 [Mesoaxial synostotic syndactyly (MSSD, MIM609432)], inherited in autosomal recessive fashion, and has been reported in two consanguineous pedigrees of Turkish and Pakistani origin (Percin *et al.*, 1998; Malik *et al.*, 2004). In both of these cases, affected individuals presented mesoaxial shortening of fingers, malformed thumbs, osseous synostosis of 3rd and 4th metacarpals resulting into a single digit, and hypoplastic and clinodactyly of the 5th finger. The X-linked form, named as Orel-Holmes type, showed fusion of 4th and 5th metacarpals with a clear ulnar deviation of the 5th finger. In addition, 4th and 5th metacarpals were

short with significant separation between their distal ends (Orel, 1928; Holmes *et al.*, 1972).

Three families (A, B, C), after failing to show linkage to known genes, were subjected to human genome scan using SNP markers. In the family A, linkage was established on chromosome 8q21.13-q24.12. The linkage interval of the mapped locus was 30.3 cM long, which corresponds to 37.0 Mb and flanked by SNP rs2053962 (89.88 cM, 80.87 Mb) and rs2514582 (119.3 cM, 119.5 Mb). Maximum multipoint LOD score of 2.82 with SNP rs2300490 along the disease interval strongly supported the linkage to this chromosomal region. Whole exome sequencing using Next generation sequencing (NGS) was then performed in an affected individual (V-3) at the University of Washington, Center for Mendelian Genomics. The identified mutation was validated and sequenced by Sanger cycle method in the remaining family members. The only variant that cosegregated with the phenotype was a nonsense mutation (p.Arg160*) in the *FAM92A1* gene on chromosome 8q21.13-q24.12 (Figure 3.9).

In family B, linkage analysis identified two regions on two different chromosomes harboring a disease causing gene. This included a locus of 37.0 Mb on chromosome 2p14-q12.1, flanked by SNPs rs6755128 and rs10177144, and another locus of 22.3 Mb on chromosome 6p22.3-p21.1, flanked by rs6459448 and rs6904723. Maximum possible LOD score of 1.92 was obtained with SNP markers on both the chromosomes.

Earlier, Tsai *et al.* (2009) described a Chinese girl, born to non-consanguineous parents, with multiple clinical features including duplication of great toes, clinodactyly, a saddle nose, have low-set ears, and tapering fingers. These authors using array-CGH and Real-time quantitative PCR, revealed a microdeletion of chromosome 2q31.1-31.2 in the patient. The deleted region spanned approximately 3.4 Mb was flanked by a centromeric marker D2S2188 (184.00 cM, 175.4 Mb) and a telomeric marker D2S300 (186.92 cM, 178.8 Mb). This region contains 30 genes according to the Human Genome Sequences (Build 36.3, 2008), including the entire HOXD gene cluster. Mutations in the HOXD genes including *HOXD13* have been found to be associated with a variety of limb abnormalities (Goodman, 2002). The linkage interval of 37.0 Mb (66.80–104.12 Mb) for autosomal recessive PAP type A

locus, mapped in the family B, on chromosome 2p14-q12.1 clearly indicates that this does not overlap with the linkage interval for PAP locus reported by Tsai *et al*. (2009). The two loci are 74.68 Mb apart, suggesting that two different genes are responsible for autosomal dominant and autosomal recessive PAP type A disorders mapped on chromosome 2.

Search using UCSC Genome Browser database (Karolchik *et al*., 2014) identified several known and predicted genes, and expressed sequence tags (ESTs) in the linkage interval flanked by SNPs rs6755128 and rs10177144 on chromosome 2p14-q12.1, mapped in the family B. Among 239 protein coding genes, present in the linkage interval, the most plausible candidates include *SPRED2* (MIM 609292), *BMP10* (MIM 608748), *FAM136A* (NM_032822), *CYP26B1* (MIM 605207), *HK* (MIM 612358), *GGCX* (MIM 137167) and *EIF2AK3* (MIM 604032). The second possible locus of 22.3 Mb, flanked by rs6459448 and rs6904723 on chromosome 6p22.3-p21.1, mapped in the family B, contains many known and predicted genes and expressed sequence tags (ESTs). Among 359 protein coding genes, six most possible candidates include *COL11A2* (MIM 120290), *CYP21A2* (MIM 613815), *PRL* (MIM 176760), *SCUBE3* (MIM 614708), *SLC17A4* (MIM 604216) and *TNF* (MIM 191160). Basis of considering the aforementioned genes as possible candidates, for the phenotype observed in the family B, include their functions in bone formation, expression in bones or digits, structural homology to genes involved in limb development or bone growth, and involvement in signaling pathways or cellular processes essential for shaping the limb. Specific information about each gene was obtained from the UCSC human genome database, OMIM and PUBMED (http://www.ncbi.nlm.nih.gov/omim/pubmed).

In the family C, linkage was established on chromosome 21q21.3-q22.3. Linkage interval of 16.3 Mb was flanked by SNP rs2829950 (25.19cM, 27.22 Mb) and rs566038 (62.77 cM, 44.74 Mb) on chromosome 21q21.3-q22.3. Maximum multipoint LOD score of 2.52 was obtained with the SNP rs761372. This interval contains 141 protein coding genes. Based on the available putative functional and expression data of these genes in the University of California- Santa Cruz (UCSC) human genome database (March 2009, http://genome.ucsc.edu/cgi-bin/hgGateway), six genes including *APP* (MIM 104760), *ADAMTS1* (MIM 605174), *SOD1* (MIM

147450), *RUNX* (MIM 151385), *ETS2* (MIM 164740), and *CBS* (MIM 613381) can be considered as the most plausible candidates for the phenotype observed in the family C.

To date, four autosomal dominant and only two autosomal recessive for postaxial polydactyly (PAP) loci have been mapped on different human chromosomes. The present study mapped three new PAP loci, segregating in autosomal recessive manner, on human chromosomes. Further, a disease causing gene *FAM92A1* has been identified on a locus mapped on chromosome 8q21.13-q24.12. Exome sequencing is in progress to search for the disease causing genes in two other families, mapped to novel loci. Identifying new genes and characterizing their functions will most likely unravel the pathways involved in limb development.
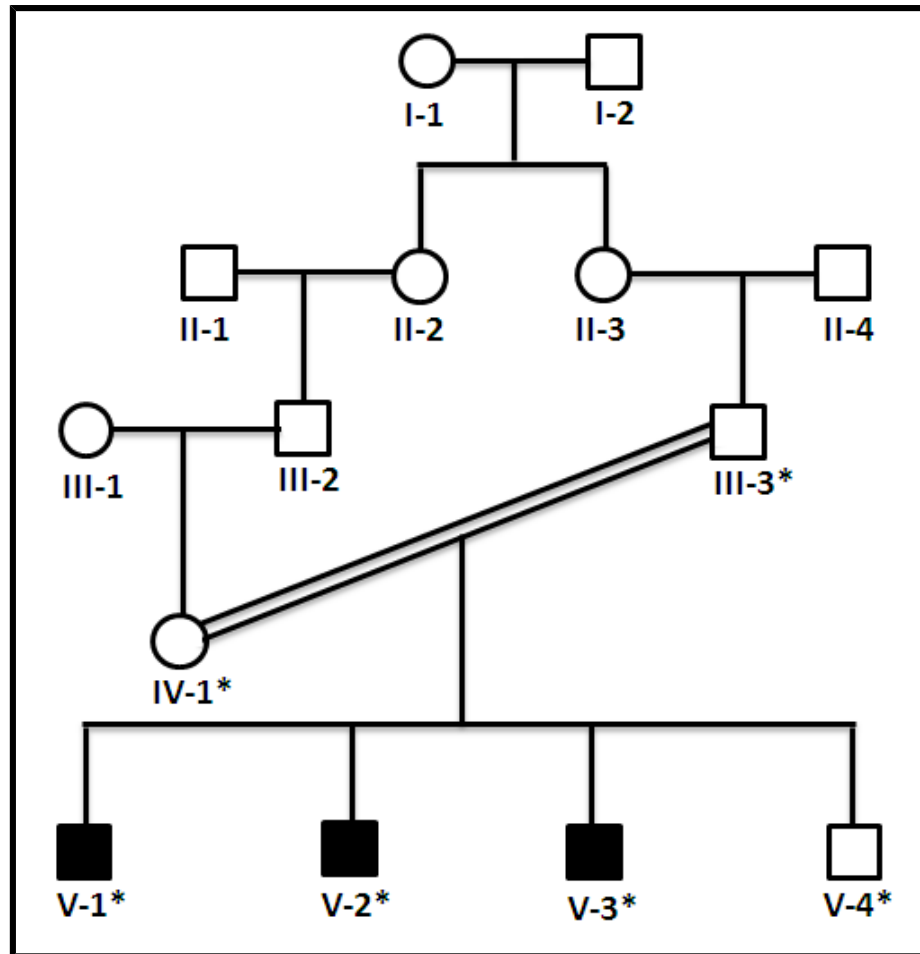
Figure 3.1: Pedigree drawing of family A with an autosomal recessive Postaxial Polydactyly type A. Clear symbols represents unaffected individuals while filled symbols represent affected individuals. Double line indicates the cousin marriage. The individual numbers labeled with asterisks indicate the samples which were available for this study.
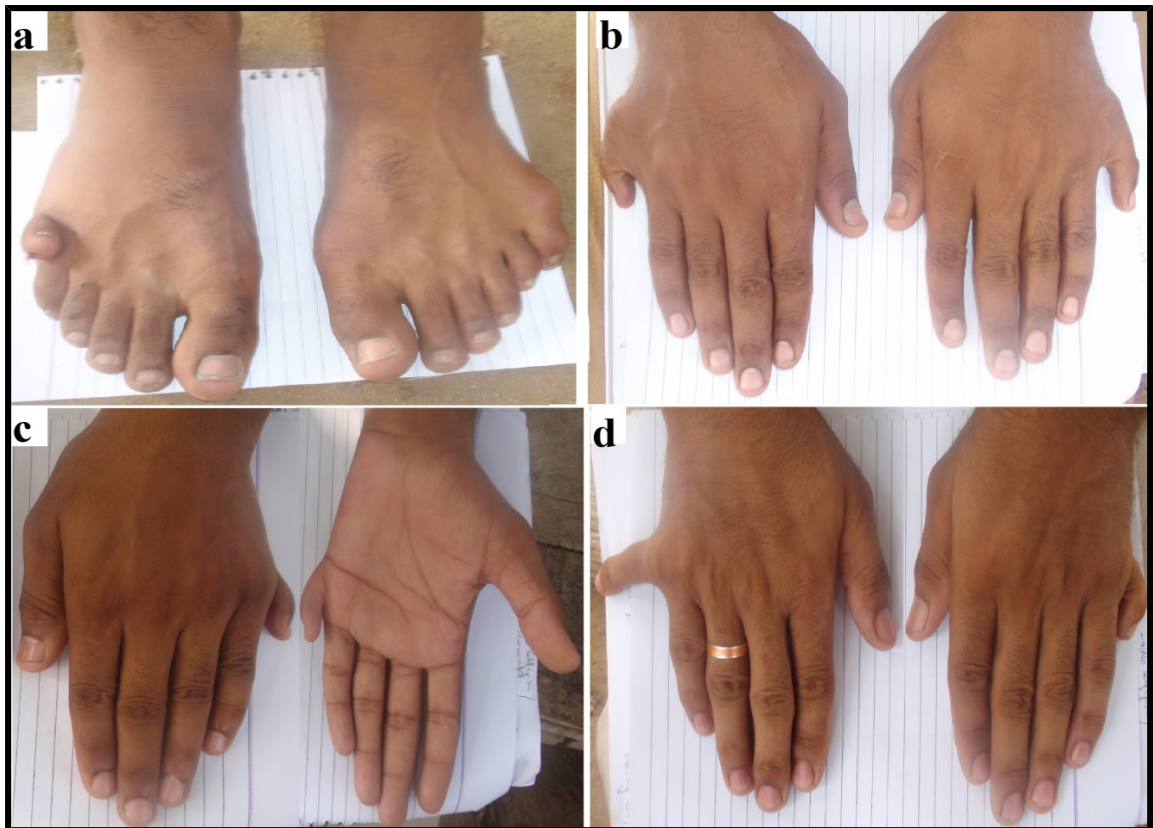
Figure 3.2: Clinical features of autosomal recessive PAP-A in the family A. Patient (V-1) showing bilateral PAP type A in feet (a), bilateral PAP type A in hands (b), the dorsum (dorsal view) and the palm (ventral view) of the left hand showing PAP type A (c), patient (V-3) showing extra finger deviated to the ulnar side in the right hand and under developed finger in the left hand (d).
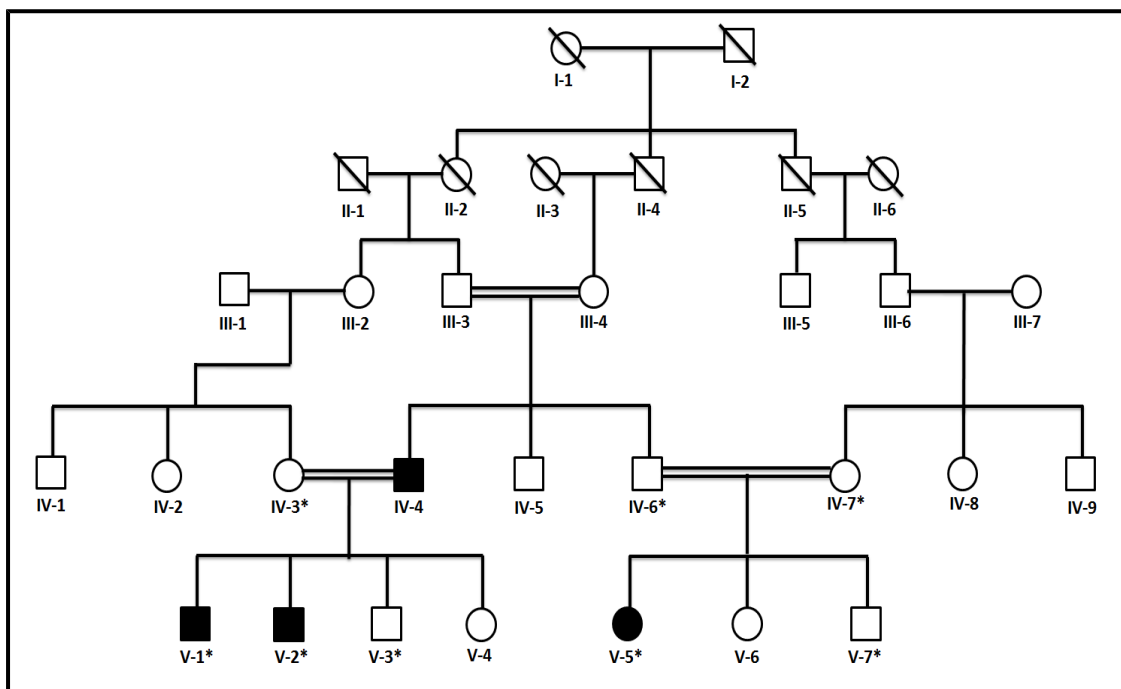
Figure 3.3: Pedigree drawing of family B with an autosomal recessive Postaxial Polydactyly type A. Clear symbols represents unaffected individuals while filled symbols affected individuals. Symbols with bars represent deceased individuals. Double line indicates intra-familial marriage. The individual numbers labeled with asterisks indicate the samples which were available for this study.
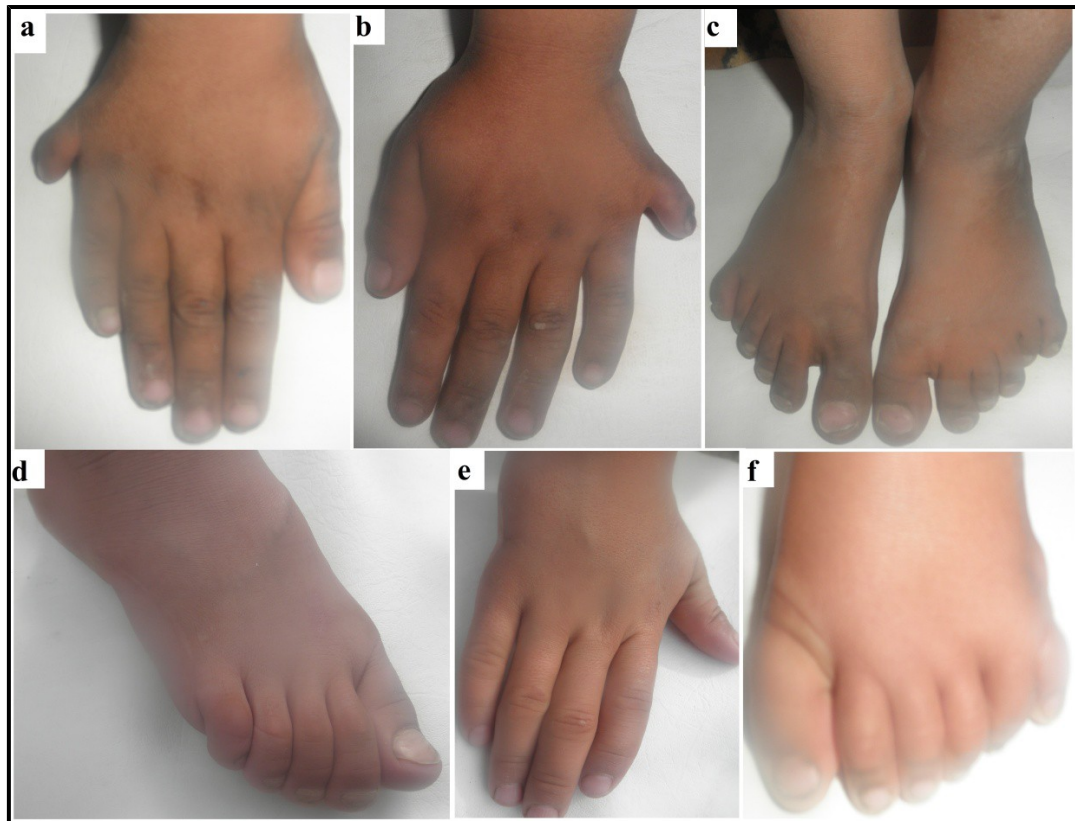
Figure 3.4: Clinical features of autosomal recessive PAP-A in family B. Patient (V-1) showing bilateral PAP type A in hands (a, b), bilateral PAP type A in feet (c). Following amputation of the extra digits, hand and foot of an affected individual (V-2) (d, e). Patient (V-5) showing PAP type A (f).
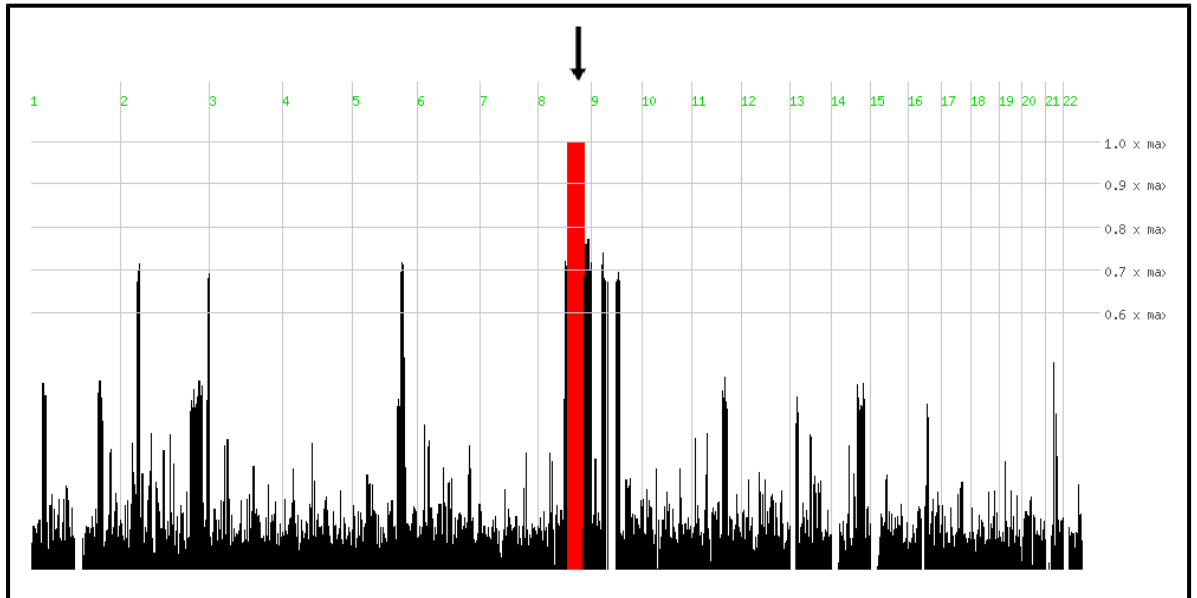
Figure 3.5: Genome-wide homozygosity peaks revealed by HomozygosityMapper. Black arrow indicates chromosomal location of PAP A locus identified in family A.
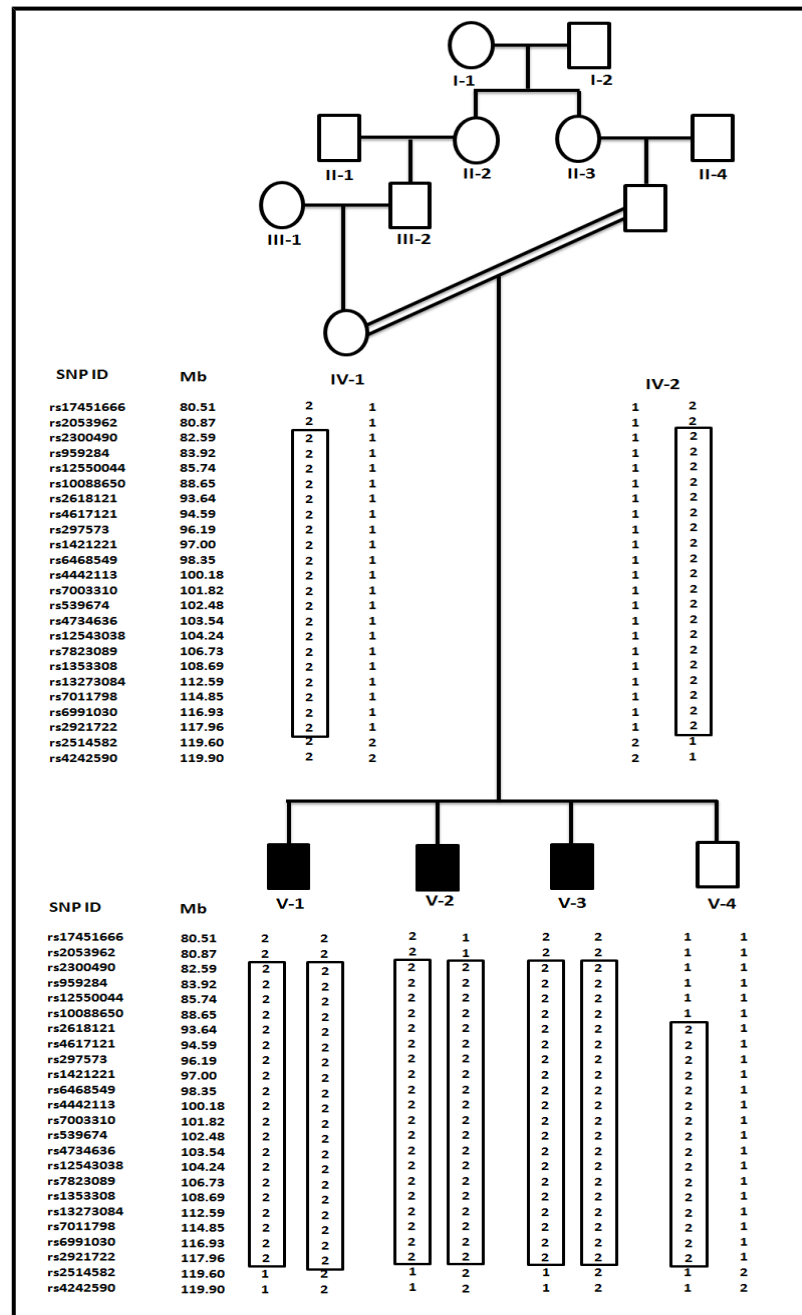
Figure 3.6: Haplotype of family A, segregating autosomal recessive postaxial polydactyly type A. Disease interval is flanked by SNPs rs2053962 and rs2514582 on chromosome 8q21.13-q24.12. For genotyped individuals, haplotypes are shown beneath each symbol revealing that all affected individuals share the same haplotypes. Physical distances in Megabase (Mb) are according to the UCSC genome browser build 37.

SNP ID	Mb	III-1	
rs7563131	65.25	1	2
rs6755128	65.65	1	2
rs6716792	66.69	1	2
rs10205913	67.90	1	2
rs6740317	68.52	1	2
rs4852283	69.79	1	2
rs3732233	71.63	1	2
rs1809265	72.01	1	2
rs6546824	73.59	1	2
rs13407946	74.85	1	2
rs759445	75.55	1	2
rs10172954	76.96	1	2
rs1354592	77.57	1	2
rs2177098	79.06	1	2
rs6719738	79.76	1	2
rs7561634	81.02	1	2
rs6713854	82.67	1	2
rs13432342	85.41	1	2
rs7597598	87.48	1	2
rs3105104	95.82	1	2
rs7603462	99.85	1	2
rs2942906	101.31	1	2
rs3771188	102.84	1	2
rs10177144	104.42	1	2
rs1441105	104.52	1	2

SNP ID	Mb	IV-1		IV-2		IV-3	
rs7563131	65.25	2	2	2	2	2	1
rs6755128	65.65	2	2	2	2	2	1
rs6716792	66.69	2	2	2	2	2	1
rs10205913	67.90	2	2	2	2	2	1
rs6740317	68.52	2	2	2	2	2	1
rs4852283	69.79	2	2	2	2	2	1
rs3732233	71.63	2	2	2	2	2	1
rs1809265	72.01	2	2	2	2	2	1
rs6546824	73.59	2	2	2	2	2	1
rs13407946	74.85	2	2	2	2	2	1
rs759445	75.55	2	2	2	2	2	1
rs10172954	76.96	2	2	2	2	2	1
rs1354592	77.57	2	2	2	2	2	1
rs2177098	79.06	2	2	2	2	2	1
rs6719738	79.76	2	2	2	2	1	1
rs7561634	81.02	2	2	2	2	1	1
rs6713854	82.67	2	2	2	2	2	1
rs13432342	85.41	2	2	2	2	2	1
rs7597598	87.48	2	2	2	2	1	1
rs3105104	95.82	2	2	2	2	1	1
rs7603462	99.85	2	2	2	2	2	1
rs2942906	101.31	2	2	2	2	2	1
rs3771188	102.84	2	2	2	2	1	1
rs10177144	104.42	1	2	1	2	1	2
rs1441105	104.52	1	2	1	2	1	2

Figure 3.7: Haplotype of family B segregating autosomal recessive postaxial polydactyly type A. Disease interval is flanked by SNPs rs6755128 and rs10177144 on chromosome 2p14-q12.1. For genotyped individuals, haplotypes are shown beneath each symbol revealing that all affected individuals share the same haplotypes. Physical distances in Megabase (Mb) are according to the UCSC genome browser build 37.
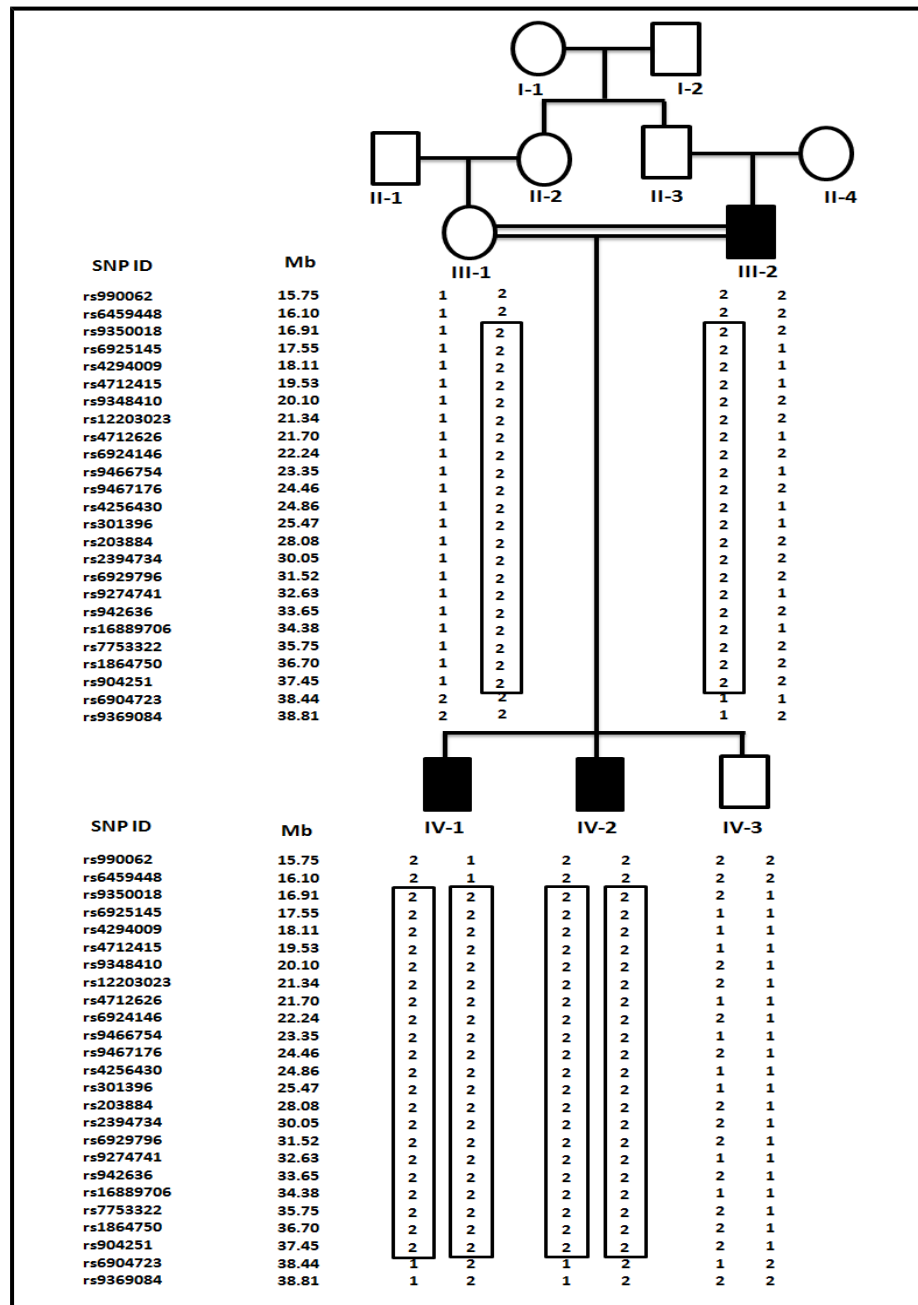
Figure 3.8: Haplotype of family B segregating autosomal recessive postaxial polydactyly type A. Disease interval is flanked by SNPs rs6459448 and rs6904723 on chromosome 6p22.3-p21.1. For genotyped individuals, haplotypes are shown beneath each symbol revealing that all affected individuals share the same haplotypes. Physical distances in Megabase (Mb) are according to the UCSC genome browser build 37.

Table 3.1: Multipoint and Two point LOD score between polydactyly type A locus and SNP markers on chromosome 8q21.13-q24.12.

SNP ID	Mb	Multipoint LOD	2-point LOD (Recombination fraction=)						
			0.000	0.010	0.050	0.100	0.200	0.300	0.400
rs17451666	80,510,544	-Infinity	-Infinity	-0.732	-0.127	0.058	0.122	0.061	-0.013
rs2053962	80,870,910	-Infinity	-Infinity	-0.604	-0.010	0.163	0.209	0.130	0.029
rs2300490	82,589,694	2.820	2.432	2.385	2.194	1.947	1.433	0.903	0.389
rs959284	83,920,104	2.820	1.819	1.778	1.612	1.402	0.976	0.555	0.185
rs12550044	85,741,835	2.820	1.460	1.428	1.297	1.130	0.782	0.426	0.117
rs10088650	88,647,577	2.820	1.719	1.680	1.523	1.323	0.919	0.517	0.166
rs2618121	93,637,168	2.820	1.819	1.774	1.592	1.366	0.918	0.496	0.155
rs4617121	94,587,666	2.820	1.701	1.658	1.486	1.272	0.850	0.451	0.133
rs297573	96,186,655	2.820	1.978	1.930	1.739	1.499	1.021	0.566	0.190
rs1421221	97,004,203	2.820	1.666	1.624	1.455	1.245	0.831	0.439	0.127
rs6468549	98,350,880	2.819	1.580	1.540	1.380	1.181	0.786	0.410	0.113
rs4442113	100,180,871	2.819	1.687	1.645	1.474	1.262	0.842	0.446	0.131
rs7003310	101,821,033	2.819	1.591	1.550	1.390	1.189	0.791	0.414	0.115
rs539674	102,484,486	2.819	1.706	1.663	1.491	1.276	0.853	0.453	0.134
rs4734636	103,542,538	2.820	1.674	1.632	1.463	1.252	0.835	0.442	0.129
rs12543038	104,244,309	2.820	2.013	1.965	1.772	1.529	1.045	0.583	0.199
rs7823089	106,730,235	2.820	2.244	2.194	1.992	1.736	1.219	0.715	0.272
rs1353308	108,686,594	2.815	1.580	1.540	1.380	1.181	0.786	0.410	0.113
rs13273084	112,589,344	2.802	1.527	1.488	1.335	1.142	0.759	0.392	0.104
rs7011798	114,848,963	2.797	1.625	1.584	1.419	1.215	0.809	0.425	0.120
rs6991030	116,934,158	2.779	2.102	2.053	1.856	1.607	1.109	0.631	0.224
rs2921722	117,960,147	2.646	1.780	1.735	1.557	1.334	0.895	0.480	0.147
rs2514582	119,596,377	-1.760	-1.156	-0.706	-0.221	-0.038	0.055	0.038	0.002
rs4242590	119,897,215	-1.669	-1.151	-0.696	-0.209	-0.026	0.066	0.045	0.006

Mb, Mega base pairs

Table 3.2: Multipoint and Two point LOD score between polydactyly type A locus and SNP markers on chromosome 2p14-q12.1.

SNP ID	Mb	Multipoint LOD	2-point LOD (Recombination fraction=)						
			0.000	0.010	0.050	0.100	0.200	0.300	0.400
rs7563131	65,248,271	-Infinity	-Infinity	-1.439	-0.754	-0.471	-0.209	-0.084	-0.022
rs6755128	65,653,199	-Infinity	-Infinity	-1.116	-0.485	-0.261	-0.093	-0.030	-0.005
rs6716792	66,687,843	1.881	0.933	0.906	0.799	0.668	0.426	0.222	0.077
rs10205913	67,903,473	1.905	0.846	0.821	0.723	0.604	0.384	0.200	0.068
rs6740317	68,515,530	1.915	0.827	0.803	0.707	0.591	0.376	0.196	0.066
rs4852283	69,794,350	1.919	0.814	0.791	0.696	0.582	0.370	0.193	0.065
rs3732233	71,633,275	1.922	0.844	0.819	0.721	0.603	0.383	0.200	0.068
rs1809265	72,013,617	1.925	1.278	1.245	1.110	0.943	0.622	0.341	0.127
rs6546824	73,587,331	1.926	1.170	1.138	1.010	0.853	0.554	0.298	0.108
rs13407946	74,849,953	1.925	0.478	0.467	0.421	0.362	0.242	0.131	0.043
rs759445	75,551,754	1.925	0.799	0.776	0.683	0.571	0.363	0.189	0.064
rs10172954	76,957,370	1.926	1.422	1.387	1.244	1.066	0.719	0.407	0.160
rs1354592	77,572,079	1.925	0.816	0.792	0.698	0.583	0.371	0.193	0.065
rs2177098	79,061,185	1.925	0.959	0.931	0.821	0.687	0.438	0.229	0.079
rs6719738	79,760,238	1.925	1.191	1.162	1.045	0.896	0.603	0.330	0.111
rs7561634	81,025,111	1.923	0.943	0.919	0.821	0.697	0.452	0.227	0.056
rs6713854	82,668,227	1.921	0.585	0.569	0.506	0.428	0.278	0.147	0.049
rs13432342	85,414,647	1.918	0.528	0.514	0.460	0.392	0.259	0.138	0.046
rs7597598	87,481,274	1.917	1.071	1.044	0.936	0.799	0.529	0.280	0.085
rs3105104	95,816,365	1.912	1.226	1.196	1.077	0.926	0.626	0.346	0.119
rs7603462	99,847,890	1.900	0.628	0.610	0.540	0.455	0.294	0.155	0.052
rs2942906	101,308,711	1.886	0.635	0.617	0.546	0.460	0.297	0.156	0.052
rs3771188	102,840,348	1.861	1.658	1.624	1.487	1.310	0.947	0.588	0.258
rs10177144	104,415,982	-3.025	-1.880	-1.188	-0.598	-0.350	-0.141	-0.054	-0.016
rs1441105	104,521,151	-3.025	-1.880	-1.188	-0.598	-0.350	-0.141	-0.054	-0.016

Mb, Mega base pairs

Table 3.3: Multipoint and Two point LOD score between polydactyly type A locus and SNP markers on chromosome 6p22.3-p21.1.

SNP ID	Mb	Multipoint LOD	2-point LOD (Recombination fraction=)						
			0.000	0.010	0.050	0.100	0.200	0.300	0.400
rs990062	15,746,779	-Infinity	-Infinity	-1.668	-0.839	-0.478	-0.178	-0.060	-0.012
rs6459448	16,098,290	-Infinity	-Infinity	-1.710	-0.914	-0.557	-0.235	-0.091	-0.023
rs9350018	16,910,129	1.823	0.712	0.691	0.610	0.511	0.327	0.171	0.057
rs6925145	17,550,158	1.894	1.007	0.982	0.878	0.748	0.490	0.254	0.071
rs4294009	18,106,076	1.915	1.207	1.178	1.059	0.910	0.613	0.338	0.115
rs4712415	19,525,075	1.920	1.121	1.094	0.981	0.839	0.559	0.301	0.096
rs9348410	20,097,963	1.922	0.768	0.746	0.657	0.550	0.350	0.182	0.061
rs12203023	21,337,783	1.924	0.864	0.839	0.739	0.617	0.392	0.204	0.070
rs4712626	21,701,841	1.925	1.186	1.157	1.040	0.893	0.600	0.328	0.110
rs6924146	22,238,088	1.925	0.582	0.567	0.503	0.426	0.277	0.147	0.049
rs9466754	23,347,873	1.926	1.500	1.467	1.335	1.165	0.821	0.488	0.198
rs9467176	24,464,907	1.925	0.571	0.556	0.495	0.419	0.274	0.145	0.048
rs4256430	24,863,075	1.926	1.165	1.136	1.021	0.875	0.586	0.319	0.105
rs301396	25,466,889	1.926	1.195	1.166	1.049	0.900	0.606	0.332	0.112
rs203884	28,077,374	1.925	0.634	0.616	0.545	0.459	0.296	0.156	0.052
rs2394734	30,046,246	1.924	0.629	0.612	0.542	0.456	0.295	0.155	0.052
rs6929796	31,522,669	1.924	0.566	0.551	0.490	0.416	0.272	0.144	0.048
rs9274741	32,637,994	1.923	1.171	1.142	1.026	0.880	0.590	0.322	0.107
rs942636	33,651,129	1.917	1.008	0.979	0.864	0.725	0.463	0.244	0.085
rs16889706	34,384,852	1.902	1.291	1.261	1.137	0.981	0.669	0.377	0.136
rs7753322	35,748,086	1.854	0.640	0.622	0.550	0.463	0.298	0.157	0.052
rs1864750	36,704,807	1.758	0.752	0.730	0.644	0.539	0.343	0.179	0.060
rs904251	37,451,696	1.558	0.797	0.774	0.682	0.570	0.363	0.189	0.064
rs6904723	38,436,317	-2.884	-1.890	-1.196	-0.604	-0.354	-0.143	-0.054	-0.015
rs9369084	38,813,081	-2.873	-1.506	-0.852	-0.307	-0.111	0.000	0.002	-0.013

Mb, Mega base pairs
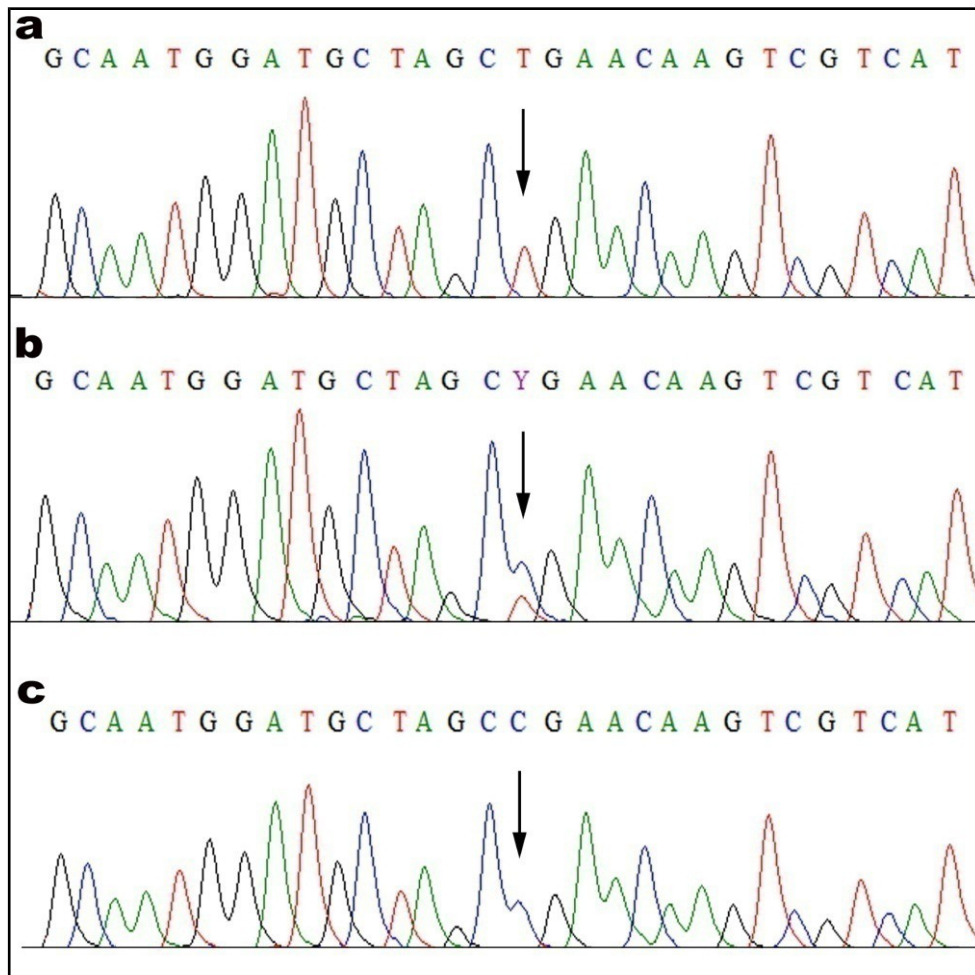
Figure 3.9: DNA sequence analysis of a novel nonsense mutation (c.478C>T, p.Arg160*) in the *FAM92A1* gene identified in the family A. The upper panel (a) represents the nucleotide sequence in the affected individual, the middle panel (b) in the heterozygous carriers and the lower panel (c) in the unaffected individual. The arrows represent position of the mutation.
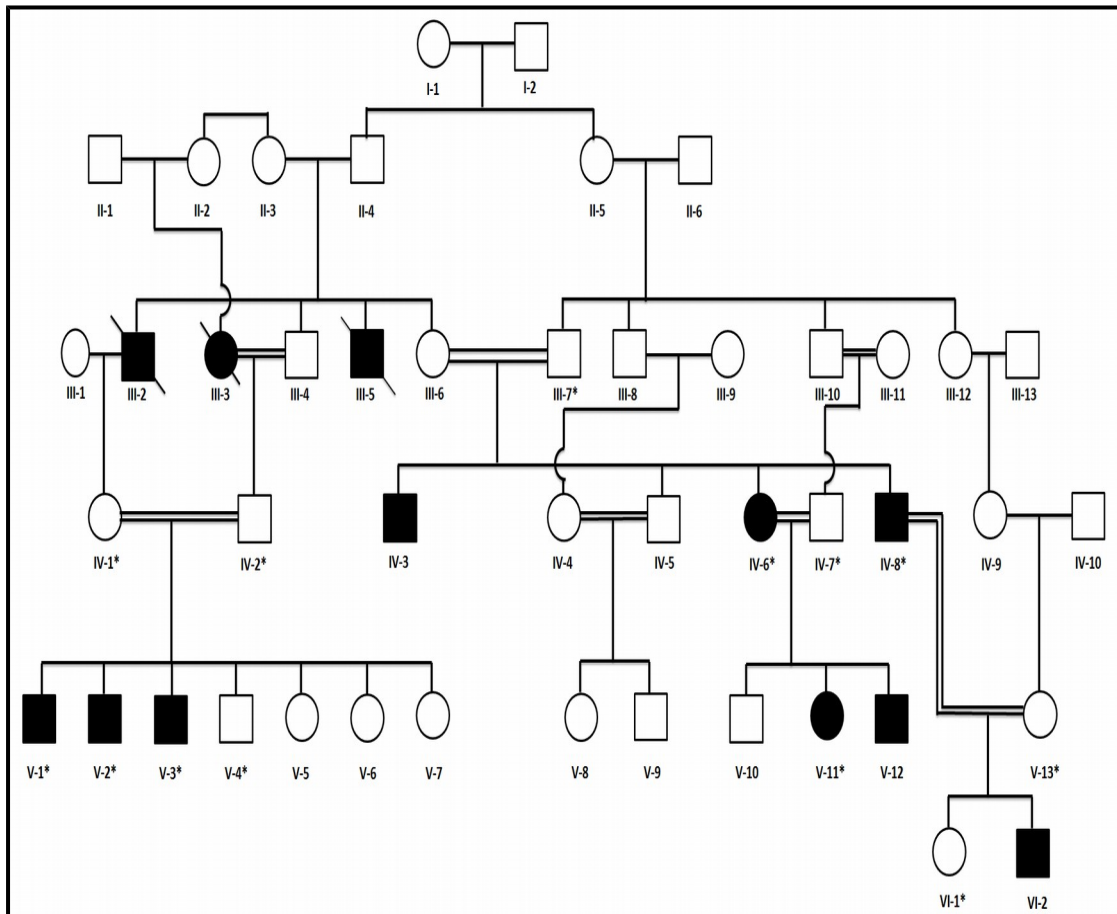
Figure 3.10: Pedigree drawing of family C segregating an autosomal recessive Syndactyly. Clear symbols represent unaffected individuals while filled symbols affected individuals. Symbols with bars represent deceased individuals. Double line indicates intra-familial marriages. The individual numbers labeled with asterisks indicate the samples which were available for this study.
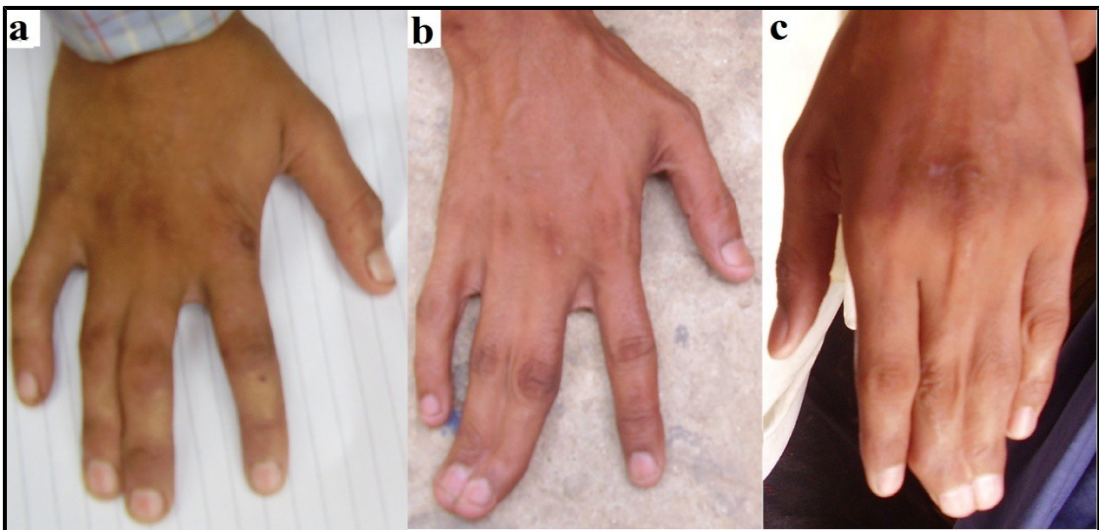
Figure 3.11: Clinical features of autosomal recessive syndactyly in the family C. Patient (V-1) showing bilateral syndactyly in hands (a), patient (V-2) showing clinodactyly and fusion of 3rd and 4th fingers (b), clinodactyly of the middle finger and cutaneous fusion of 3rd and 4th fingers was observed in patient V-3 (c).
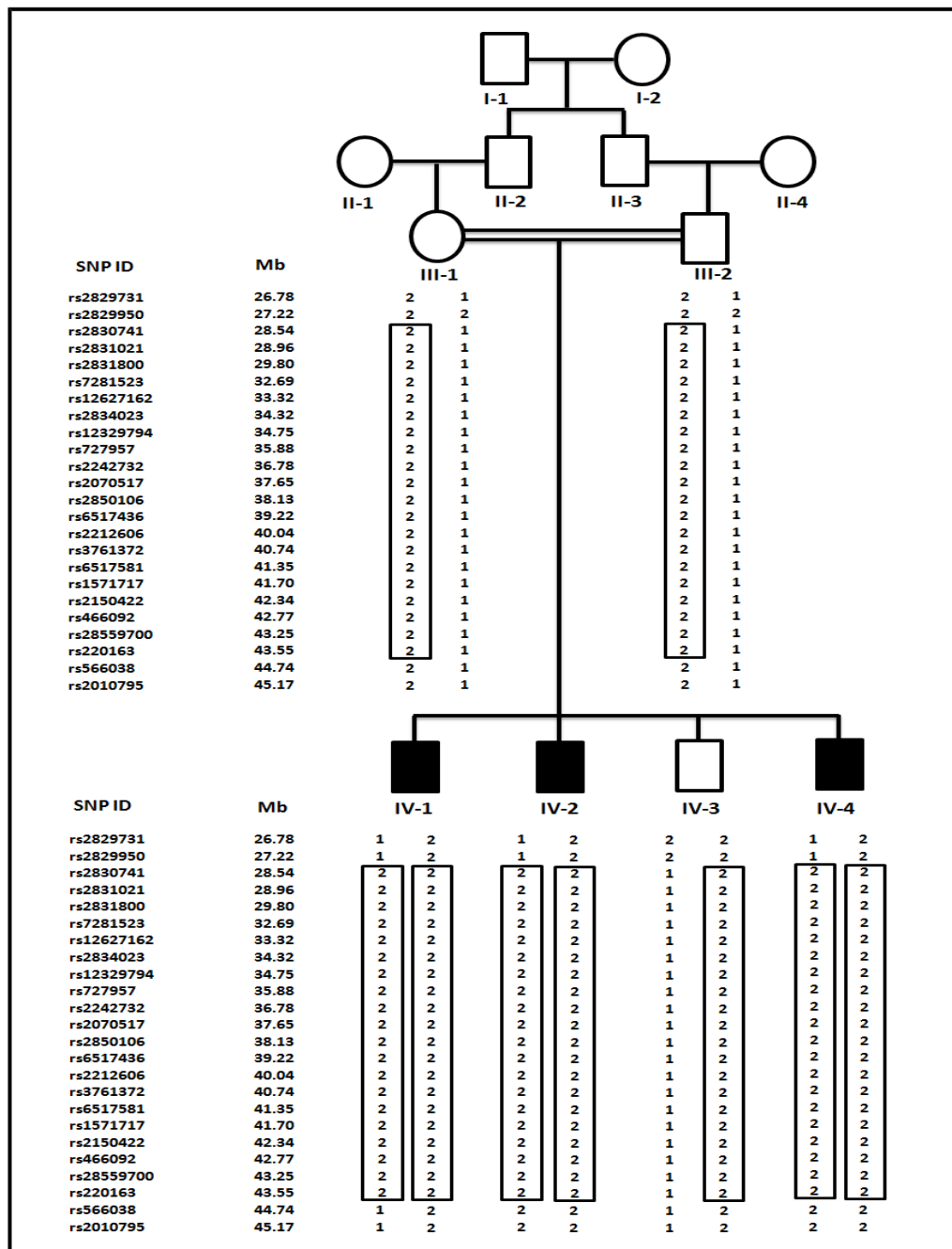
Figure 3.12: Haplotype of family C segregating syndactyly in autosomal recessive manner. Disease interval is flanked by SNPs rs2829950 and rs566038 on chromosome 21q21.3-q22.3. For genotyped individuals, haplotypes are shown beneath each symbol revealing that all affected individuals share the same haplotypes. Physical distances in Megabase (Mb) are according to the UCSC genome browser build 37.

Table 3.4: Multipoint and Two point LOD score between syndactyly locus and SNP markers on chromosome 21q21.3-q22.3.

SNP ID	Mb	Multipoint LOD	2-point LOD (Recombination fraction=)						
			0.000	0.010	0.050	0.100	0.200	0.300	0.400
rs2829731	26,784,019	-1.941	-1.332	-0.651	-0.175	-0.063	-0.057	-0.054	-0.022
rs2829950	27,223,152	-1.976	-1.205	-0.555	-0.032	0.136	0.178	0.100	0.010
rs2830741	28,540,905	2.145	1.466	1.430	1.286	1.105	0.735	0.374	0.085
rs2831021	28,956,641	2.443	2.081	2.035	1.852	1.620	1.150	0.689	0.275
rs2831800	29,799,861	2.465	1.254	1.222	1.090	0.922	0.575	0.233	-0.014
rs7281523	32,691,163	2.493	1.565	1.527	1.375	1.184	0.798	0.423	0.117
rs12627162	33,322,819	2.506	1.599	1.561	1.406	1.212	0.820	0.439	0.126
rs2834023	34,319,085	2.513	1.676	1.636	1.475	1.273	0.867	0.474	0.147
rs12329794	34,753,038	2.517	1.262	1.229	1.097	0.929	0.581	0.239	-0.010
rs727957	35,880,072	2.521	2.093	2.048	1.864	1.631	1.160	0.697	0.280
rs2242732	36,781,033	2.521	1.576	1.538	1.385	1.193	0.806	0.429	0.120
rs2070517	37,650,235	2.521	1.769	1.727	1.560	1.349	0.927	0.518	0.172
rs2850106	38,134,511	2.521	1.523	1.486	1.338	1.151	0.772	0.403	0.104
rs6517436	39,223,338	2.522	1.722	1.681	1.517	1.310	0.896	0.495	0.159
rs2212606	40,044,940	2.522	1.726	1.685	1.520	1.313	0.899	0.497	0.160
rs3761372	40,743,845	2.523	1.953	1.909	1.731	1.506	1.054	0.613	0.228
rs6517581	41,354,868	2.522	1.608	1.569	1.414	1.218	0.825	0.443	0.129
rs1571717	41,698,322	2.522	1.756	1.715	1.548	1.339	0.918	0.512	0.168
rs2150422	42,343,159	2.521	1.775	1.733	1.566	1.354	0.931	0.521	0.174
rs466092	42,774,541	2.520	1.447	1.411	1.269	1.089	0.723	0.364	0.078
rs28559700	43,246,223	2.520	1.710	1.669	1.506	1.301	0.889	0.490	0.156
rs220163	43,550,518	2.521	1.865	1.822	1.649	1.430	0.991	0.566	0.200
rs566038	44,742,746	-Infinity	-Infinity	0.012	0.547	0.643	0.539	0.338	0.140
rs2010795	45,172,628	-Infinity	-Infinity	-0.305	0.248	0.369	0.326	0.193	0.066

Mb, Mega base pairs

Chapter 4

Split-Hand/Foot Malformation

Clinical and Molecular Characterization of Human Hereditary Skeletal Disorders in Consanguineous Families

SPLIT-HAND/FOOT MALFORMATION

Split-hand/foot malformation (SHFM) is a congenital limb malformation of median clefts of hands and feet, and aplasia and/or hypoplasia of the phalanges. The clinical picture varies in severity from patient to patient as well between the limbs in the same individual (Duijf *et al*., 2003; Elliott and Evans, 2008). Mode of inheritance of SHFM may be autosomal dominant, autosomal recessive or X-linked. This condition exists as an isolated (non-syndromic) or part of a complex syndrome.

To date, seven different types of non-syndromic SHFM have been mapped on different human chromosomes. Four of these forms (SHFM-1, SHFM-3, SHFM-4, SHFM-5) are inherited in autosomal dominant, one (SHFM-2) in X-linked and one (SHFM-6) in autosomal recessive form. The four autosomal dominant forms were mapped on chromosome 7q21 (SHFM-1, Scherer *et al.,* 1994), 10q24 (SHFM-3, Nunes *et al.,* 1995; Gurrieri *et al.,* 1996; Raas-Rothschild *et al.,* 1996), 3q27 (SHFM-4, Ianakiev *et al.,* 2000) and 2q31 (SHFM-5, Boles *et al.,* 1995). The only autosomal recessive form (SHFM-6) known has been mapped on chromosome 12q13.11-q13 (Ugur and Tolun, 2008). The X-linked form was mapped on Xq26 and later refined to a small region of 5.0 cM region (Faiyaz-Ul-Haque *et al.,* 2005). Gurnett *et al.* (2006) suggested a novel locus on chromosome 8q21.11–q22.3 on the basis of a genome-wide linkage analysis in single family. For these seven loci, only three (SHFM1, SHFM4, SHFM6) have been solved at the gene level. A gene wingless-type MMTV integration site family, member 10 (*WNT10B,* MIM 601906) has been identified for locus SHFM-6 (Ugur and Tolun, 2008). Ianakiev *et al.* (2000) reported another gene *TP63* (tumor protein p63, MIM 603273), encoding a homolog of the tumor suppressor, responsible for SHFM-4 phenotype. Shamseldin *et al.* (2011) reported a mutation in the gene *DLX5* for SHFM-1in a consanguineous family. Goodman *et al.* (2002) proposed that SHFM-5 and other digit defects may be caused by haploinsufficiency of the 5' *HOXD, EVX2,* or *DLX1* and *DLX2* genes.

Three consanguineous Pakistani families (D, E, F) showing split hand and foot malformation phenotypes were ascertained and presented in the present chapter of the dissertation. Linkage in the families was established by genotyping microsatellite

markers and automated DNA sequencing was employed to identify the sequence variants.

Family D

Family D (Figure 4.1) belongs to a remote area in district Kohat of Khyber Pakhtunkhwa (KPK) province of the country. Affected individuals segregated SHFM phenotype in the fourth generation in autosomal recessive inheritance pattern. The blood samples were obtained from two affected (IV-3, IV-4) and four unaffected individuals (III-1, III-2, IV-1, IV-2) of the family.

Clinical Features

Affected individuals were clinically investigated at National Institute of Rehabilitation Medicine (NIRM), Islamabad, Pakistan. The SHFM condition among the affected individuals in the family exhibited a great degree of phenotypic variability. Males and females were equally affected. The affected individuals including a seventeen years old male (IV-3) and his fourteen years old sister (IV-4) were born after normal pregnancies. Clinical features of the affected individuals are presented in Figure 4.2. Male affected member (IV-3) showed syndactyly in the left foot as the only abnormality. The right foot and both hands in this member showed normal development. Female affected member (IV-4) exhibited SHFM phenotype with involvement of hands and feet. Abnormalities such as polydactyly/syndactyly, dysplastic hands and cleft feet were observed in this affected member.

Abnormalities of face, skin, teeth, nails, ear and heart were not found in any of the two affected individuals of the family. Abnormalities of mammary gland in affected females were not reported. Parents of the affected individuals in the family were healthy and clinically indistinguishable from normal individuals of the family.

Family E

This family (E) belongs to Upper Dir district of Khyber Pakhtunkhwa (KPK) Province. The family has two affected (IV-3, IV4) and four unaffected (III-1, III-2, IV-1, IV-2) individuals, aged between 15-25 years at the time of the study (Figure 4.3). The blood samples were obtained from all affected and unaffected individuals of the family.

Clinical Features

Affected individuals were clinically investigated at Pakistan Institute of Medical Sciences (PIMS), Islamabad, Pakistan. Both the affected individuals showed typical features of the hereditary SHFM. The patient IV-4 showed cleft hand deformity associated with central type of syndactyly in left hand and absence of central digit in right hand. The other patient (IV-3) exhibited cleft hand deformity with pre-axial syndactyly and radial deviation of ring finger. In addition, both the affected members exhibited cleft foot deformity, hallux valgus deformity of big toe and rudimentary bud of lesser toes (Figure 4.4).

Teeth, nails, sweating and hearing were normal in both the affected individuals. Neurological problems and facial dysmorphism were not observed in any of the affected individuals. Heterozygous carrier individuals had normal hands and feet, and were clinically indistinguishable from genotypically normal individuals.

Family F

Family F with autosomal recessive form of split-hand/foot malformation was recruited from Sindh Province of Pakistan (Figure 4.5). The family had three affected members including a deceased member (III-3). Blood samples of five family members including two affected (IV-1, IV-2), and their normal brother (IV-3), normal sister (IV-4) and mother (III-4) were available for the present study.

Clinical Features

Two affected individuals of the family (IV-1, IV-2) were clinically examined at local government hospital. Both the affected individuals were born after normal pregnancies. In male affected member (IV-1) hands were normal while central type of syndactyly and polydactyly was observed in the feet. On the other hand, female affected member (IV-2) showed cleft hand and foot deformity associated with absence of middle finger and large proximal phalanx of ring finger in both hands (Figure 4.6).

Skin, face, teeth, nails, eyes and heart abnormalities were not observed in the affected individuals of the family. Parents of the affected individuals showed no abnormalities and were healthy like other normal individuals of the family.

Genotyping and Sequencing *WNT10B*

Linkage in the three families (D, E, F) was tested by typing microsatellite markers linked to five autosomal dominant and an autosomal recessive SHFM loci. This included SHFM-1 at chromosome 7q21 (D7S524, D7S644, D7S630, D7S627, D7S646, D7S1820, D7S2482, D7S554), SHFM-3 at chromosome 10q24 (D10S547, D10S571, D10S1758, D10S198, D10S1265, D10S1239, D10S1268, D10S254), SHFM-4 at chromosome 3q27 (D3S1602, D3S2436, D3S3628, D3S2398, D3S2747, D3S3054, D3S2455, D3S3043), SHFM-5 at chromosome 2q31 (D2S2195, D2S1281, D2S 376, D2S326, D2S2307, D2S2981, D2S324, D2S324), SHFM-6 at chromosome 12q11-q13 (D12S1621, D12S291, D12S1701, D12S339, D12S347, D12S1604), and another potential locus on chromosome 8q21.11–q22.3 (D8S2324, D8S164, D8S1143, D8S556, D8S1132). PCR amplification of the microsatellite markers was performed as described in Chapter 2. The amplified PCR products were resolved on 8% non-denaturing poly acrylamide gel, stained with ethidium bromide and scored the alleles by manual inspection. Genotyping data and haplotype analysis showed segregation of homozygous pattern of alleles, obtained with microsatellite markers linked to the gene *WNT10B* (Figure 4.7, 4.8, 4.9), only in affected individuals of the family. Normal individuals were heterozygous at this locus, thus establishing linkage in all three families (D, E, F) to the gene *WNT10B* on chromosome 12q11–q13.

A gene *WNT10B* mapped at SHFM-6 on chromosome 12q13.11–q13 was previously reported causing SHFM phenotype (Ugurand Tolun, 2008), therefore the same gene was sequenced in all affected and unaffected members of the families. In family D, sequence analysis revealed a 4-bp deletion mutation (c.1165_1168delAAGT) in exon-5 of the gene in both affected individuals. This deletion mutation was present in heterozygous state in obligate carriers of the family (Figure 4.10). In family E, sequence analysis identified 7-bp duplication (c.300_306dupAGGGCGG) in exon 3 of the *WNT10B* gene. This mutation was present in heterozygous state in the obligate carriers of the family (Figure 4.11). In the family F, entire coding region and splice junctions of *WNT10B* gene were screened in two affected and one normal individual of the family. However, sequence analysis failed to detect pathogenic sequence variant suggesting that probably the mutation is present in regulatory sequences of the gene.

To exclude nonpathogenic nature of the two mutations identified in exons 3 and 5 of the gene in two families (D and E), genomic DNA collected from 200 ethnically matched control individuals was sequenced and these were not identified outside the families. In order to verify the mutation in the *WNT10B* mRNA, an attempt was made to extract it from the blood of both affected and unaffected individuals but it was not successful.

Discussion

This chapter of the dissertation described clinical and molecular analysis of three consanguineous families exhibiting autosomal recessive split hand and feet malformation (SHFM) phenotype. Prior to this study, only three families segregating autosomal recessive form of SHFM-6 were described (Ugur and Tolun, 2008; Blattner *et al.,* 2010; Khan *et al*., 2012).

Affected members of the three families exhibited SHFM phenotype with involvement of hands and feet. Bone abnormalities such as ectrodactyly, polydactyly/syndactyly, dysplastic hands and cleft feet were observed in affected members of all the three families. The phenotypic variability has been observed not only among families but also among affected members with in the same family. In certain individuals, one extremity was found more affected than the other. Features observed in the three families were similar to those reported in affected members of the families presented by Khan *et al*. (2012) and Ugur and Tolun (2008). However, absences of thumb and fingers seen in few affected members of the family reported by Khan *et al.* (2012) have not been observed in the present three families. Similarly, associated abnormalities such as deafness and cardiac defects reported in few individuals with SHFM-1 and SHFM-5 (Elliott *et al.,* 2008) were not found in any individual of the present families. The SHFM phenotypic variability grading from mild preaxial to post-axial involvement as simple syndactyly to severe central clefting of the autopods is not restricted to families with autosomal recessive mode of inheritance but was also reported in families mapped to five autosomal dominant loci (Ianakiev *et al.,* 2000).

Linkage in the families, presented here, was established to SHFM-6 locus on chromosome 12q11-q13. This locus and the candidate gene causing SHFM were identified earlier by Ugur and Tolun, (2008). The *WNT10B* gene contains five exons

encoding 389 amino acids protein. Previously, only three mutations including two missense p.Arg332Trp in a Turkish family and p.Thr329Arg in a Pakistani family, and one duplication (c.458_461dupAGCA) in a Swiss woman were reported in the gene *WNT10B* (Blattner *et al.,* 2010; Khan *et al.*, 2012;Ugur and Tolun, 2008). The present study has led to the identification of two novel mutations in the gene *WNT10B* including 4-bp deletion (c.1165_1168delAAGT) in both affected individuals of family D and 7-bp duplication (c.300_306dupAGGGCGG) in both affected individuals of family E. The 4-bp deletion (c.1165_1168delAAGT), identified in the family D, created a new termination codon after incorporating additional codons for 36 illegitimate amino acids (p.Lys388Glufs*36). Molecular docking studies revealed that a significant conformational shift was detected in the active binding site of mutated WNT10B (p.Lys388Glufs*36), influencing binding with Fzd8 which might affect the canonical signaling pathway (Figure 4.12). The second mutation, 7-bp duplication (c.300_306dupAGGGCGG) identified in the *WNT10B* gene in family E, created a premature stop codon (TGA) 163 bps downstream probably resulting in production of a mutant transcript, which is most likely degraded by nonsense mediated mRNA decay.

The gene *WNT10B* is one of the members of WNT gene family, which contains at least 18 other genes. Proteins encoded by these genes bind cell surface frizzled (FZD) and low-density lipoprotein receptor related proteins resulting in activation of a conserved "canonical" signaling pathway (Peifer and Polakis, 2000). The Wnt signaling through proteins such as Wnt6, Wnt10a and Wnt10b play an important role in development and maintenance of many organs and tissues including bones (Cadigan and Nusse, 1997; Cawthorn *et al.,* 2012). The role of Wnt signaling pathway has been investigated in the developing limb bud that controls multiple processes such as limb patterning and limb morphogenesis. Several Wnt genes such as *WNT3, WNT4, WNT6, WNT7A, WNT7B, WNT9B, WNT10A, WNT10B* and *WNT16* are highly expressed in the ectoderm and apical ectoderm ridge (AER) during early limb development (Witte *et al.*, 2009). Moreover, Wnt signaling plays a critical role in the determining of dorso-ventral limb identity (Galceran *et al.,* 1999). During late limb morphogenesis, Wnt signaling is determining the position and morphology of limb structures such as muscles, tendons and skeletal elements (Yang, 2003). Wnt signaling is also involved in bone formation by regulating chondrogenic differentiation from

mesenchymal progenitors as well as osteoblast proliferation (Hartmann and Tabin, 2001; Rudnicki and Brown, 1997). In null mice Stevens *et al.* (2010) have studied that both alleles of the *WNT10B* gene are required for maintenance of adult bone density and loss of *WNT10B* results in reduction of the numbers of bone marrow-derived mesenchymal progenitors. Andrade *et al.* (2007), and Zhou *et al*. (2008), have shown that WNT10B expresses in several stem cell compartments including, postnatal growth plate, bone marrow, and osteoblastic precursors.

In summary, the study presented in this chapter provided detailed clinical and molecular aspects of hereditary SHFM in three consanguineous families of Pakistani origin. Prior to this investigation, only one family from Pakistan was reported segregating SHFM phenotype. Considering that SHFM6 is the only known autosomal recessive locus known and mapped in Pakistani population therefore, *WNT10B* gene mutation analysis can be included in routine molecular analysis of SHFM phenotype at least in this part of the world. Sequence analysis of the gene in one family presented in the present chapter, failed to detect disease causing mutation. Since genotyping clearly and without any doubt established linkage of the family to SHFM6 locus, it would be interesting to subject DNA from affected members for third generation sequencing. Recently Rehman *et al*. (2014) have shown that occurrence of intra familial locus heterogeneity, including intra-sibship heterogeneity, is not rare and that taking intra-familial locus heterogeneity into account while analyzing pedigree data can increase the success rate in the identification of causal variants for Mendelian traits. It is more likely that this effort will result in revealing a potential sequence variant in intron or other regulatory sequences of the *WNT10B* gene. Presence of second gene involved in causing SHFM phenotype at the same locus cannot be ruled out as well.

Figure 4.1: Pedigree drawing of the family D segregating autosomal recessive congenital SHFM. Clear symbols represents unaffected individuals while filled symbols represent affected individuals. Double line indicates the cousin marriage. The individual numbers labeled with asterisks indicate the samples available for this study.

Figure 4.2: Clinical features of SHFM phenotypes observed in affected members of the family D. Patient (IV-4) showing absence of middle finger, and large proximal phalanx of ring finger in the left hand (a), dysplasia of distal phalanx of index finger and absence of middle phalanx of 3rd middle finger in the right hand (b). Patient (IV-3) showing pre-axial syndactyly of toe 1–2 and post-axial syndactyly of toe 3–4 in patient (c). Patient IV-4 showing a classical cleft foot deformity (d). Radiographic features of left hand of patient IV-4 showing redial ray malformation including hypoplasia of 1st metacarpal, absent middle finger (e), and right hand showing polydactyly, absent phalanx, radial ray hypoplasia (f). Left foot of patient IV-3 showing accessory sesamoid of hallux (g). Right foot of patient IV-4 showing claw foot, hellux valgus, claw toe deformity, basel syndactyly formation, absence of tarsal and metatarsal bones, and prominent 5th metatarsal presenting varus angulation at metatarsophalangeal joint (h). Left foot showing accessory sesamoid of hallux, dysplastic middle and distal phalynx of lesser four toes, and fusion of middle and distal phalynx of the 5th toe.
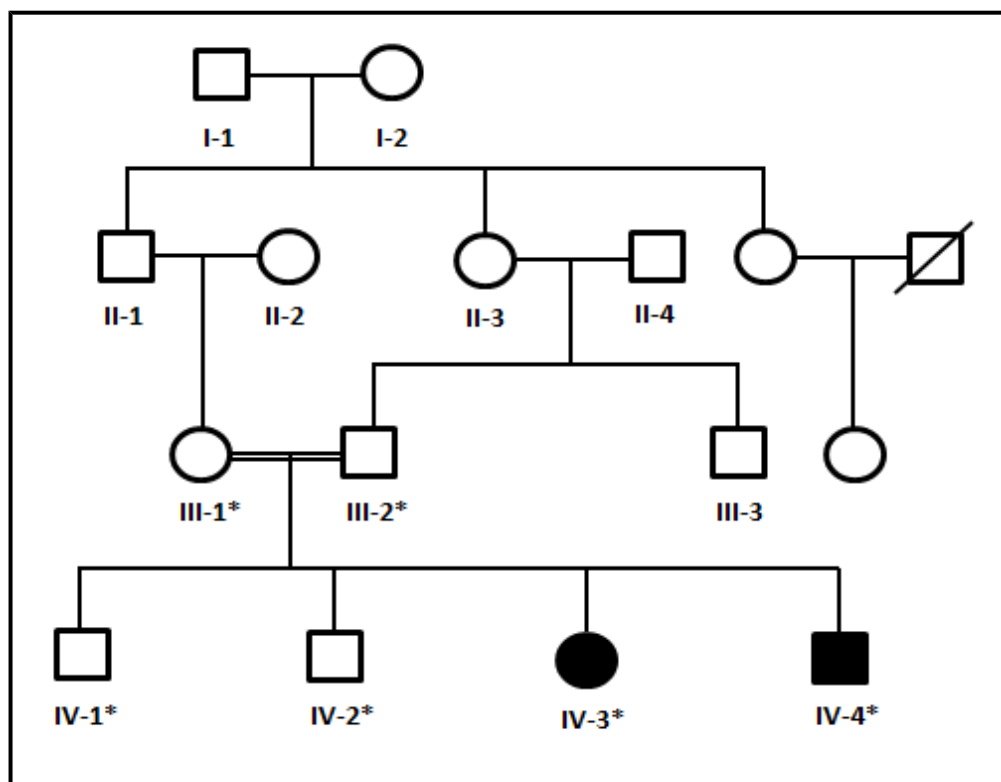
Figure 4.3: Pedigree drawing of the family E segregating autosomal recessive congenital SHFM. Clear symbols represents unaffected individuals while filled symbols represent affected individuals. Symbols with crossed lines represent deceased individuals. Double lines indicate a cousin marriage. The individual numbers labeled with asterisks indicate the samples available for this study.
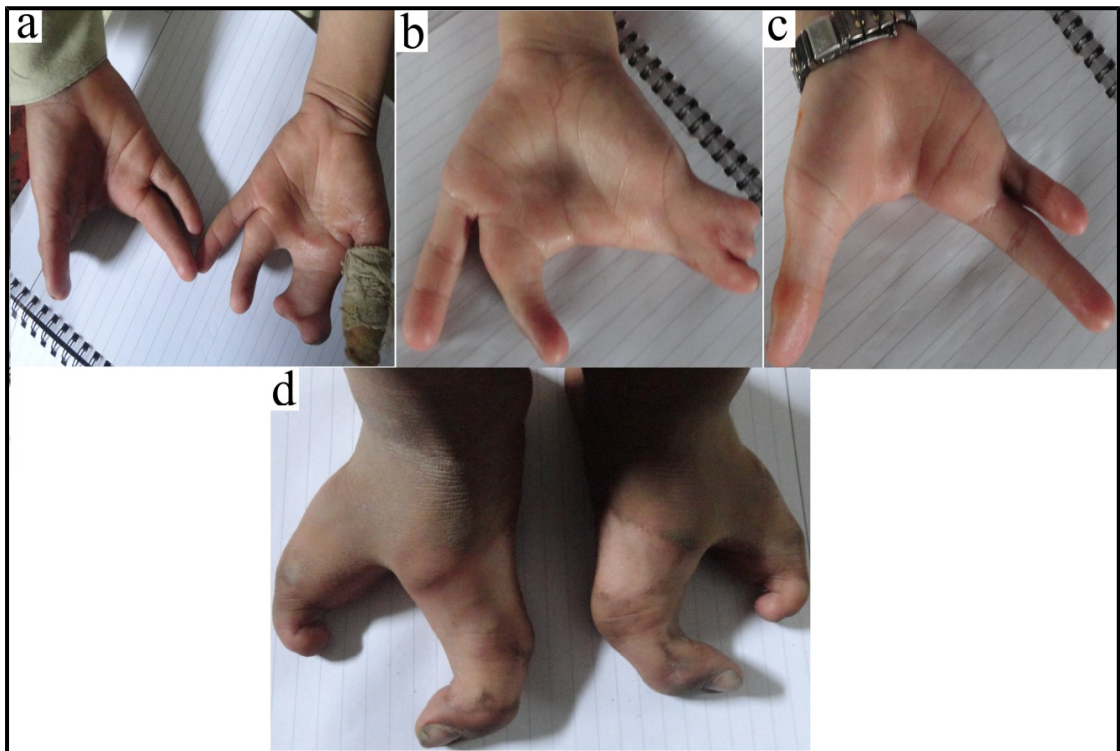
Figure 4.4: Clinical features observed in affected individuals in the family E. Patient (IV-4) showing cleft hand deformity associated with central type of syndactyly in left hand and absence of central digit in right hand (a). Patient (IV-3) exhibiting cleft hand deformity with pre-axial syndactyly and radial deviation of ring finger (b). Patient (IV-3) with cleft hand deformity of central type (c). Patient (IV-4) showing cleft foot deformity i.e. central deficiency and hallux valgus deformity of big toe and varus deformity of lessor toe (d).
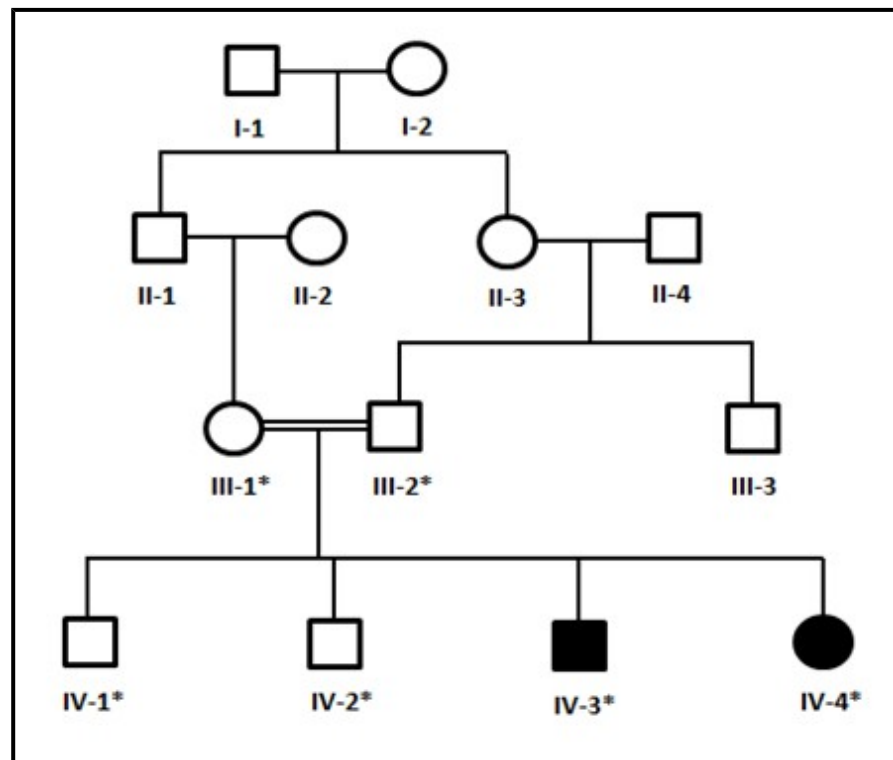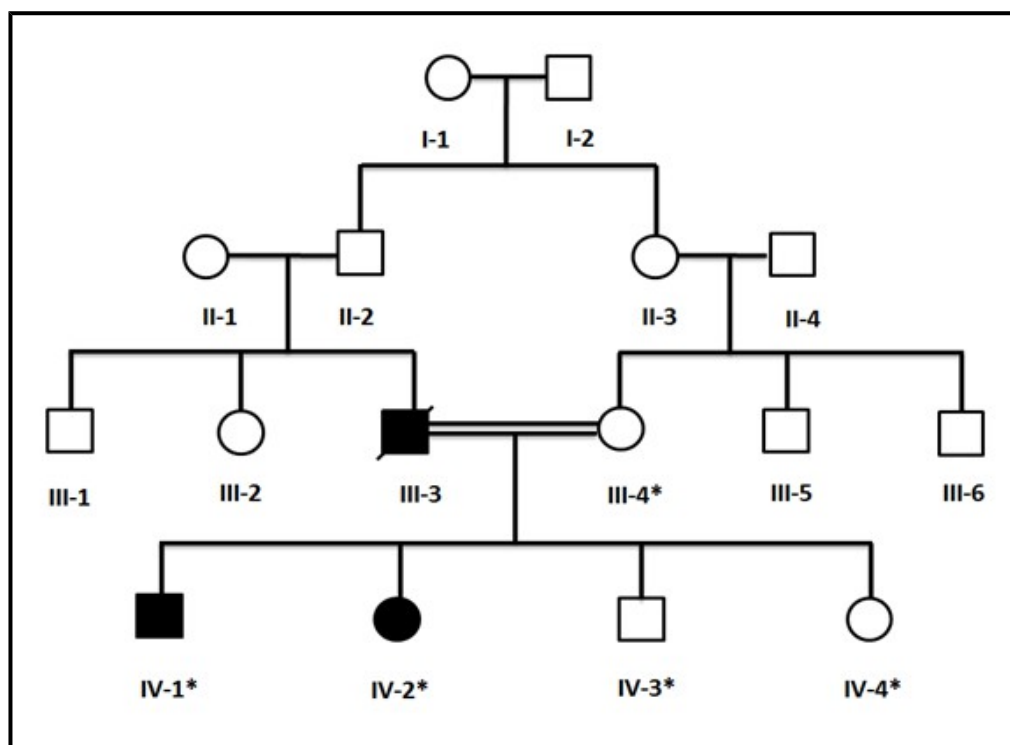
Figure 4.5: Pedigree drawing of the family F segregating autosomal recessive congenital SHFM. Clear symbols represents unaffected individuals while filled symbols represent affected individuals. Symbols with crossed lines represent deceased individuals. Double line indicates the cousin marriage. The individual numbers labeled with asterisks indicate the samples available for this study.
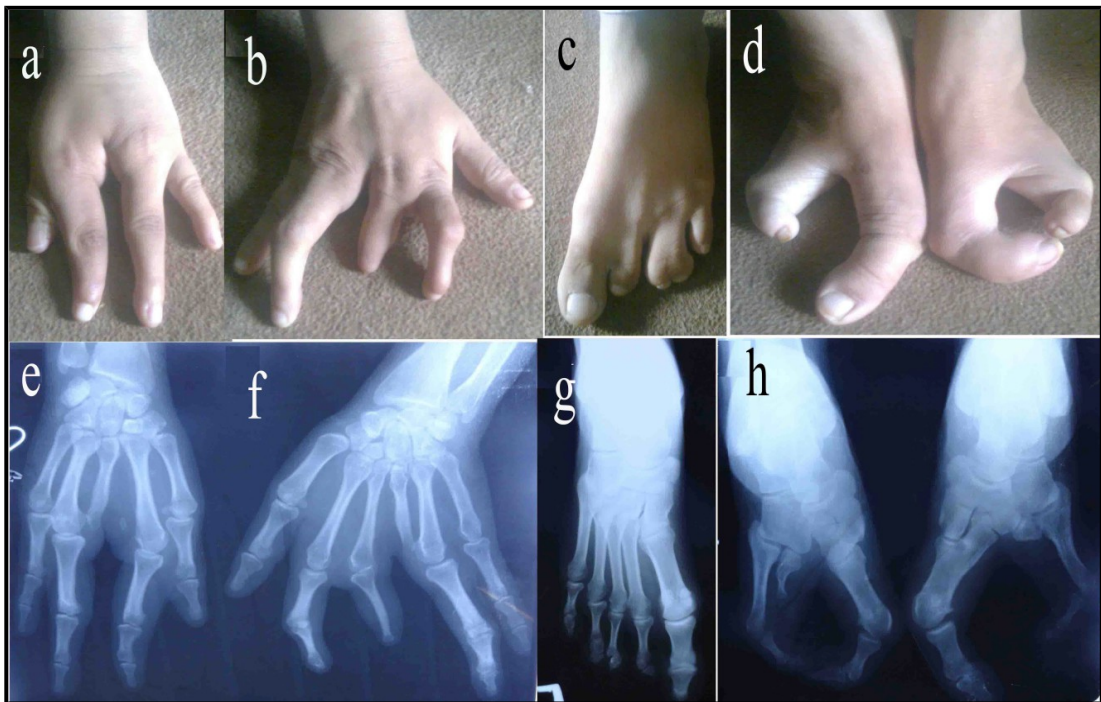
Figure 4.6: Clinical features observed in affected individuals in the family F. Patient (IV-1) showing syndactyly of 3rd and 4th toes (a), central type of polydactyly along with syndactyly in the right foot (b). Patient (IV-2) showing dysplastic cleft hand associated with camptodactyly of a little finger, and central ray radial deficiency (c, d). Patient (IV-2) showing cleft foot characterized by central deficiency with rudimentary bud of lesser toe (e). Patient (IV-2) demonstrating cleft foot with central deficiency and hallux valgus deformity (f).
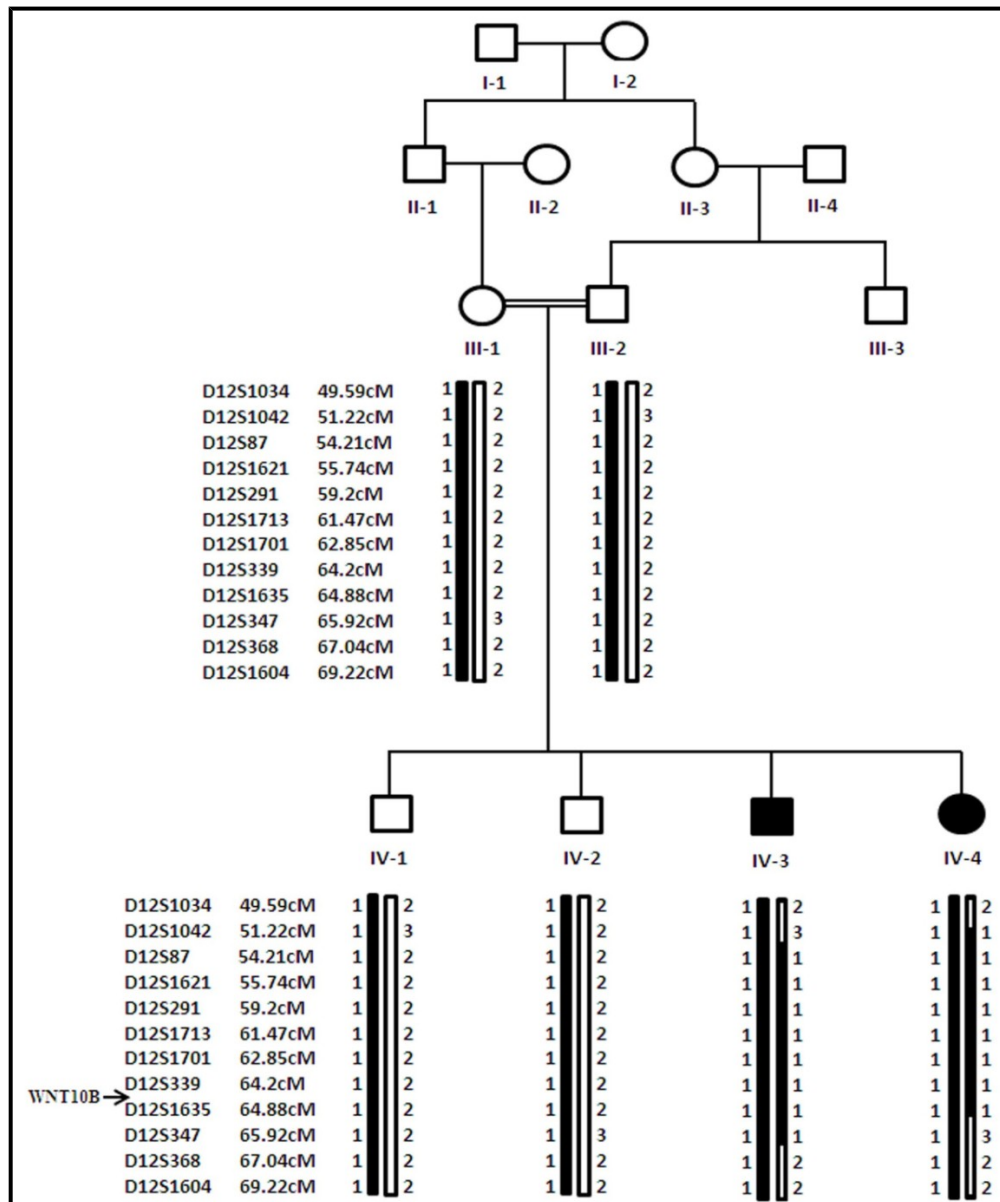
Figure 4.7: Haplotype of family D segregating SHFM6. Alleles forming the risk haplotype are shaded black, while alleles not co-segregating with the disease are shown in white. Disease-interval is flanked by markers D12S1042 and D12S347. Genetic distances in centi-Morgans (cM) are depicted according to the Rutgers combined linkage-physical map (Build 36.2) (Matise *et al.,* 2007).
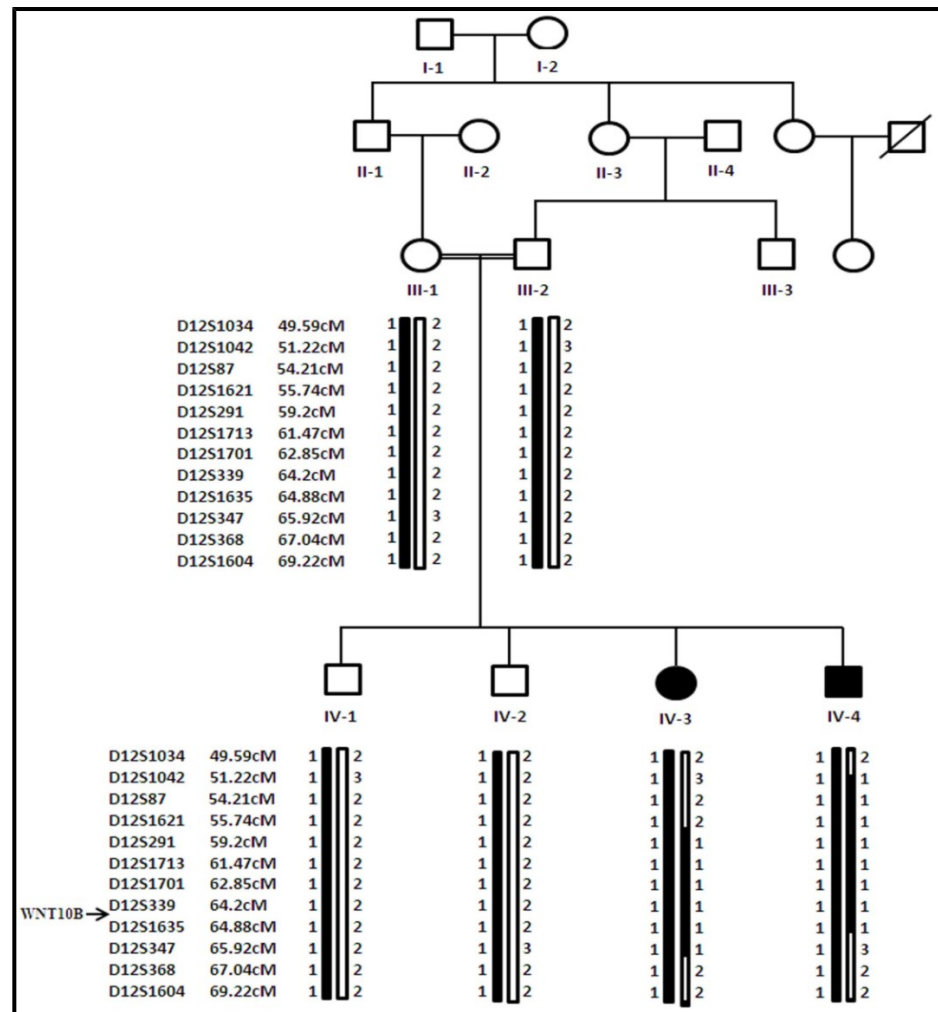
Fig. 4.8: Haplotype of family E segregating SHFM6. Alleles forming the risk haplotype are shaded black, while alleles not co-segregating with the disease are shown in white. Disease-interval is flanked by markers D12S1621 and D12S347. Genetic distances in centi-Morgans (cM) are depicted according to the Rutgers combined linkage-physical map (Build 36.2) (Matise *et al.,* 2007).
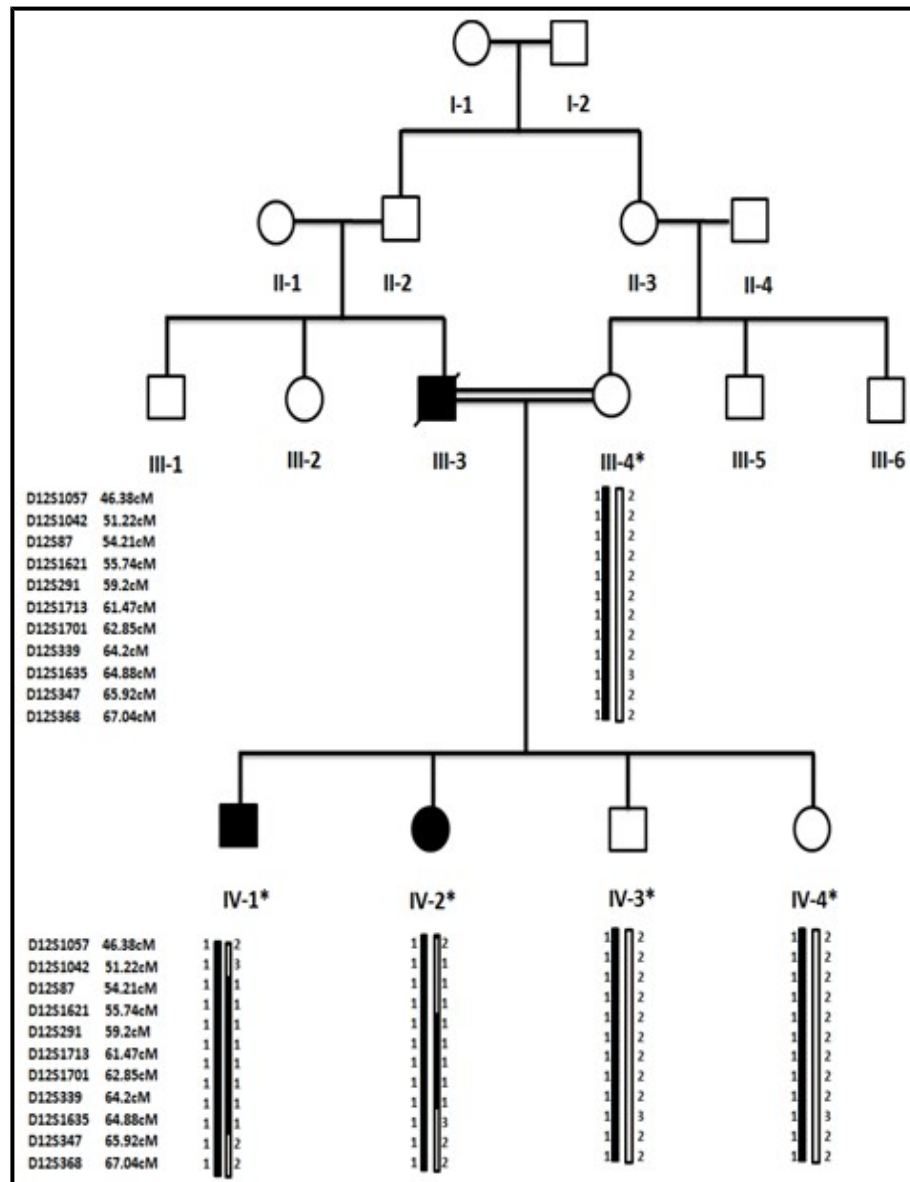
Figure 4.9: Haplotype of family F segregating SHFM6. Alleles forming the risk haplotype are shaded black, while alleles not co-segregating with the disease are shown in white. Disease-interval is flanked by markers D12S1621 and D12S1635. Genetic distances in centi-Morgans (cM) are depicted according to the Rutgers combined linkage-physical map (Build 36.2) (Matise *et al.,* 2007).
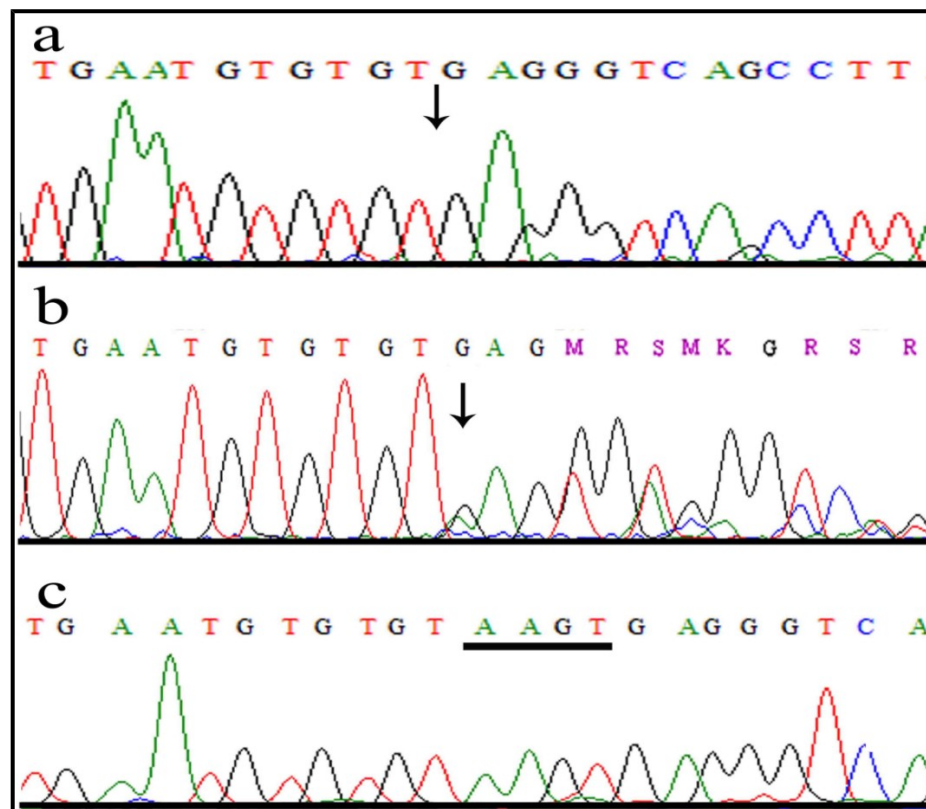
Figure 4.10: Sequence analysis of a novel mutation in the gene *WNT10B*. A 4-bp deletion (c.1165_1168delAAGT) identified in the family D. The upper panel (a) represent the nucleotide sequences in the affected individuals, the middle panel (b) in the heterozygous carriers and the lower panel (c) in the unaffected individuals. The 4-bp underlined in panel c represents the sequence deleted in affected individuals in the family in the panel (a).
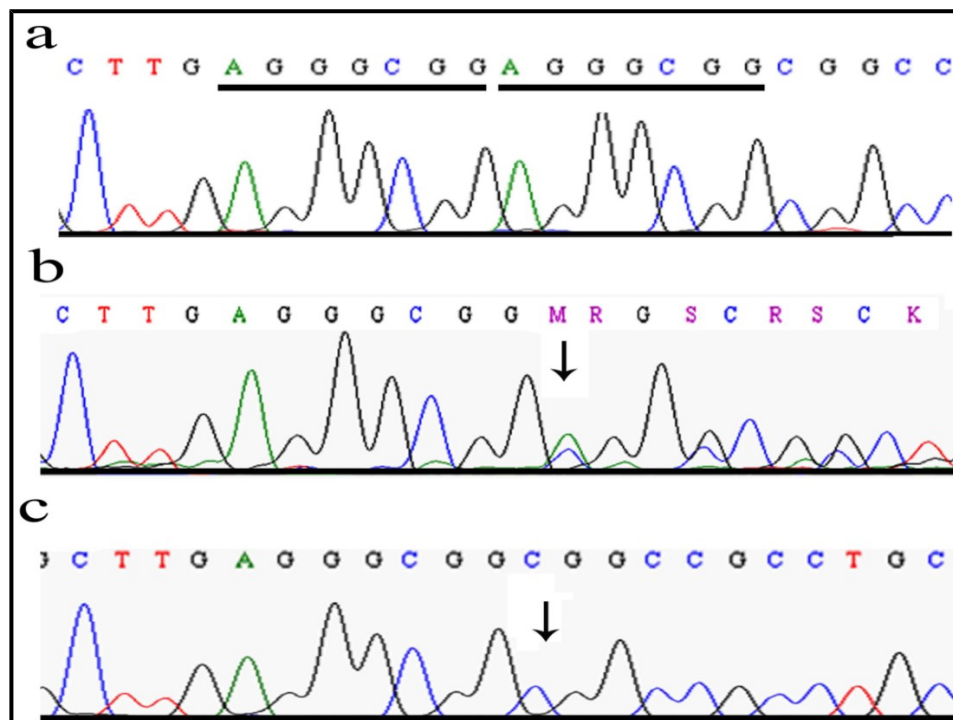
Figure 4.11: Sequence analysis of a novel mutation in the gene *WNT10B*. 7-bp duplication (c.300_306dupAGGGCGG) detected in family E. The upper panel (a) represents the nucleotide sequences in the affected individuals, the middle panel (b) in the heterozygous carriers and the lower panel (c) in the unaffected individuals. The 7-bp sequence underlined in panel (a) represents the sequence duplicated in the affected individuals in the family.
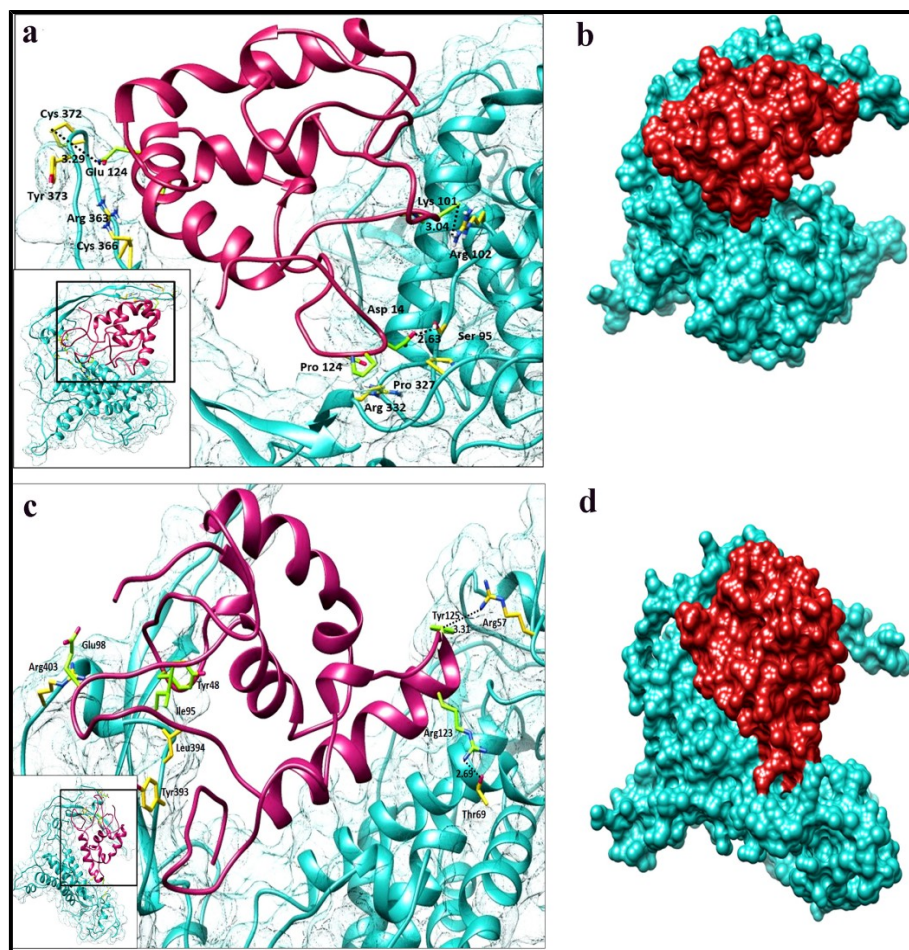
Figure 4.12: Visualization of the best docked WNT10B-Fz8 complex normal WNT10B represented by cyan color ribbons (a). Surface view of normal WNT10B (b). Mutated WNT10B represented by cyan color ribbons (c) and surface view of mutated WNT10B (d). Interacting residues are shown in atomic representations and H-bonds are shown by dotted black lines. H-bond distances are indicated in Å.

Chapter 5

ELLIS-VAN CREVELD SYNDROME

Clinical and Molecular Characterization of Human Hereditary Skeletal Disorders in Consanguineous Families

ELLIS-VAN CREVELD SYNDROME

Ellis–van Creveld syndrome (EvC, MIM 225500) is an autosomal recessive skeletal dysplasia, first described by Richard Ellis and Simon Van Creveld in 1940 (Zangwill *et al*., 1998). EvC syndrome is commonly observed in Amish community of Lancaster, Pennsylvania, where the incidence is estimated to be 5/1000 live births as compared to 7/10,00,000 in non-Amish population (Stoll *et al*., 1989; Dugoff *et al*.,2001). Since 1940 large number of cases of the syndrome has been reported in different ethnic groups including at least four in Pakistani population.

Congenital heart defects occur in 50–60% of EvC cases, and are a major cause of reduced life expectancy (Digilio *et al.,* 1999). AVCD (Atrioventricular Canal Defect), CA (Common Atrium), LSVC (Left Superior Vena Cava) and pulmonary venous abnormalities are most commonly heart defects reported in EvC patients (Digilio *et al*., 1999; Hills *et al.,* 2011). In addition to cardiac abnormalities, several different forms of skeletal defects have been reported as well. This include disproportionate dwarfism with short ribs and exceptionally long and narrow trunk, distal shortening of upper and lower limbs, short broad hands with bilateral postaxial polydactyly type A, partial cutaneous syndactyly and genu velgum. The radiographic analysis identified short middle and distal phalanges, coned shaped epiphysis, hamate and capitate bone fusion, mild bowing of humerus, complete or partial fusion of metacarpal and metatarsal bones, fusion of proximal tibia and fibula (Ulucan *et al*., 2008; Vinay *et al*., 2009; Kalsoom *et al*., 2010). Oral and dental anomalies associated with EvC are maxillary and mandibular labiogingival adherences causing a lip to present a V shaped notch in the mid line, submucosal clefts, multiple frenula, dystrophic philtrum, hypodontia, conical and microdontic teeth, natal and neonatal teeth, malocclusion, delayed teeth eruption and enamel hypoplasia (Sarnat *et al*., 1980; Deborah *et al*., 1988; Hunter and Roberts, 1998; Atasu and Biren, 2000; Cahuana *et al*., 2004; Tompson *et al*., 2007; Ulucan *et al*., 2008; Kalsoom *et al*., 2010). Nearly nails in all the EvC patients are short, thin, hypoplastic and often spoon shaped (Al-khenaizan *et al*., 2001; Gorlin *et al*., 2001; Kalsoom *et al*., 2010).

Ellis-van Creveld syndrome is caused by mutations in two genes, *EVC* (MIM 604831) and *EVC2* (MIM 607261), arranged in head to head configuration and separated by 2.6 kb genomic sequence on chromosome 4p16 (Ruiz-Perez *et al.,* 2003). The *EVC*

and *EVC2* express in the heart, kidney, lungs and developing bones. In bones, the expression was observed in the developing vertebral bodies, ribs and both upper and lower limbs being higher in the distal limbs compared with the proximal limbs (Ruiz-Perez *et al.,* 2000). The EvC phenotype caused by mutations in either of the two genes is indistinguishable, which indicates that both the genes are involved in common signaling pathway (Tompson *et al*., 2007; Valencia *et al.,* 2009).

Both EVC and EVC2 act as positive regulators of hedgehog (hh) signal transduction pathway by localizing at the basal body and membrane of chondrocyte cilia, in a co-dependent manner. Their co-localization requires the interaction between the intracellular C-terminus portions of EVC and EVC2 (Ruiz-Perez *et al.,* 2007; Blair *et al*., 2011). *EVC* is also expressed in the primary cilia of osteoblasts thus transducing the hh signals in osteoblast. Pacheco *et al*. (2012) have reported that EVC is involved in promoting chondrocyte proliferation and hypertrophy, and differentiation of osteoblasts in the perichondrium. These authors have further shown normal Indian hedgehog (Ihh) expression in *EVC* knockout mice but reduced expression of Ihh downstream targets *Ptch1*, *Gli1* and *Pthrp* in chondrocytes. Due to low Pthrp level, the proliferation rate of chondrocytes was reduced thus causing them to become hypertrophic prematurely. Additionally, onset of osteoblastogenesis was delayed and expression of the transcription factor Runx2, a principal trigger of osteoblast differentiation and a perichondrial target of Ihh signaling, was also reduced in the perichondrium.

Pakistani Consanguineous Families with EvC Syndrome

Three consanguineous families (G, H, I), segregating Ellis–van Creveld syndrome, were ascertained from different areas of the country. They were clinically and genetically characterized and the results obtained are made part of the present chapter of the dissertation. Summary of the clinical features noted in affected members of the three families are presented in Table 5.1.

Family G

This family with clinical manifestations of EvC syndrome was recruited from Rawalpindi District of Pakistan. Rawalpindi is one of the most populated cities and situated next to Islamabad, Capital of the country. Analysis of the family pedigree

drawing (Figure 5.1) provided convincing evidence of an autosomal recessive mode of inheritance of the phenotype. Affected individuals (IV-3, IV-4) in the family were the product of first cousin marriage (III-1, III-2). For DNA analysis, blood samples were obtained from two affected (IV-3, IV4) and four unaffected (III-2, III-3, IV-1, IV-2) individuals of the family.

Clinical Features

Two affected individuals of the family including a 3.5 years old girl (IV-3) and her 7 months old brother (IV-4) were born after normal pregnancies. They were short stature, had low set shoulders, and bilateral postaxial polydactyly of hands. Their hands were broad and swollen with short misaligned fingers. Fingernails were short, hypoplastic and absent on both sixth fingers (Figure 5.2).

Electrocardiography of the affected individual (IV-4) showed partial atrioventricular septal defect (Figure 5.2g). Teeth abnormalities were observed in both the patients. In individual IV-3, serrated teeth and missing maxillary lateral incisors and right central incisor were found. High arch palate and gum hypoplasia were also present (Figure 5.2a). In individual IV-4, facial features including short/thin upper lips, short multiple frenula, irregular alveolar ridge and long philtrum were observed. Neonatal teeth were present while lateral incisors were missing. Macroglossia was visible in the infant, however the mucous membrane under the tongue was short (ankyloglossia). Sweating and hair were normal in both the patients. Radiological study of an affected individual (IV-4, Figure 5.2f) revealed bilateral rhizomelia of the humerus and short ribs with narrow chest.

Family H

This is the second family, H, with EvC syndrome, recruited from Rawalpindi District of the country. The family has two affected (IV-2, IV-3) and four unaffected (III-1, III-2, IV-1, IV-4) individuals (Figure 5.3). The blood samples were obtained from both affected and unaffected individuals of the family.

Clinical Features

Two affected individuals of the family (IV-2, IV-3) were clinically examined at local government hospital. Both the affected individuals were born after normal pregnancies. Broad swollen hands with short misaligned fingers, bilateral postaxial

polydactyly, short hypoplastic finger nails were observed in both the affected members (Figure 5.4). Ankyloglossia or tongue-tie and macroglossia were prominent in the affected individuals. Gum hypoplasia, high arch palate, short/thin upper lips, irregular alveolar ridge and long philtrum were observed. Bilateral rhizomelia of the hands, short ribs with narrow chest and distended abdomen were present. Radiographs of the affected individual IV-2 were not available. Electrocardiography did not identify any cardiac abnormality. Slight variation in dental anomalies was observed in the two patients.

Family I

Family I (Figure 5.5) belongs to a remote area in district Kohat of Khyber Pakhtunkhwa (KPK) province of the country. Similar to two other families (G and H) affected members in this family also showed segregation of EvC phenotype in the autosomal recessive pattern. For genetic analysis, blood samples were obtained from one affected (IV-5) and five unaffected individuals (III-2, III-3, III-4, IV-2, IV-3) of the family.

Clinical Features

Lone affected individual (IV-5) in the family showed several well characterized features of EvC syndrome. He was short statured, had low set shoulders, developed deformity of legs and knees called genu valgum, and bilateral postaxial polydactyly of hands and feet. His hands were broad with short misaligned fingers. Fingernails were short, dystrophic and also present on both the sixth fingers. He had no facial dysmorphic features except for a relatively narrow and long face. Feet were broad and swollen with thick nails and the great toe was laterally deviated (Figure 5.6). Electrocardiography did not identify any cardiac abnormality. Slight variation in dental anomalies was observed in the patient. Ankyloglossia or tongue-tie was prominent in the individual and this could be the contributing factor to his speech problem. Additionally, fissured tongue and connective tissue deposition in the gums were also observed.

Sweating, skin, eyes and heart abnormalities were missing in the affected individual of the family. Parents of the affected individual showed no abnormalities and were healthy like other normal individuals of the family.

Genotyping and Sequencing *EVC and EVC2* Genes

Linkage in the three families (G, H, I) was tested by genotyping microsatellite markers mapped in the known locus of EvC syndrome on chromosome 4p16. The markers flanking the region, encompassing both *EVC* and *EVC2* genes, and typed in the three families are presented in the Table 2.1. Affected individuals in the families were homozygous for nine markers (D4S90, D4S343, D4S2957, D4S2285, D4S2366 D4S3007, D4S394, D4S545, D4S2983) in the region. Analysis of the haplotypes provided convincing evidence of linkage in the two families (G and H) to the EvC genes (Figure 5.7, 5.8). In the third family (I), nine typed markers showed heterozygous pattern of alleles thus predicting the involvement of another gene in causing EvC syndrome (Figure 5.9).

The *EVC* and *EVC2* genes were sequenced using genomic DNA available from affected and unaffected members in the two families (G and H) as described in Materials and Methods. The primers used for amplification of *EVC* and *EVC2* genes are listed in Table 2.3 and 2.4, respectively.

In family G, sequence analysis detected a novel nonsense mutation involving transition of G to A at nucleotide position 702 (c.702G>A) in exon 8 of the *EVC2* gene in both affected individuals. This resulted in substitution of a codon for amino acid tryptophan with a premature stop codon (p.Try234*) (Figure 5.10). In family H, sequence analysis identified 15-bpduplication (c.1932_1946dupAGCCCTCCGGAGGCT) in exon 14 of the *EVC* gene (Figure 5.11). Both the mutations, identified here, were present in heterozygous state in the obligate carriers of the family.

To exclude non pathogenic nature of the two mutations identified in exons 8 and 14 of the *EVC*2 and *EVC* genes in the two families (G and H), genomic DNA collected from 250 ethnically matched control individuals was sequenced and these were not identified outside the families.

Discussion

This chapter describes detailed clinical and molecular analysis of three families (G, H, I) segregating autosomal recessive form of EvC syndrome. Several cases of the syndrome have been reported in families originating from different ethnic groups

around the world. However, prior to this study, from Pakistan only one family with EvC syndrome has been reported (Kalsoom *et al.*, 2010). Two of the families, in the present study, showed disease causing novel sequence variants in the *EVC* and *EVC2* genes. However, the third family with EvC syndrome failed to show linkage to the known genes suggesting presence of another gene in the human genome causing EvC syndrome.

The EvC related features observed in affected members of the three families, characterized here, included cardiac defect, upper-lip defect, long philtrum, neonatal teeth, short stature, broad swollen hands with short misaligned fingers, postaxial polydactyly of hands, hypodontia, serrated teeth, multiple oral frenula, tongue-tie (ankyloglossia), macroglossia, irregular alveolar ridge, short, hypoplastic nails, bilateral rhizomelia of the humerus and short ribs with narrow chest. The partial atrioventricular septal defect and multiple oral frenula observed in affected members of family G were not present in affected members of family H and I. Some of the most commonly reported features associated with EvC syndrome including cone shaped epiphysis of phalanges, fusion of the capitate and hamate bones of the wrist, bowing of the humerus and fusion of the proximal tibia and fibula were not observed in the patients described here. High arch palate was observed in all the affected individuals of the two families (G, H) which were not reported previously.

Establishing linkage of the two families (G, H) on chromosome 4p16 followed by DNA sequencing led to the identification of a novel mutation each in *EVC2* and *EVC* gene. A nonsense mutation (p.Trp234*) in *EVC2* and 15-bpduplication (c.1932_1946dupAGCCCTCCGGAGGCT) in the *EVC* gene were detected in family G and H, respectively.

The *EVC2* gene holds 22 coding exons spanning 150 kb on genomic DNA. The gene encoding 1,308 amino acids protein, predicted to have a transmembrane segment, three coil coiled regions, and a RhoGEF domain (Schultz *et al.,* 1998; Letunic *et al.,* 2002; Ruiz-Perez *et al.,* 2003). The other gene *EVC* contains 21 coding exons spanning 120 kb on genomic DNA and gives rise to 992 amino acids protein with three putative nuclear localization signal sequences (82-88, 249-255, 923-939 amino acids), a leucine zipper motif (635-656 amino acids) and a putative transmembrane domain (27-47 amino acids) (Ruiz-Perez *et al.,* 2000). *EVC* and *EVC2* are arranged in

a divergent orientation separated by 2.6 kb on genomic sequence. The two genes encode proteins with no significant homology to each other or to any other protein (Ruiz-Perez *et al.*, 2003).

To date, several mutations have been reported in both *EVC2* and *EVC* genes. Majority of the mutations are either of nonsense type or frameshift introducing premature nonsense codons and, thus are likely to be considered as loss of function mutations (Tompson *et al.,* 2007; Ruiz-Perez and Goodship, 2009). A novel nonsense mutation (p.Trp234*), identified in *EVC2* gene in the family G, predicts an absence of functional mRNA following nonsense mediated mRNA decay, and absence of functional protein. The other mutation, 15-bp duplication (c.1932_1946dupAGCCCTCCGGAGGCT), identified in the *EVC* gene in the family H, adds 5 additional amino acids and therefore predicts to disrupt the leucine zipper motif in DNA-binding region of the protein. The leucine zipper motif encodes by *EVC* gene play dual role in the replication process in the nucleus. It promotes RepA-RepA interaction in the dimerization and cooperativity at oriV, and interaction between RepA and other host replication factors involved in replication (García-de-Viedma *et al.,* 1996).

The two mutually dependent endogenous ciliary proteins Evc and Evc2 play a key role in the Sufu/Gli3 dissociation and Gli3 recruitment to the cilium tip through direct interaction with Smo and in this manner modulate Hh signaling. Simultaneously, Evc and Evc2 appear to be needed for the activation of pathway in the absence of Sufu (Caparrós-Martín *et al.,* 2013). EVC syndrome shares some phenotypic similarities with oral-facial-digital-syndrometype-1 (OFDI) such as orofacial and nail abnormalities and cardiovascular defects. It has been suggested that SHH signaling pathway is disrupted in both EVC and OFDI as the protein mutated in OFD1 plays a role in ciliogenesis (Ferrante *et al.,* 2006; Goddeeris *et al.,* 2008).

In conclusion, the study presented here, have revealed two novel disease causing mutations in the *EVC2 and EVC* genes, which further extend the spectrum of mutation in these genes resulting in the EvC syndrome. This is only the second study describing EvC syndrome in Pakistani population. In addition to identifying novel mutations, another interesting aspect of the present study is the characterization of EvC syndrome in a family which is not linked to *EVC* and *EVC2* genes. Although,

due to short of time, an attempt was not made to scan the human genome to find the disease causing gene in this family but at least this reflects the presence of one more gene for this syndrome in the human genome.

Table 5.1: Clinical Features of affected individuals of family G, H and I

Clinical features	Family H		Family I		Family J
	IV-3	IV-4	IV-2	IV-3	III-5
Cardiac defects					
partial atrioventricular septal defect	+	+	-	-	-
Skeletal features					
Postaxial polydactyly of hands	+	+	+	+	+
Postaxial polydactyly of feet	-	-	-	-	+
Short stature	+	+	+	+	+
Limb shortening	+	+	+	+	-
Narrow chest	+	+	+	+	+
Nail hypoplasia	+	+	+	+	+
Dysplastic nails	+	+	+	+	+
Facial Features					
Short/thin upper lip	+	+	+	+	-
Short/multiple frenula	+	+	-	-	-
Irregular alveolar ridge	+	+	+	+	-
High arch palate*	+	+	+	+	-
Hypodontia	+	+	+	+	-
Natal teeth	+	-	+	-	-
Macroglossia	+	+	+	+	-
Ankyloglossia	+	+	+/-	+/-	+
Short broad nose	+	+	+	+	-
Long philtrum	+	+	+	+	-
Radiological Features					
Short long bones	+	+	+	+	-
Short ribs with narrow chest	+	+	+	+	+

In the columns describing the patients + indicates a feature is present and – indicates a feature is absent. In the column describing features * indicates novel findings.

Figure 5.1: Pedigree drawing of the family G with autosomal recessive Ellis-van Creveld (EvC) syndrome. Squares and circles represent males and females, respectively. Clear symbols represents unaffected individuals while filled symbols represent affected individuals. Double line indicates consanguineous union. The individual numbers labeled with asterisks indicate the samples available for this study.

Figure 5.2: Clinical features of EvC syndrome observed in the family G. Patient (IV-3) showing hypodontia with serrated teeth, missing maxillary lateral and right central incisor, high arch palate and gum hypoplasia (a). Patient (IV-3) showing bilateral postaxial polydactyly of hands, which are broad and swollen with short misaligned fingers (b). In the same patient, fingernails are short, hypoplastic and absent on both the sixth fingers(c). Patient IV-4 showing neonatal teeth, missing lateral incisors, short multiple frenulum's and irregular alveolar ridge (d). In the same patient (IV-4), small thin upper lips, and long philtrum can be noted (e). Radiological study of an affected member (IV-4) revealed bilateral rhizomelia of the humerus and short ribs with narrow chest (f). Electrocardiography analysis of the affected individual (IV-4) revealed partial atrioventricular septal defect (g).
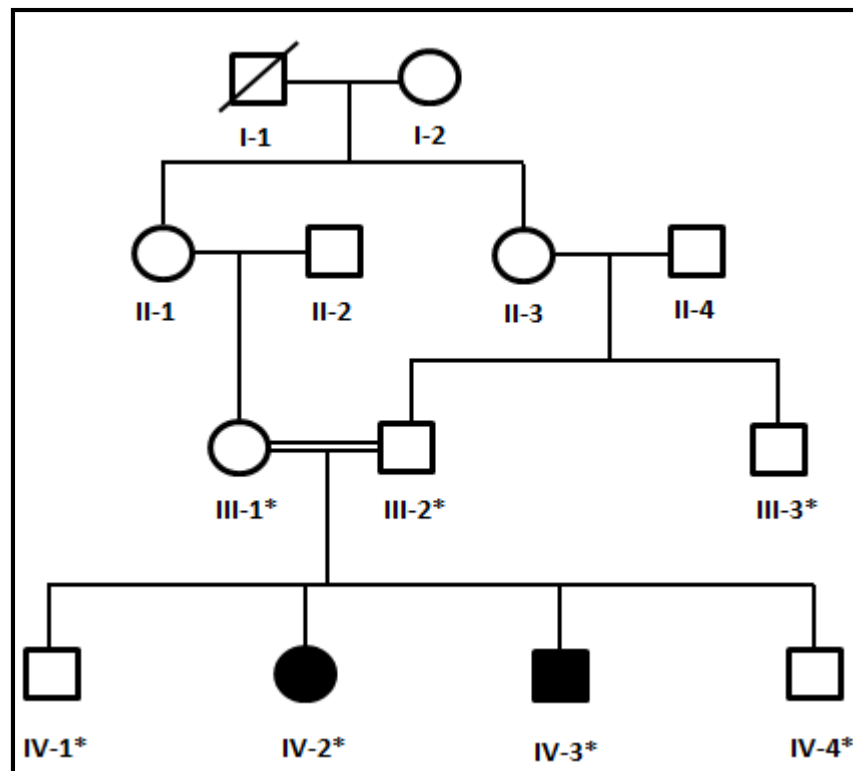
Figure 5.3: Pedigree drawing of the family H with autosomal recessive Ellis-van Creveld syndrome. Squares and circles represent males and females, respectively. Clear symbols represents unaffected individuals while filled symbols represent affected individuals. Symbols with crossed lines represent deceased individuals. Double line indicates consanguineous union. The individual numbers labeled with asterisks indicate the samples available for this study.
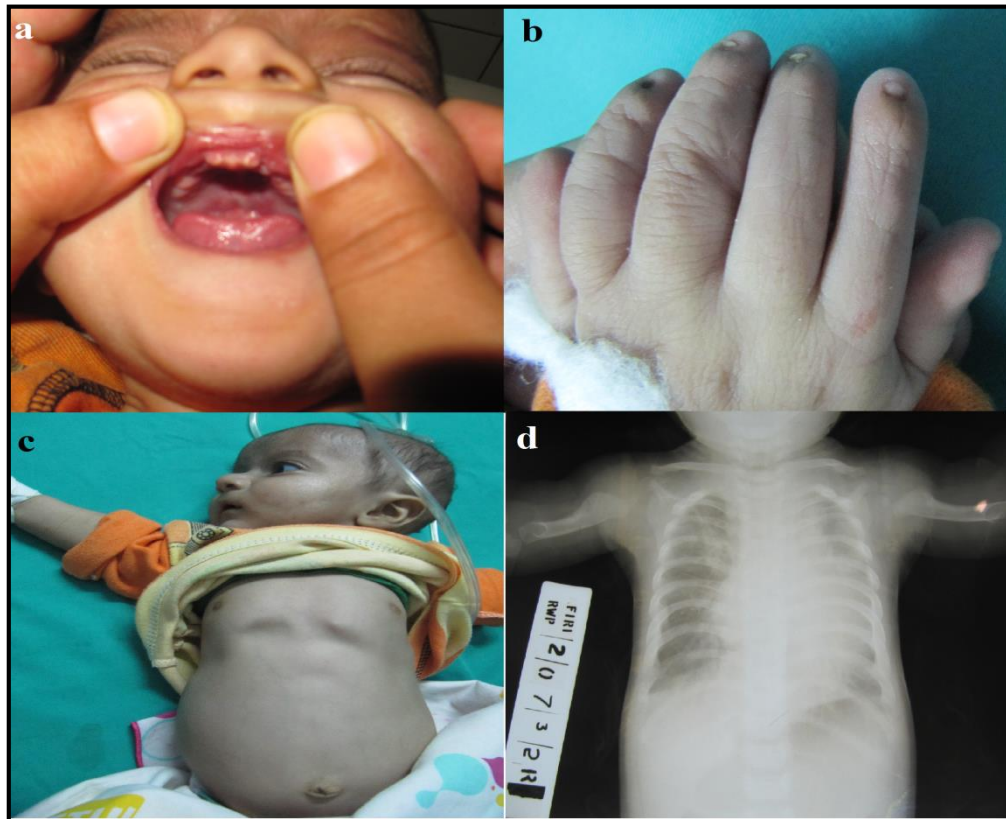
Figure 5.4: Clinical features of EvC syndrome observed in the family H. Patient (IV-3) showing ankyloglossia or tongue-tie and macroglossia, gum hypoplasia, high arch palate, neonatal teeth, missing lateral incisors and irregular alveolar ridge (a). The same patient (IV-3) showing bilateral postaxial polydactyly of hands, broad and swollen hands with short misaligned fingers, short fingernails which are hypoplastic (b), narrow chest and distended abdomen (c). Radiological study of the patient (IV-3) revealed bilateral rhizomelia of the humerus and short ribs with narrow chest (d).
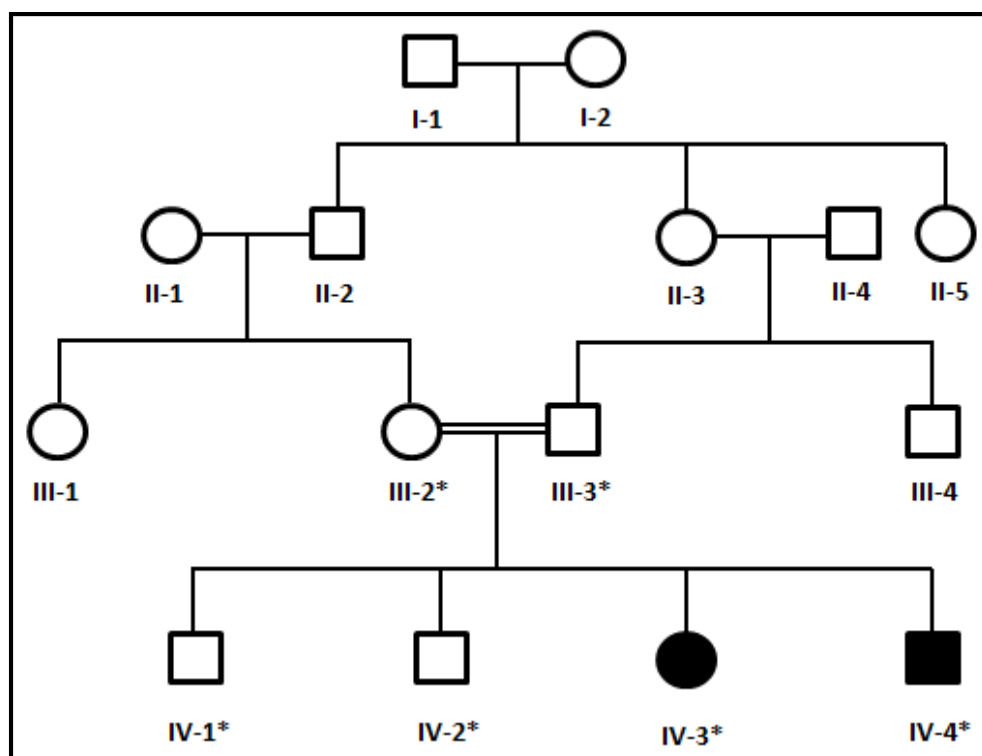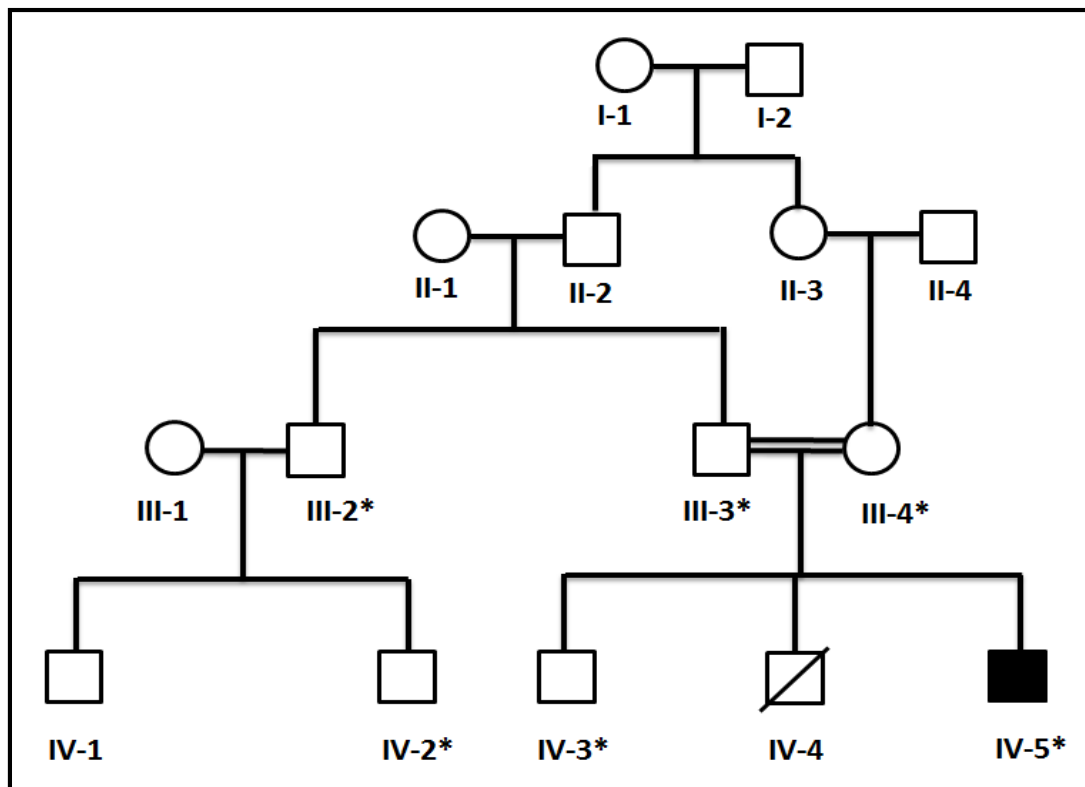
Figure 5.5: Pedigree drawing of the family I with autosomal recessive Ellis-van Creveld syndrome. Squares and circles represent males and females, respectively. Clear symbols represents unaffected individuals while filled symbols represent affected individuals. Symbols with crossed lines represent deceased individuals. Double line indicates consanguineous union. The individual numbers labeled with asterisks indicate the samples available for this study.

Figure 5.6: Clinical features of EvC syndrome observed in the family I. Patient (IV-5) showing broad and short hands with postaxial polydactyly associated with camptodactyly of ring finger (a). The same patient (IV-5) showing relatively narrow and long face, short stature, and low set shoulders (b), broad feet with thick nails and the great toe laterally deviated and postaxial polydactyly (c).
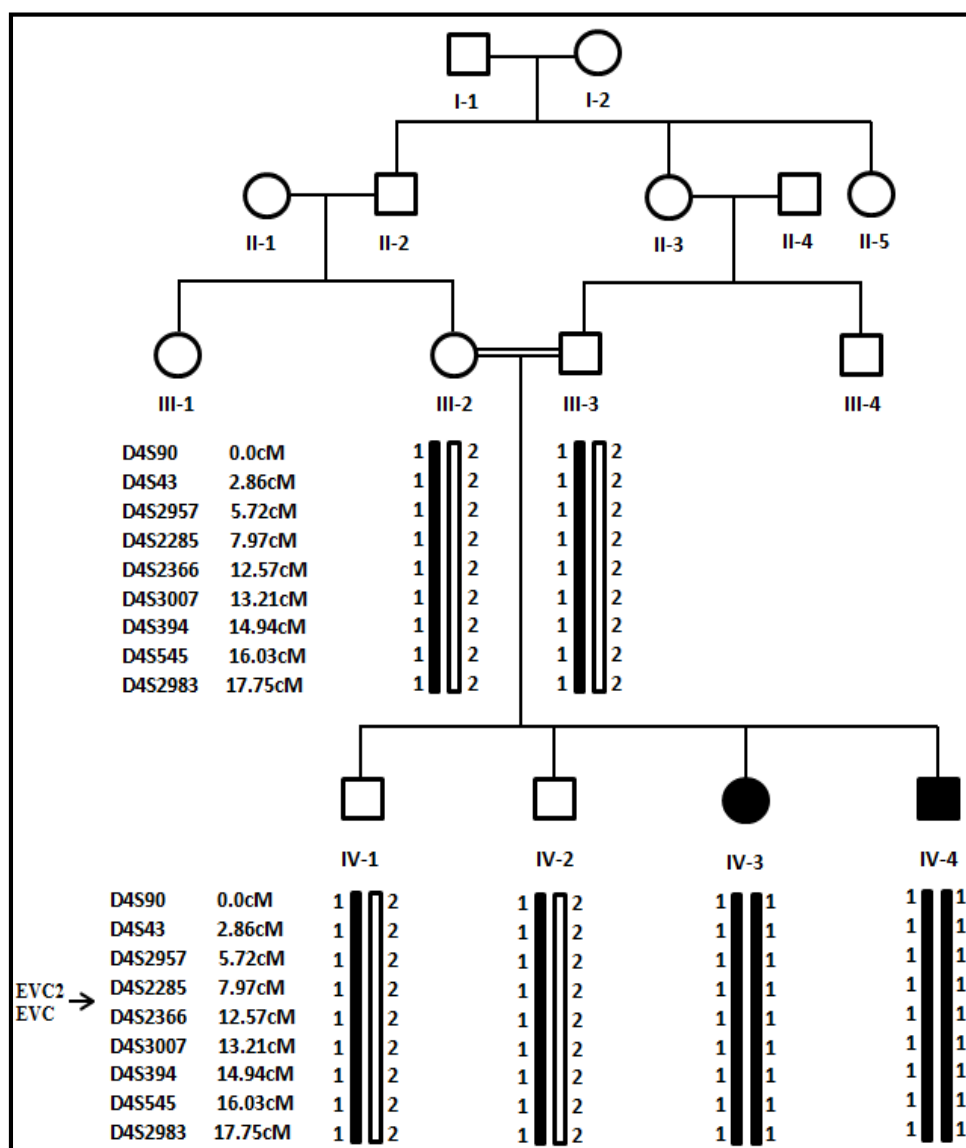
Figure 5.7: Haplotype analysis of the family G segregating autosomal recessive Ellis-van Creveld syndrome. Haplotypes of the most closely linked microsatellite markers are shown below the genotyped individuals. Black bars indicate disease haplotype. The genetic positions (centi-Morgan) and arrangement of microsatellite markers is according to Rutgers combined linkage physical map built 36.2 (Matise *et al*., 2007).
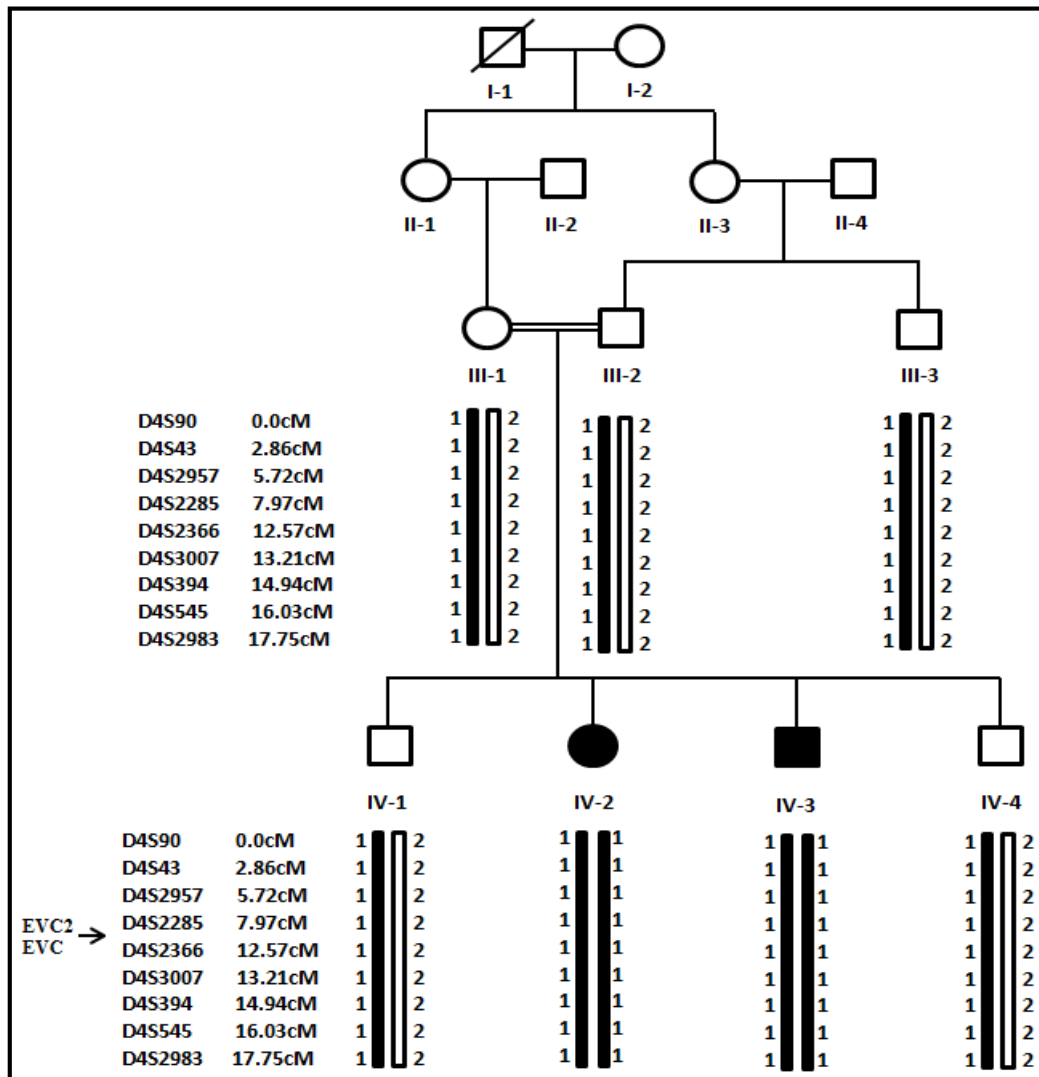
Figure 5.8: Haplotype analysis of the family H segregating autosomal recessive Ellis-van Creveld syndrome. Haplotypes of the most closely linked microsatellite markers are shown below the genotyped individuals. Black bars indicate disease haplotype. The genetic positions (centi-Morgan) and arrangement of microsatellite markers is according to Rutgers combined linkage physical map built 36.2 (Matise *et al*., 2007).
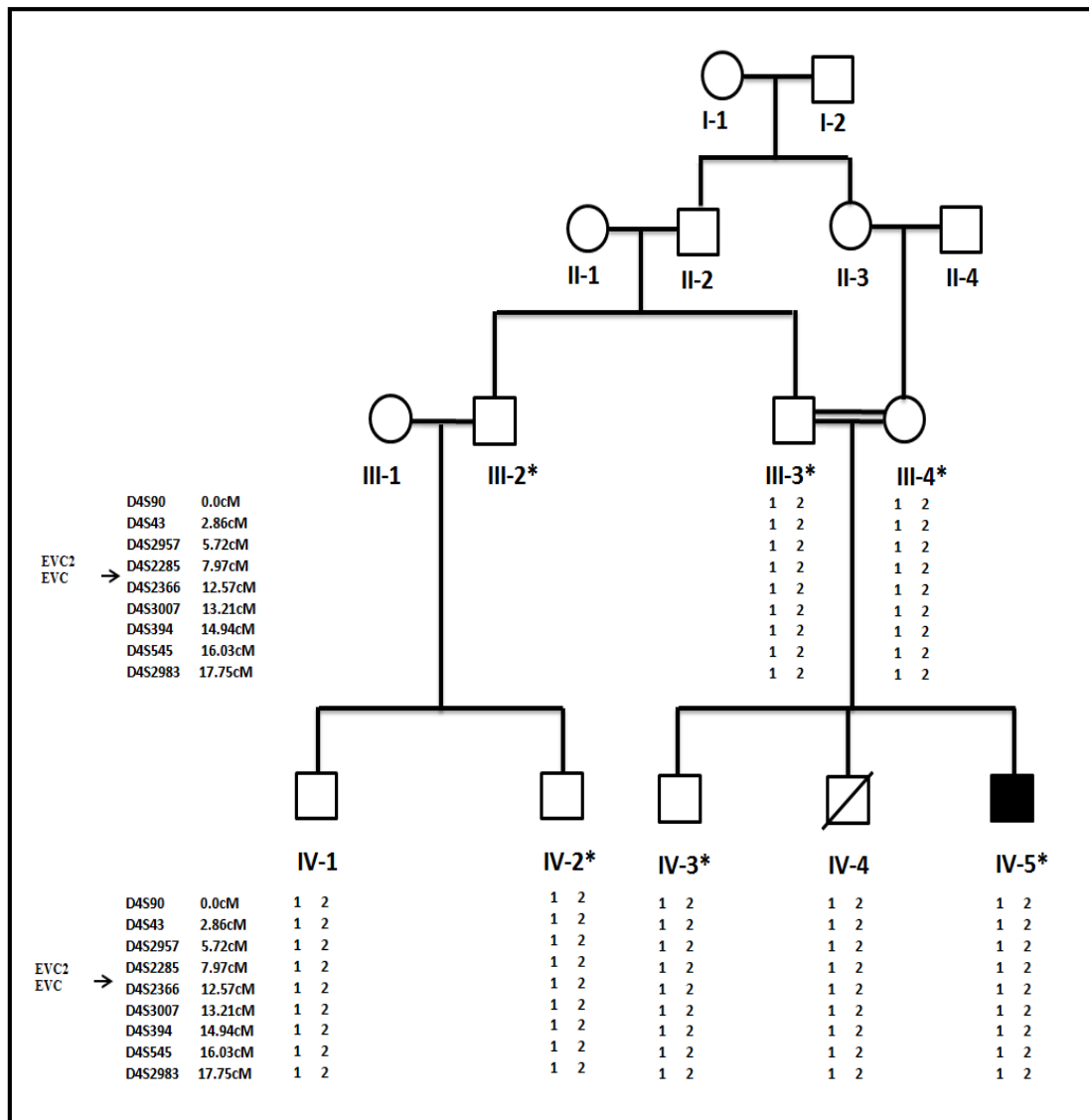
Figure 5.9: Haplotype analysis of the family I segregating autosomal recessive Ellis-van Creveld syndrome. Haplotypes of the most closely linked microsatellite markers are shown below the genotyped individuals. The arrows represent position of the two genes. The genetic positions (centi-Morgan) and arrangement of microsatellite markers is according to Rutgers combined linkage physical map built 36.2 (Matise *et al.*, 2007).
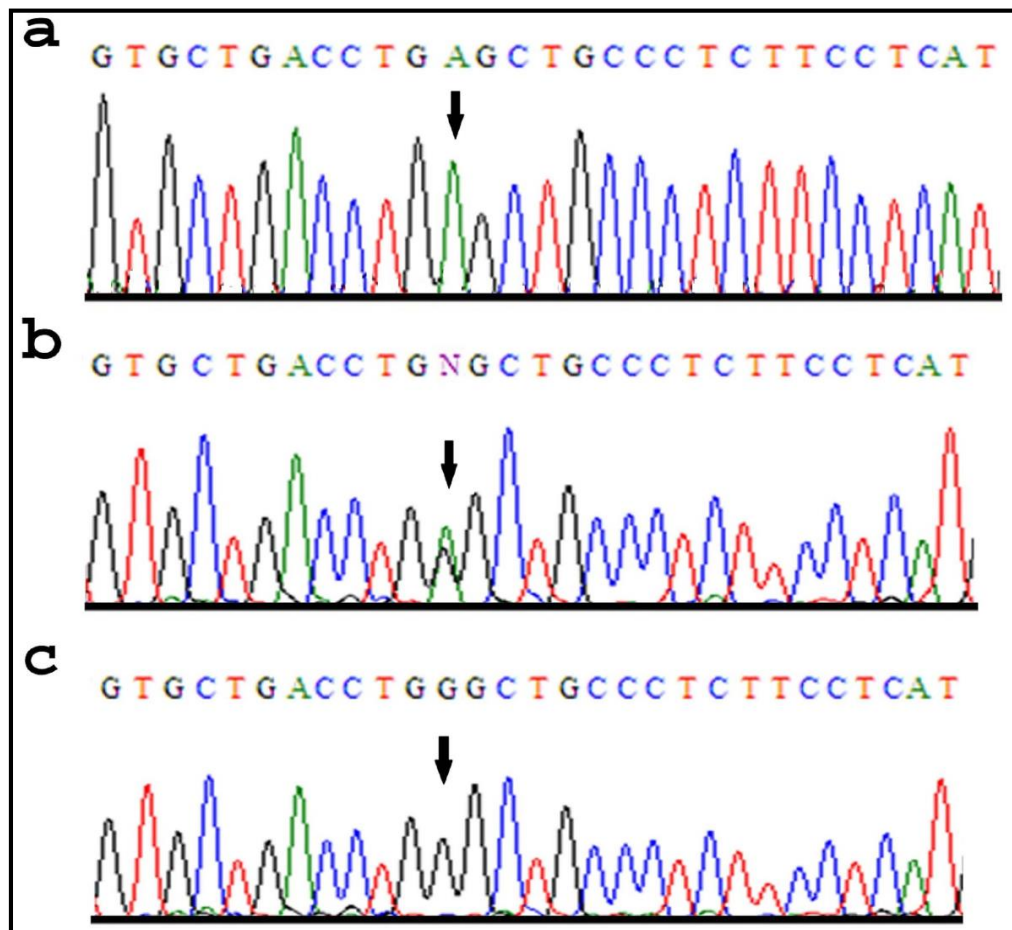
Figure 5.10: DNA Sequence analysis of a novel nonsense mutation (c.702G>A, p.Trp234*) in the *EVC2* gene identified in the family G. The upper panel (a) represents the nucleotide sequences in the affected individual, the middle panel (b) in the heterozygous carriers and the lower panel (c) in the unaffected individual. The arrows represent position of the mutation.
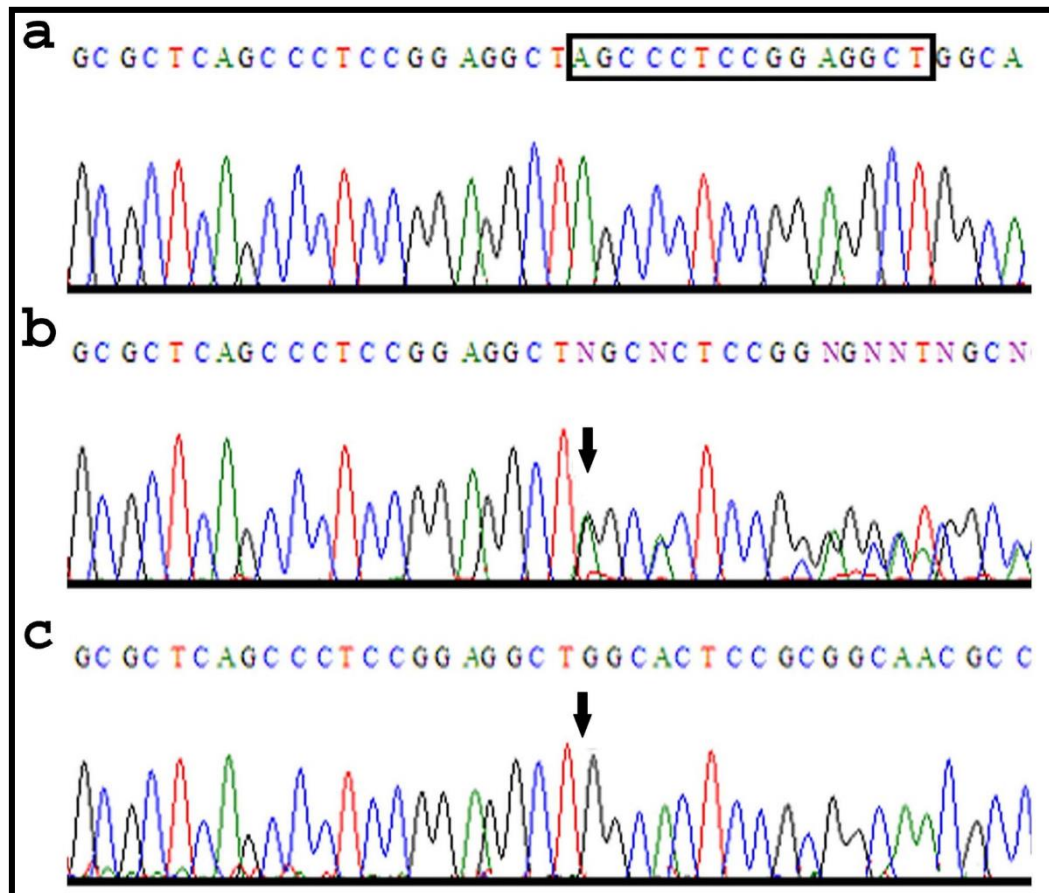
Figure 5.11: DNA Sequence analysis of a novel 15-bp duplication (c.1932_1946dupAGCCCTCCGGAGGCT) in the *EVC* gene detected in family H. The upper panel (a) represent the nucleotide sequence in the affected individual, the middle panel (b) in the heterozygous carriers and the lower panel (c) in the unaffected individual. The arrows represent position of the mutation. The 15-bp sequence boxed, represents the sequence duplicated in the affected individual in the panel a.

Chapter 6

Acromesomelic Dysplasia

Clinical and Molecular Characterization of Human Hereditary Skeletal Disorders in Consanguineous Families

ACROMESOMELIC DYSPLASIA

Acromesomelic dysplasia (AMD) is a group of autosomal recessive disorders in which the patient's exhibit disproportionate shortening of the skeletal elements including forearms, forelegs, hands and feet. This form of skeletal disorder is further classified into three major types including Grebe-type Acromesomelic Dysplasia, Acromesomelic Dysplasia type Hunter-Thompson and Acromesomelic Dysplasia, type Maroteaux.

Grebe-type acromesomelic dysplasias (AMDG) is recessively inherited distinct limb developmental disorder with distinctive features of short and deformed radii/ulnae and tibiae/fibulae. Lin *et al*. (1996) mapped Grebe-type chondrodysplasia on chromosome 20q11.22. Mutations in the gene encoding cartilage-derived morphogenetic protein-1 (*CDMP-1*), mapped on chromosome 20q11.22, have been shown to cause Grebe-type acromesomelic dysplasias (AMDG) (Thomas *et al*., 1997; Faiyaz-ul-Haque *et al*., 2002; Stelzer *et al*., 2003; Al-Yahyaee *et al*., 2003; Basit *et al*., 2008).

The second type of AMD, Acromesomelic Dysplasia type Hunter-Thompson (AMDH), having autosomal recessive mode of inheritance, characterized by short humerus, radius and ulna, short femur, tibia and fibula along with dislocated ankle. Thomas *et al*. (1996) reported 22-bp (tandem-duplication) frameshift mutation in the gene *CDMP-1* in AMDH patient.

Acromesomelic Dysplasia, type Maroteaux (AMDM) is the third type of AMD, characterized by disproportionate shortening of skeletal elements, predominantly affecting the middle segments (forearms and forelegs) and distal segments (hands and feet) of appendicular skeleton. In addition, axial skeletal involvement occurs characterized by wedging of vertebral bodies, with dorsal margins being shorter than the ventral margins. Mode of inheritance of AMDM (MIM 602875) is an autosomal recessive with a prevalence of 1/1,000,000 (Langer and Garrett, 1989). Skeletal growth in AMDM patients falls off sharply after birth causing abnormal growth plate and short misshapen bones in the extremities and spine. Borrelli *et al*. (1983) observed that carrier parents of AMDM children are shorter than average.

Acromesomelic dysplasia type Maroteaux (AMDM) was mapped on chromosome 9p13-q12 (Kant *et al*., 1998). Mutations in the gene *NPR2*, encoding natriuretic peptide receptor B, result in Acromesomelic Dysplasia, Type Maroteaux (Bartels *et al.*, 2004; Khan *et al*., 2012; Amano *et al.*, 2014).

Natriuretic peptides (NPs) comprise a family of hormones involved in the regulation of various physiological processes including cardiac growth, blood pressure, axonal path finding and endochondral ossification by binding to cell surface receptors called natriuretic peptide receptors (NPRs) (Kishimoto *et al*., 2001; Tamura *et al*., 2004; Langenickel *et al*., 2006). Three different subtypes (A, B, C) of NPRs have been identified (Potter *et al.,* 2006). NPR-B is expressed in various tissues and cell populations like heart, vessels, brain, uterus and chondrocytes (Silberbach and Roberts, 2001; Potter *et al*., 2006; Pagel-Langenickel *et al*., 2007). NPR-B is a receptor for type-C natriuretic peptide (CNP) that acts locally as a paracrine and/or autocrine regulator in a wide variety of tissues (Schulz, 2005). NPR-B consist of an extracellular ligand binding domain, a single hydrophobic transmembrane region, an intracellular kinase homology domain (KHD), and carboxyl- terminal guanylyl cyclase (GC) domain (Schulz, 2005; Garbers *et al*., 2006). The NPR-A and NPR-B mediate their biological function through GC domains.

The present chapter describes clinical and genetic investigation of a consanguineous Pakistani family segregating acromesomelic Dysplasia, Type Maroteaux in autosomal recessive pattern. The clinical investigation was performed with the assistance of medical officers serving the government hospitals. Linkage in the family was established by genotyping microsatellite markers and automated DNA sequencing was employed to identify the sequence variants.

Family J Segregating Acromesomelic Dysplasia

Family J with autosomal recessive form of acromesomelic dysplasia was recruited from lower Dir, a district of Khyber Pakhtunkhwa (KPK) Province of the country (Figure 6.1). The family had five affected members including a deceased member (IV-2). Blood samples of six family members including two affected (IV-1, IV-5) and four unaffected (III-1, III-2, IV-6, V-1) were available for the present study.

Clinical Features

Affected individuals of the family showed clinical features of acromesomelic dysplasia, type Maroteaux (AMDM), segregated in an autosomal recessive manner. At the time of study, ages of the two patients IV-1 (81 cm) and IV-5 (111 cm) were 40 and 25 years, respectively. They exhibit marked shortening in the middle and distal segments of limbs. Hands and feet were short with broad fingers and redundant skin. A skeletal survey revealed disproportionate mesomelic shortening of the arms, phalanges and metacarpal bones. Both affected individuals showed vertebral abnormalities including short thoracic and lumbar spine (mild platyspondyly) (Figure 6.2).

Genotyping and Sequencing *NPR2*

Linkage in the family was tested by genotyping microsatellite markers mapped in the flanking regions of *NPR2* gene on chromosome 9p13-q12. The markers typed in the family are listed in the Table 2.1. Affected individuals in the family were homozygous for five markers (D9S1118, D9S1845, D9S1817, D9S50, D9S1874) in the region. Analysis of the haplotype provided convincing evidence of linkage in the family to the *NPR2* gene (Figure 6.3).

To search for underlying mutation in the gene *NPR2*, all 22 exons and splice junctions were PCR amplified from genomic DNA using primers designed from intronic sequences of the gene (Chapter 2: Materials and Methods: Table 2.5). The entire coding and splice junctions of the *NPR2* gene were then sequenced bidirectionally in two affected and one unaffected individual in the family. Sequence analysis with standard sequence of the exons and splice junctions of this gene (www.ensembl.org/Homosapiens) failed to identify any potential sequence variant, which could be responsible for generating AMDM phenotypes in the family, suggesting that probably the mutation is present in regulatory sequences of the gene.

Discussion

This chapter of the dissertation described clinical and molecular analysis of a consanguineous Pakistani family exhibiting typical features of Acromesomelic Dysplasia, type Maroteaux (AMDM). Clinical and physical features observed in

affected members of the family included extremely short and broad fingers with redundant skin of hands and feet, short middle and distal segments, misshaped long bones and reduced thoracic and lumbar spines. The features observed in the present family were similar to those reported earlier in several other families with different ethnic origins (Kant *et al*., 1998; Bartels *et al*., 2004; Olney *et al*., 2006; Hachiya *et al*., 2007; Khan *et al*., 2012).

Genotyping analysis in the family established linkage to the gene *NPR2,* mapped earlier on chromosome 9p13-q12 (Kant *et al*., 1998; Bartels *et al*., 2004). DNA sequence analysis of the gene failed to identify any potential sequence variant, which could be responsible for generating AMDM phenotype in the family, suggesting that probably the mutation is present in regulatory sequences of the gene. Recently Rehman *et al*. (2014) have shown that occurrence of intra familial locus heterogeneity, including intra-sibship heterogeneity, is not rare and that taking intra-familial locus heterogeneity into account while analyzing pedigree data can increase the success rate in the identification of causal variants for Mendelian traits.

The human gene *NPR2* spans about 16.5 kb, contains 22 exons encoding 1047 amino acids protein (Kant *et al*., 1998). Potter (2006) has shown that guanylyl cyclase-linked natriuretic peptide receptors consist of 450 amino acids extracellular ligand-binding domain, 20 amino acids of single hydrophobic transmembrane domain and 570 amino acids of intracellular domain. Intracellular domain contains 3 subdomains including a kinase homology domain of 250-260 amino acids, a coiled-coil dimerization domain of 40 amino acids, and carboxyl-terminal guanylyl cyclase catalytic domain of 250 amino acids (Tamura and Garbers, 2003).

To date, 27 mutations in the gene *NPR2* have been reported in families segregating AMDM (Bartels *et al*., 2004; Olney *et al*., 2006; Hachiya *et al*., 2007; Khan *et al.,* 2012; Hannema *et al.*, 2013; Amano *et al.*, 2014). This included 4 nonsense, 5 frameshift, 3 splice site and 15 missense mutations in 31 families with AMDM (Table 6.1). Mostly the missense mutations caused receptors to retain in the endoplasmic reticulum, and never reached the cell surface and as a result decreased the number of receptors available to extracellular ligands (Hume *et al.,* 2009). A couple of other reports indicated that missense mutations produce receptors with less binding affinity

to their ligand (Hume *et al*., 2009) or with an impaired ligand-induced guanylyl cyclase activity (Hachiya *et al.,* 2007). A novel activating *NPR2* mutation (p.Arg655Cys) located in the kinase homology domain, which results in extremely tall stature without severe skeletal abnormalities. This activating mutation indicates that the kinase homology domain, whose function is still poorly understood, is crucially involved in regulating guanylyl cyclase activity of NPR2 (Hannema *et al.*, 2013). Recently, Amano *et al*. (2014) identified two novel heterozygous *NPR2* mutations (p.Arg110Cys; p.Gln417Glu) causing a loss of C-type natriuretic peptide-dependent cGMP generation capacities and having dominant-negative effects. A homozygous mutation (p.Arg110Cys) caused NPR2 defective in trafficking from the endoplasmic reticulum to the Golgi apparatus. In contrast, another homozygous missense mutation (p.Gln417Glu) showed clear cell surface expression.

At least two studies have shown that mutations in GC-binding domain in the gene *Npr2* result in impaired endochondral ossification and severe dwarfism in mice (Tamura *et al*., 2004, Weischenfeldt *et al*., 2005). Since NPR-B mediate its biological function through GC domain, it is highly likely that the effect on the structure of NPR-B will affect the natriuretic peptide-dependent physiological response occurs through synthesis of cGMP. This in turns will affect the cGMP signaling effects which occurs through cGMP binding proteins including cGMP dependent protein kinase (PKG), cGMP binding phosphodiesterases (PDEs) and cyclic nucleotide-gated ion channels. The best studied cGMP signaling effects occurs through PKGs. Deletion of a membrane bound PKGII, which has been found in high concentration in brain, chondrocytes and bones (Smolenski *et al*., 1998), results in dwarfism in rodents (Pfeifer *et al*., 1996; Smolenski *et al*., 1998). The genetic data pertaining to mutations identified in Cnp and Npr-b in mice and NPR-B in human clearly showed the involvement of CNP/NPR-B/cGMP signaling pathway in bone development.
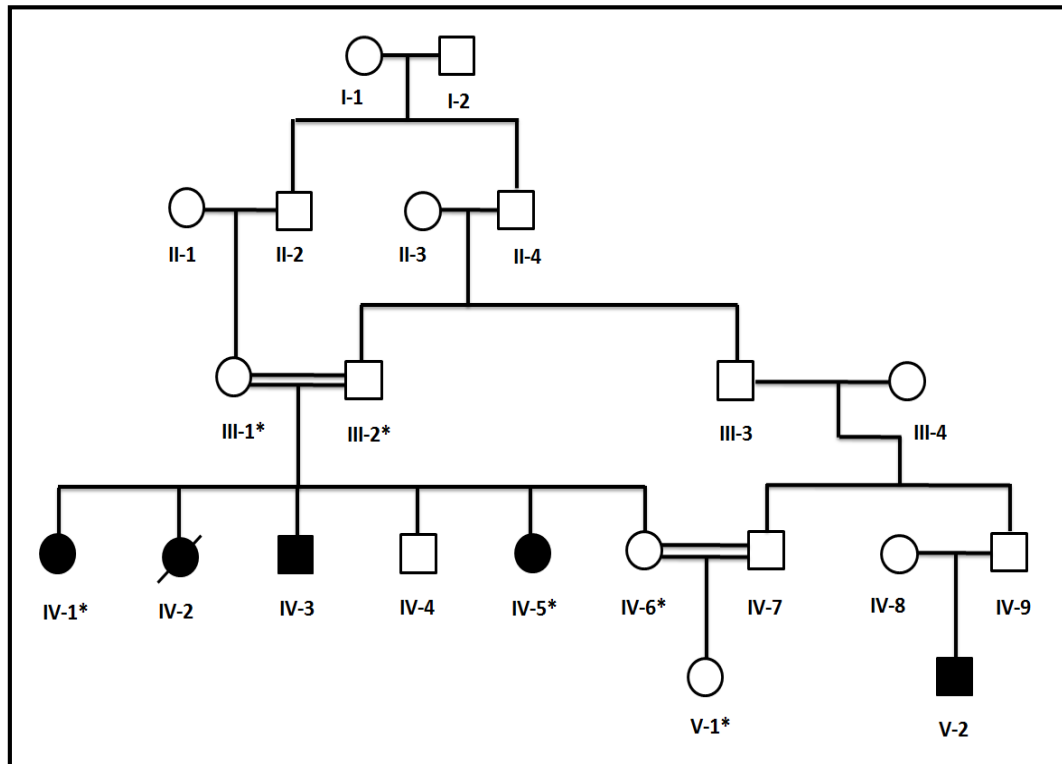
Figure 6.1: Pedigree drawing of the family J segregating acromesomelic dysplasia in autosomal recessive pattern. Squares and circles represent males and females, respectively. Clear symbols represents unaffected individuals while filled symbols affected individuals. Symbols with bars represent deceased individuals. Double lines indicate consanguineous union. The individual numbers labeled with asterisks indicate samples available for this study.

Figure 6.2: Clinical features of acromesomelic dysplasiatype Maroteaux (AMDM), observed in the family J. Patients (IV-1, 81cm) age 40 years, and Patient (IV-5, 111 cm) age 25 years (a). Short fingers and redundant skin in affected individual IV-1 (b,c) and IV-5 (d, e).
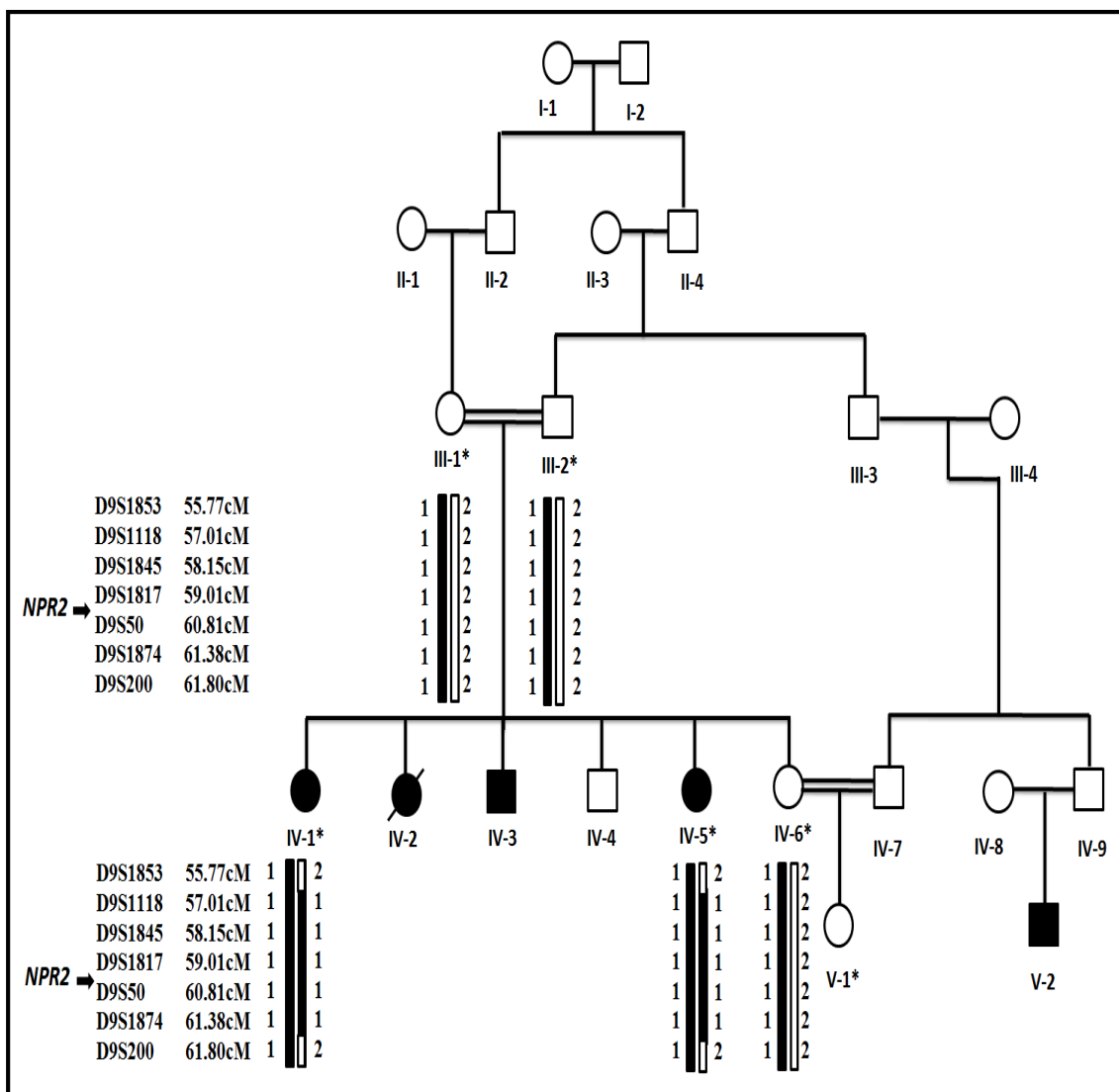
Figure 6.3: Haplotype analysis of the family J segregating acromesomelic dysplasia in autosomal recessive manner. Haplotypes of the most closely linked microsatellite markers are shown below the genotyped individuals. Black bars indicate disease haplotype. The genetic positions (centi-Morgan) and arrangement of microsatellite markers is according to Rutgers combined linkage physical map built 36.2 (Matise *et al.*, 2007).

Table 6.1: List of mutations in the gene *NPR2* reported to date

S.NO	Mutation	cDNA	Protein	Reference
1	Missense	c.94C>A	p.Pro32Thr	Bartels *et al.,* 2004
2	Missense	c.343T>G	p.Trp115Gly	Bartels *et al.,* 2004
3	Missense	c.528T>A	p.Asp176Glu	Bartels *et al.,* 2004
4	Nonsense	c.1162C>T	p.Arg388*	Bartels *et al.,* 2004
5	Nonsense	c.844C>T	p.Gln282*	Bartels *et al.,* 2004
6	Missense	c.890C>T	p.Thr297Met	Bartels *et al.,* 2004
7	Missense	c.1013A>G	p.Tyr338Cys	Bartels *et al.,* 2004
8	Nonsense	c.1111C>T	p.Arg371*	Bartels *et al.,* 2004
9	Deletion	c.1314_1315delCT	p.Pro438fs*441	Bartels *et al.,* 2004
10	Missense	c.1225G>A	p.Ala409Thr	Bartels *et al.,* 2004
11	Missense	c.1238GrA	p.Gly413Glu	Bartels *et al.,* 2004
12	Deletion	c.1294delC	p.Pro432fs*476	Bartels *et al.,* 2004
13	Nonsense	c.1498C>T	p.Gln500*	Bartels *et al.,* 2004
14	Splice-site	c.1887-2T>A	p. Gly630fs*	Bartels *et al.,* 2004
15	Missense	c.2123A>G	p.Tyr708Cys	Bartels *et al.,* 2004
16	Deletion-Insertion	c.2304_2307delTTGG insCTGATGGA	p.Trp769*	Bartels *et al.,* 2004
17	Missense	c.2326C>T	p.Arg776Trp	Bartels *et al.,* 2004
18	Missense	c.2869C>T	p.Arg957Cys	Bartels *et al.,* 2004
19	Missense	c.2876G>C	p.Gly959Ala	Bartels *et al.,* 2004
20	Splice-site	c.1436-1G>T	p.Lys480*	Bartels *et al.,* 2004
21	Deletion	c.3059delG	p.Arg1020fs*1025	Bartels *et al.,* 2004
22	Missense	c.1972C>T	p.Leu658Phe	Hachiya *et al.,* 2007
23	Missense	c.2720 C > T	p.Thr907Met	Khan *et al.,* 2012
24	splice site	c.2986 + 2 T > G		Khan *et al.,* 2012
25	Missense	c.1963C>T	p.Arg655Cys	Hannema *et al.,* 2013
26	Missense	c.328C>T	p.Arg110Cys	Amano *et al.,* 2014
27	Missense	c.1249C>G	p.Gln417Glu	Amano *et al.,* 2014

Clinical and Molecular Characterization of Human Hereditary Skeletal Disorders in Consanguineous Families

Chapter 7

References

Clinical and Molecular Characterization of Human Hereditary Skeletal Disorders in Consanguineous Families

CONCLUSION

In Pakistan, a country of 180 million populations, consanguineous marriages are preferred due to socio-cultural advantages including low rate of domestic violence, reduced divorce rate, reduced dowry, and stable and more compatible relationships (Hamamy 2012; Perveen and Rehman 2012). However, in addition to limited access to medical services in rural areas, such a culture of intra-familial marriages has led to large family size with high rate of genetic disorders. The risks of the cousin marriage are highest among families with sever segregating autosomal recessive conditions (Perveen and Rehman 2012).

Large families are suitable for genetic linkage studies as they allow the inheritance pattern to be unequivocally determined, each phenotype and its variability to be well described, and present an ideal solution to the problem of genetic heterogeneity. This is of particular importance for the recessively inherited phenotypes, which are abundant among the Pakistani families. Thus, this population has turn out to be an important resource for research on genetic disorders.

Over the last years a big effort has been made to understand the molecular and cellular mechanisms involved in controlling development of various organs and systems. Much information on the genes that are important for the developmental plan has been revealed using linkage studies in large human pedigrees segregating genetic disorders. However, very little is known on the pathologies that are the consequence of abrupt gene function and subsequent malformation. Elucidating when and how signaling molecules and transcription factors dictate organ development initiation, morphology and growth will open new horizons to the developmental biology discipline and will create new challenges. Advances in genomic technologies, including dense SNP arrays, whole exome and whole genome sequencing, have promoted a new era in genetic analysis of rare diseases.

Skeletal dysplasia is a collection of disorders of the skeleton that result from derangement of growth, development and/or differentiation of the skeleton. Visiting some of the remote areas in the country identified ten consanguineous families, segregating autosomal recessive forms of skeletal deformities, which were then

clinically and genetically characterized in the present study. Scanning three families with postaxial polydatcyly/syndactyly led to the mapping of three novel loci on human chromosomes. Further, using exome sequencing, the first disease causing mutation was identified in the gene *FAM92A1* in one such case. In the other two families exome sequencing is in progress to search for the disease causing genes.

Two novel mutations were identified in *WNT10B* gene in two families segregating split hand and foot malformation phenotypes. Similarly, in two other families segregating Ellis-van-Creveld syndrome, novel mutations were detected in the *EVC* and *EVC2* genes. Another family with the later syndrome failed to show linkage to *EVC* genes indicating locus heterogeneity for this particular phenotype.

Identification/mapping of at least three new genes, in the present study, further increases the list of the disease genes involved in skeletal deformities. The previously known genes encode a huge variety of molecules including extracellular matrix proteins, enzymes, hormones, cytokines and their receptors, and transcription factors, which reflects complexity of the skeletal formation. Functional characterization of the genes mapped here would be a step further in defining pathways involved in developing of human skeleton.

The variety reflects the complexity of skeletal formation in vivo. Using the human disease genes as starting points, we can clarify the complex mechanism. The study of the rare monogenic diseases can bring a breakthrough for clarifying the genetic aspects of common diseases. Thus, as regards medicine and basic science, research into skeletal dysplasia will give us a lot of knowledge. Integration of clinical and genetic information is the key to success for research in the genome era.

The identification of the causative mutation for a Mendelian disease enables molecular diagnosis and carrier testing in the patient and his or her family. This is of great importance for patient management and family counseling, and serves as a starting point for therapeutic interventions. Furthermore, the identification of Mendelian disease genes contributes to our understanding of gene functions and biological pathways underlying health and disease in general, and lessons learned from rare diseases are often also relevant to common disease. Research aimed at the identification of genes that cause Mendelian disease has received a boost over the past

couple of years by the introduction of new technologies that enable the sequencing of DNA at a much higher throughput and at much lower costs than previously possible.

Considering the number of various types of skeletal disorders, prevailing in various ethnic groups in Pakistani population, use of exome sequencing will not only help in identifying the disease genes but will open the doors to rapid genetic diagnosis and screening.

These data suggest that premarital genetic, social counseling and mass media efforts need to increase public awareness about genetic risks associated with cousin marriage.

Conclusion

Clinical and Molecular Characterization of Human Hereditary Skeletal Disorders in Consanguineous Families

REFERENCES

Ahmad M, Abbas H, Haque S, Flatz G (1987). X-chromosomally inherited split-hand/split-foot anomaly in a Pakistani kindred. Hum Genet 75: 169-173.

Akarsu AN, Ozbas F, Kostakoglu N (1997). Mapping of the second locus of postaxial polydactyly type A (PAP-A2) to chromosome 13q21–q32. Am J Hum Genet 6: A265.

Akiyama H (2008). Control of chondrogenesis by the transcription factor Sox 9. Mod Rheumatol 18: 213-219.

Akiyama H, Kim JE, Nakashima K, Balmes G, Iwai N, Deng JM, Zhang Z, Martin JF, Behringer RR, Nakamura T, de Crombrugghe B (2005). Osteo-chondroprogenitor cells are derived from Sox9 expressing precursors. Proc Natl Acad Sci USA 102: 14665-14670.

Al-khenaizan S, Al-sannaa N, Teebi AS (2001). What syndrome is this? Chondroectodermal dysplasia-The Ellis-van Creveld syndrome. Pediatr Dermatol 18: 68-70.

Altshuler D, Durbin RM, Abecasis GR, Bentley DR, Chakravarti A, Clark AG, Collins FS, De La Vega FM, Donnelly P, Egholm M, Flicek P, Gabriel SB *et al.* (2010). A map of human genome variation from population-scale sequencing. Nature 467: 1061-1073.

Al-Yahyaee SA, Al-Kindi MN, Habbal O, Kumar DS (2003). Clinical and molecular analysis of Grebe acromesomelic dysplasia in an Omani family. Am J Med Genet 121: 9-14.

Amano N, Mukai T, Ito Y, Narumi S, Tanaka T, Yokoya S, Ogata T, Hasegawa T (2014). Identification and functional characterization of two novel *NPR2* mutations in Japanese patients with short stature. J Clin Endocrinol Metab 99: 713-718.

Andrade AC, Nilsson O, Barnes KM, Baron J (2007). Wnt gene expression in the postnatal growth plate: regulationwith chondrocyte differentiation. Bone 40: 1361-1369.

Atasu M, Biren S (2000). Ellis-van Creveld syndrome: Dental, clinical, genetic and dermatoglyphic findings of a case. J Clin Pediatr Dent 24: 141-145.

Aziz A , Irfanullah, Khan S, Zimri FK, Muhammad N, Rashid S, Ahmad W (2014). Novel homozygous mutations in the *WNT10B* gene underlying autosomal recessive split hand/foot malformation in three consanguineous families. Gene 534: 265-271.

Bai S, Kopan R, Zou W, Hilton MJ, Ong CT, Long F, Ross FP, Teitelbaum SL (2008). NOTCH1 regulates osteoclastogenesis directly in osteoclast precursors and indirectly via osteoblast lineage cells. J Biol Chem 283: 6509-6518.

Bartels CF, Bükülmez H, Padayatti P, Rhee DK, van Ravenswaaij-Arts C, Pauli RM, Mundlos S, Chitayat D, Shih LY, Al-Gazali LI, Kant S, Cole T, Morton J, Cormier-Daire V, Faivre L, Lees M, Kirk J, Mortier GR, Leroy J, Zabel B, Kim CA, Crow Y, Braverman NE, van den Akker F, Warman ML (2004). Mutations in the transmembrane natriuretic peptide receptor NPR-B impair skeletal growth and cause acromesomelic dysplasia, type Maroteaux. Am J Hum Genet 75: 27-34.

Basit S, Naqvi SK, Wasif N, Ali G, Ansar M, Ahmad W (2008). A novel insertion mutation in the cartilage-derived morphogenetic protein-1 (*CDMP1*) gene underlies Grebe-type chondrodysplasia in a consanguineous Pakistani family. BMC Med Genet 9: 102.

Bell J (1951). On brachydactyly and symphalangism. In: Treasury of human inheritance. Penrose LS (ed), Vol 5, Cambridge University Press, London, pp 1-31.

Bell J (1953). On syndactylies and its association with polydactyly. In: The treasury of human inheritance. Cambridge University Press, London, pp 30-50.

Bennett RL, French KS, Resta RG, Doyle DL (2008). Standardized human pedigree nomenclature: update and assessment of the recommendations of the National Society of Genetic Counselors. J Genet Couns 17: 424-433.

Berdon-Zapata V, Granillo-Alvarez M, Valdés-Flores M, Garcia-Ortiz JE, Kofman-Alfaro S, Zenteno JC (2004). *p63* gene analysis in Mexican patients with syndromic and non-syndromic ectrodactyly. J Orthop Res 22: 1-5.

Bi W, Deng JM, Zhang Z, Behringer RR, de Crombrugghe B (1999). Sox9 is required for cartilage formation. Nat Genet 22: 85-89.

Biesecker LG (2010). Exome sequencing makes medical genomics a reality. Nat Genet 42: 13-14.

Blair HJ, Tompson S, Liu YN, Campbell J, MacArthur K, Ponting CP, Ruiz-Perez VL, Goodship JA (2011). Evc2 is a positive modulator of Hedgehog signalling that interacts with Evc at the cilia membrane and is also found in the nucleus. BMC Biol 9: 14.

Blattner A, Huber AR, Rothlisberger B (2010). Homozygous nonsense mutation in WNT10B and sporadic split-hand/foot malformation (SHFM) with autosomal recessive inheritance. Am J Med Genet A 152: 2053-2056.

Blauth W, Olason AT (1988). Classification of polydactyly of the hands and feet. Arch Orthop Trauma Surg 107: 334-344.

Boles RG, Pober BR, Gibson LH, Willis CR, McGrath J, Roberts DJ, Yang-Feng TL (1995). Deletion of chromosome 2q24-q31 causes characteristic digital anomalies: case report and review. Am J Med Genet 55: 155-160.

Bonewald LF (1999). Regulation and regulatory activities of transforming growth factor beta. Crit Rev Eukaryot Gene Expr 9: 33-44.

Borrelli P, Fasanelli S, Marini R (1983). Acromesomelic dwarfism in a child with an interesting family history. Pediatr Radiol 13: 165-168.

Bosse K, Betz RC, Lee YA, Wienker TF, Reis A, Kleen H, Propping P, Cichon S, Nöthen MM (2000). Localization of a gene for syndactyly type 1 to chromosome 2q34-q36.Am J Hum Genet 67: 492- 497.

Buck-Gramcko D (1998). Angeborene Fehlbildungen der Hand. In: Handchirurgie. Nigst H, Buck-Gramcko D, Milesi H (eds), Thieme, Stuttgart, pp 12.1-12.115.

Bulman MP, Kusumi K, Frayling TM, McKeown C, Garrett C, Lander ES, Krumlauf R, Hattersley AT, Ellard S, Turnpenny PD (2000). Mutations in the human delta homologue, *DLL3*, cause axial skeletal defects in spondylocostal dysostosis. Nat Genet 24: 438-441.

Cadigan KM, Nusse R (1997). Wnt signaling: a common theme in animal development. Genes Dev 11: 3286-3305.

Cahuana A, Palma C, Gonzαles W, Geαn E (2004). Oral manifestations in Ellis-van Creveld syndrome: Report of five cases. Pediatr Dent 26: 277-281.

Carey JD, Hommell M, Fineman RM, Hall BD (1990). Hallucal polydactyly in infants of diabetic mothers a clinical marker and possible clue to teratogenesis. Proc Greenwood Genet Center 9: 95.

Castilla E, Paz JE, Mutchinick O, Munoz E, Giorgiutti E, Gelman Z (1973). Polydactyly a genetic study in South America. Am J Hum Genet 25: 405-412.

Castilla EE, da Graca Dutra M, Lugarinho da Fonseca R, Paz JE (1997). Hand and foot postaxial polydactyly: two different traits. Am J Med Genet 73: 48-54.

Castilla EE, Paz JE, Orioli-Parreiras IM (1980). Syndactyly: frequency of specific types. Am J Med Genet 5: 357-364.

Cawthorn WP, Bree AJ, Yao Y, Du B, Hemati N, Martinez-Santibañez G, MacDougald OA (2012). Wnt6, Wnt10a andWnt10b inhibit adipogenesis and stimulate osteoblastogenesis through a β-catenin-dependent mechanism. Bone 50: 477-489.

Cenani A, Lenz W (1967). Totale Syndaktylie und totale radioulnare Synostose bei zwei Bru¨dern.Ein Beitrag zur Genetik der Syndaktylien. Ztschr Kinderheilk 101: 181-190.

Chai Y, Maxson RE Jr (2006). Recent advances in craniofacial morphogenesis. Dev Dyn 235: 2353-2375.

Chiang C, Litingtung Y, Lee E, Young KE, Corden JL, Westphal H, Beachy PA (1996). Cyclopia and defective axial patterning in mice lacking sonic hedgehog gene function. Nature 383: 407-413.

Clinical and Molecular Characterization of Human Hereditary Skeletal Disorders in Consanguineous Families

Choi M, Scholl UI, Ji W, Liu T, Tikhonova IR, Zumbo P, Nayir A, Bakkaloğlu A, Ozen S, Sanjad S, Nelson-Williams C, Farhi A, Mane S, Lifton RP (2009). Genetic diagnosis by whole exome capture and massively parallel DNA sequencing. Proc Natl Acad Sci USA 106: 19096-19101.

Creuzet S, Couly G, Le Douarin NM (2005). Patterning the neural crest derivatives during development of the vertebrate head: insights from avian studies. J Anat 207: 447-459.

Crossley PH, Minowada G, Macarthur CA, Martin GR (1996). Roles for FGF-8 in the induction, initiation and maintenance of chick limb development. Cell 84: 127-136.

Dawson K, Seeman P, Sebald E, King L, Edwards M, Williams J, Mundlos S, Krakow D (2006). GDF5 is a second locus for multiple-synostosis syndrome. Am J Hum Genet 78: 708-712.

de Crombrugghe B, Lefebvre V, Behringer RR, Bi W, Murakami S, Huang W (2000). Transcriptional mechanisms of chondrocyte differentiation. Matrix Biol 19: 389-394.

de Crombrugghe B, Lefebvre V, Nakashima K (2001). Regulatory mechanisms in the pathways of cartilage and bone formation. Curr Opin Cell Biol 13: 721-727.

de Mollerat XJ, Gurrieri F, Morgan CT, Sangiorgi E, Everman DB, Gaspari P, Amiel J, Bamshad MJ, Lyle R, Blouin JL, Allanson JE, Le Marec B, Wilson M, Braverman NE, Radhakrishna U, Delozier-Blanchet C, Abbott A, Elghouzzi V, Antonarakis S, Stevenson RE, Munnich A, Neri G, Schwartz CE (2003). A genomic rearrangement resulting in a tandem duplication is associated with split hand-split foot malformation 3 (SHFM3) at 10q24. Hum Mol Genet 12: 1959-1971.

Debeer P, Mols R, Huysmans C, Devriendt K, Van de Ven WJ, Fryns JP (2002b). Involvement of a palindromic chromosome 22-specific low-copy repeat in a constitutional t(X; 22) (q27; q11). Clin Genet 62: 410-414.

Debeer P, Schoenmakers EF, Twal WO, Argraves WS, De Smet L, Fryns JP, Van De Ven WJ (2002a). The fibulin-1 gene (*FBLN1*) is disrupted in a t(12;22) associated with a complex type of synpolydactyly. J Med Genet 39:98-104.

Deborah A, Himelhoch DA, Mostofi R (1988). Oral abnormalities in the Ellis-van Creveld syndrome: Case report. Pediatr Dent 10: 309-313.

Dequeant ML, Pourquie O (2008). Segmental patterning of the vertebrate embryonic axis. Nat Rev Genet 9: 370-382.

Digilio MC, Marino B, Ammirati A, Borzaga U, Giannotti A, Dallapiccola B (1999). Cardiac malformations in patients with oral-facial-skeletal syndromes: Clinical similarities with heterotaxia. Am J Med Genet 84: 350-356.

Dowd CN (1896). Cleft hand: a report of a case successfully treated with the use of periosteal flaps. Ann Surg 24: 210-216.

Ducy P, Zhang R, Geoffroy V, Ridall AL, Karsenty G (1997). Osf2/Cbfa1: a transcriptional activator of osteoblast differentiation. Cell 89: 747-754.

Dugoff L, Thieme G, Hobbins JC (2001). First trimester prenatal diagnosis of chondroectodermal dysplasia (Ellis-van Creveld syndrome) with ultrasound. Ultrasound Obstet Gynecol 7: 86-88.

Duijf PH, van Bokhoven H, Brunner HG (2003). Pathogenesis of split-hand/split-foot

Ehlen HW, Buelens LA, Vortkamp A (2006). Hedgehog signaling in skeletal development. Birth Defects Res C Embryo Today 78: 267-279.

Elliott AM, Evans JA (2008). The association of split hand foot malformation (SHFM) and congenital heart defects. Birth Defects Res 82: 425-434.

Engin F, Yao Z, Yang T, Zhou G, Bertin T, Jiang MM, Chen Y, Wang L, Zheng H, Sutton RE, Boyce BF, Lee B (2008). Dimorphic effects of Notch signaling in bone homeostasis. Nat Med 14: 299-305.

Erlebacher A, Filvaroff EH, Gitelman SE, Derynck R (1995). Toward a molecular understanding of skeletal development. Cell 80: 371-378.

Faiyaz-Ul-Haque M, Ahmad W, Wahab A, Haque S, Azim AC, Zaidi SHE, Teebi AS, Ahmad M, Cohn DH, Siddique T, Tsui LC (2002). Frameshift mutation in the

cartilage-derived morphogenetic protein-1 (*CDMP1*) gene and severe acromesomelic chondrodysplasia resembling grebe type chondrodysplasia. Am J Med Genet 111: 31-37.

Faiyaz-Ul-Haque M, Zaidi SH, King LM, Haque S, Patel M, Ahmad M, Siddique T, Ahmad W, Tsui LC, Cohn DH (2005). Fine mapping of the X-linked split-hand/split-foot malformation (SHFM2) locus to a 5.1-Mb region on Xq26.3 and analysis of candidate genes. Clin Genet 67: 93-97.

Fallon J, Lopez A, Ros M, Savage M, Olwin B, Simandl B (1994). FGF-2, apical ectodermal ridge growth signals for chick limb development. Science 264: 104-107.

Ferrante MI, Zullo A, Barra A, Bimonte S, Messaddeq N, Studer M, Dollé P, Franco B (2006). Oral-facial-digital type I protein is required for primary cilia formation and left-right axis specification. Nat Genet 38: 112-117.

Ferreira MA (2004). Linkage analysis: principles and methods for the analysis of human quantitative traits. Twin Res 7: 513-530.

Frazier TM (1960). A note on race-specific congenital malformation rates. Am J Obstet Gynecol 80: 184-185.

Galceran J, Galceran J, Fariñas I, Depew MJ, Clevers H, Grosschedl R (1999). Wnt3a−/−−like phenotype and limb deficiency in Lef1 (−/−) Tcf1 (−/−) mice. Genes Dev 13: 709-717.

Galjaard RJ, Smits AP, Tuerlings JH, Bais AG, Bertoli Avella AM, Breedveld G, de Graaff E, Oostra BA, Heutink P (2003). A new locus for postaxial polydactyly type A/B on chromosome 7q21− q34. Eur J Hum Genet 11: 409-415.

Garbers DL, Chrisman TD, Wiegn P, Katafuchi T, Albanesi JP, Bielinski V, Barylko B, Redfield MM, Burnett JC Jr (2006). Membrane guanylyl cyclase receptors: an update. Trends Endocrinol Metab 17: 251-258.

García-de-Viedma D, Giraldo R, Rivas G, Fernandez-Tresguerres E, Diaz-Orejas R (1996). A leucine zipper motif determines different functions in a DNA replication protein. EMBO 15: 925-934.

Gerber HP, Vu TH, Ryan AM, Kowalski J, Werb Z, Ferrara N (1999). VEGF couples hypertrophic cartilage remodeling, ossificationand angiogenesis during endochondral bone formation. Nat Med 5: 623-628.

Ghadami M, Majidzadeh AK, Haerian BS, Damavandi E, Yamada K, Pasallar P, Najafi MT, Nishimura G, Tomita HA, Yoshiura KI, Niikawa N (2001). Confirmation of genetic homogeneity of syndactyly type 1 in an Iranian family. Am J Med Genet 104: 147-151.

Gibbs JR, Singleton A (2006). Application of genome-wide single nucleotide polymorphism typing: simple association and beyond. PLoS Genet 2: e150.

Gladwin A, Donnai D, Metcalfe K, Schrander-Stumpel C, Brueton L, Verloes A, Aylsworth A, Toriello H, Winter R, Dixon M (1997). Localization of a gene for oculodentodigital syndrome to human chromosome 6q22-q24. Hum Mol Genet 6: 123-127.

Goddeeris MM, Rho S, Petiet A, Davenport CL, Johnson GA, Meyers EN, Klingensmith J (2008). Intracardiac septation requires hedgehog-dependent cellular contributions from outside the heart. Development 135: 1887-1895.

Gong L, Wang B, Wang J, Yu H, Ma X, Yang J (2011). Polyalanine repeat expansion mutation of the *HOXD13* gene in a Chinese family with unusual clinical manifestations of synpolydactyly. Eur J Med Genet 54: 108-111.

Goodman FR, Majewski F, Collins AL, Scambler PJ (2002). A 117 kb microdeletion removing HOXD9, HOXD13 and EVX2 causes synpolydactyly. Am J Hum Genet 70: 547-555.

Goodman FR, Mundlos S, Muragaki Y, Donnai D, Giovannucci-Uzielli ML, Lapi E, Majewski F, McGaughran J, McKeown C, Reardon W, Upton J, Winter RM, Olsen BR, Scambler PJ (1997). Synpolydactyly phenotypes correlate with size of expansions in HOXD13 polyalanine tract. Proc Natl Acad Sci USA 94: 7458-7463.

Gorlin RJ, Cohen MMJ, Hennekam RCM (2001). Syndromes of the head and neck, 4th edition. Oxford University Press, Newyork, pp201-204.

Graham TJ, Ress AM (1998). Finger polydactyly. Hand Clin 14: 49-64.

Grcevic D, Pejda S, Matthews BG, Repic D, Wang L, Li H, Kronenberg MS, Jiang X, Maye P, Adams DJ, Rowe DW, Aguila HL, Kalajzic I (2012). In vivo fate mapping identifies mesenchymal progenitor cells. Stem Cells 30: 187-196.

Gurnett CA, Dobbs MB, Nordsieck EJ, Keppel C, Goldfarb CA, Morcuende JA, Bowcock AM (2006). Evidence for an additional locus for split hand/foot malformation in chromosome region 8q21.11-q22.3.Am J Med Genet A 140: 1744-1748.

Gurrieri F, Prinos P, Tackels D, Kilpatrick MW, Allanson J, Genuardi M, Vuckov A, Nanni L, Sangiorgi E, Garofalo G, Nunes ME, Neri G, Schwartz C, Tsipouras P (1996). A split hand-split foot (*SHFM3*) gene is located at 10q24–25. Am J Med Genet 62: 427-436.

Haas SL (1940). Bilateral complete syndactylism of all fingers. Am J Surg 50: 363-366.

Hachiya R, Ohashi Y, Kamei Y, Suganami T, Mochizuki H, Mitsui N, Saitoh M, Sakuragi M, Nishimura G, Ohashi H, Hasegawa T, Ogawa Y (2007). Intact kinase homology domain of natriuretic peptide receptor-B is essential for skeletal development. J Clin Endocrinol Metab 92: 4009-4014.

Hamamy H (2012). Consanguineous marriages: Preconception consultation in primary health care settings. J Community Genet 3: 185-192.

Hannema SE, van Duyvenvoorde HA, Premsler T, Yang RB, Mueller TD, Gassner B, Oberwinkler H, Roelfsema F, Santen GW, Prickett T, Kant SG, Verkerk AJ, Uitterlinden AG, Espiner E, Ruivenkamp CA, Oostdijk W, Pereira AM, Losekoot M, Kuhn M, Wit JM (2013). An activating mutation in the kinase homology domain of the natriuretic peptide receptor-2 causes extremely tall stature without skeletal deformities. J Clin Endocrinol Metab 98: 1988-1998.

Harada M, Murakami H, Okawa A, Okimoto N, Hiraoka S, Nakahara T, Akasaka R, Shiraishi Y, Futatsugi N, Mizutani-Koseki Y, Kuroiwa A, Shirouzu M, Yokoyama S, Taiji M, Iseki S, Ornitz DM, Koseki H (2009). FGF9 monomer-dimer equilibrium regulates extracellular matrix affinity and tissue diffusion. Nat Genet 41: 289-298.

Harpf C, Pavelka M, Hussl H (2005). A variant of Cenani-Lenz syndactyly [CLS]: review of the literature and attempt of classification. Br J Plast Surg 58: 251-257.

Hartmann C (2009). Transcriptional networks controlling skeletal development. Curr Opin Genet Dev 19: 437-443.

Hartmann C, Tabin CJ, (2001). Wnt-14 plays a pivotal role in inducing synovial joint formation in the developing appendicular skeleton. Cell 104: 341-351.

Hartung A, Sieber C, Knaus P (2006). Yin and Yang in BMP signaling: impact on the pathology of disease and potential for tissue regeneration. Signal Transduction 6: 314-328.

Hay S (1971). Incidence of selected congenital malformations in Iowa. Am J Epidemiol 94: 572-584.

Helms JA, Cordero D, Tapadia MD (2005). New insights into craniofacial morphogenesis. Development 132: 851-861.

Hill TP, Später D, Taketo MM, Birchmeier W, Hartmann C (2005). Canonical Wnt/beta-catenin signaling prevents osteoblasts from differentiating into chondrocytes. Dev Cell 8: 727-738.

Hilton MJ, Tu X, Wu X, Bai S, Zhao H, Kobayashi T, Kronenberg HM, Teitelbaum SL, Ross FP, Kopan R, Long F (2008). Notch signaling maintains bone marrow mesenchymal progenitors by suppressing osteoblast differentiation. Nat Med 14: 306-314.

Holmes LB, Wolf E, Miettinen OS (1972). Metacarpal 4-5 fusion with Xlinked recessive inheritance. Am J Hum Genet 24: 562-568.

Hsu CK (1965). Hereditary syndactylia in a Chinese family. Chin Med J 84: 482-485.

Hume AN, Buttgereit J, Al-Awadhi AM, Al-Suwaidi SS, John A, Bader M, Seabra MC, Al-Gazali L, Ali BR (2009). Defective cellular trafficking of missense NPR-B mutants is the major mechanism underlying acromesomelic dysplasia-type Maroteaux. Hum Mol Genet 18: 267-277.

Hung IH, Yu K, Lavine KJ, Ornitz DM (2007). FGF9 regulates early hypertrophic chondrocyte differentiation and skeletal vascularization in the developing stylopod. Dev Biol 307: 300-313.

Hunter ML, Roberts GJ (1998). Oral and dental anomalies in Ellis-van Creveld syndrome (Chondroectodermal dysplasia): report of a case. Int J Paediatr Dent 8: 153-157.

Hussain M, Glass GE, Moss ALH (2007). An actively mobile accessory digit arising from the dorsum of the foot: an unusual example of polydactyly. Eur J Plast Surg 29: 381-383.

Ianakiev P, Kilpatrick MW, Toudjarska I, Basel D, Beighton P, Tsipouras P (2000). Split-hand/split-foot malformation is caused by mutations in the *p63* gene on 3q27. Am J Hum Genet 67: 59-66.

Ikeda T, Kamekura S, Mabuchi A, Kou I, Seki S, Takato T, Nakamura K, Kawaguchi H, Ikegawa S, Chung UI (2004). The combination of SOX5, SOX6, and SOX9 (the SOX trio) provides signal sufficient for induction of permanent cartilage. Arthritis Rheum 50: 3561-3573.

Iyama K, Ninomiya Y, Olsen BR, Linsenmayer TF, Trelstad RL, Hayashi M (1991). Spatiotemporal pattern of type X collagen gene expression and collagen deposition in embryonic chick vertebrae undergoing endochondral ossification.Anat Rec 229: 462-472.

Janssens K, Vanhoenacker F, Bonduelle M, Verbruggen L, Van Maldergem L, Ralston S, Guañabens N, Migone N, Wientroub S, Divizia MT, Bergmann C, Bennett C, Simsek S, Melançon S, Cundy T, Van Hul W (2006). Camurati-Engelmann disease: review of the clinical, radiological, and molecular data of 24 families and implications for diagnosis and treatment. J Med Genet 43: 1-11.

Jensen ED, Gopalakrishnan R, Westendorf JJ (2010). Regulation of gene expression in osteoblasts. Biofactor 36: 25-32.

Jimenez-Escrig A, Gobernado I, Garcia-Villanueva M, Sanchez-Herranz A (2012). Autosomal recessive Emery-Dreifuss muscular dystrophy caused by a novel

mutation (R225Q) in the lamin A/C gene identified by exome sequencing. Muscle Nerve 45: 605-610.

Johnston O, Kirby Jr VV (1955).Syndactyly of the ring and little finger. Am J Hum Genet 7: 80-82.

Kalsoom U, Wasif N, Tariq M, Ahmad W (2010). A novel missense mutation in the EVC gene underlies Ellis-van Creveld syndrome in a Pakistani family. Pediatrics International 52: 240-246.

Kalsoom UE, Basit S, Kamran-ul-Hassan Naqvi S, Ansar M, Ahmad W (2012). Genetic mapping of an autosomal recessive postaxial polydactyly type A to chromosome 13q13.3-q21.2 and screening of the candidate genes. Hum Genet 131: 415-422.

Kalsoom UE, Klopocki E, Wasif N, Tariq M, Khan S, Hecht J, Krawitz P, Mundlos S, Ahmad W (2013). Whole exome sequencing identified a novel zinc-finger gene *ZNF141* associated with autosomal recessive postaxial polydactyly type A. J Med Genet 50: 47-53.

Kant SG, Polinkovsky A, Mundlos S, Zabel B, Thomeer RT, Zonderland HM, Shih L, van Haeringen A, Warman ML (1998). Acromesomelic dysplasia maroteaux type maps to human chromosome 9. Am J Hum Genet 63: 155-162.

Karolchik D, Barber GP, Casper J, Clawson H, Cline MS, Diekhans M, Dreszer TR, Fujita PA, Guruvadoo L, Haeussler M, Harte RA, Heitner S, Hinrichs AS, Learned K, Lee BT, Li CH, Raney BJ, Rhead B, Rosenbloom KR, Sloan CA, Speir ML, Zweig AS, Haussler D, Kuhn RM, Kent WJ (2014). The UCSC genome browser database: 2014 update. Nucleic Acids Res 42: D764-770.

Karsenty G, Kronenberg HM, Settembre C (2009). Genetic control of bone formation. Ann Rev Cell Dev Biol 25: 629-664.

Karsenty G, Wagner EF (2002). Reaching a genetic and molecular understanding of skeletal development. Dev Cell 2: 389-406.

Kemp T, Ravn J (1932). Ueber erbliche Hand-und Fussdeformitaeten in einem 140-koepfigen Geschlecht, nebst einigen Bemerkungen ueber Poly-und Syndaktylie beim Menschen. Acta Psychiat Neurol Scand 7: 275-296.

Kerchring T (1670). Spicilegium anatomicum continens observationum anatomicarum rariorum centuriam unam necnon osteogeniam foeruum etc. Amsterdam. In: Blauth W, Olason AT (1988). Classification of polydactyly of the hands and feet. Arch Orthop Trauma Surg 107: 334-344.

Khan S, Basit S, Zimri FK, Ali N, Ali G, Ansar M, Ahmad W (2012). A novel homozygous missense mutation in *WNT10B* in familial split-hand/foot malformation. Clin Genet 82: 48-55.

Khan S, Hussain Ali R, Abbasi S, Nawaz M, Muhammad N, Ahmad W (2012). Novel mutations in natriuretic peptide receptor-2 gene underlie acromesomelic dysplasia, type maroteaux. BMC Med Genet 13:44.

Kingsley DM (1994a). The TGF-b superfamily: New members, new receptors, and new genetic tests of function in different organisms. Genes Dev 8: 133-146.

Kinoshita A, Saito T, Tomita H, Makita Y, Yoshida K, Ghadami M, Yamada K, Kondo S, Ikegawa S, Nishimura G, Fukushima Y, Nakagomi T, Saito H, Sugimoto T, Kamegaya M, Hisa K, Murray JC, Taniguchi N, Niikawa N, Yoshiura K (2000). Domain-specific mutations in *TGFB1* result in Camurati-Engelmann disease. Nat Genet 26: 19-20.

Kishimoto I, Rossi K, Garbers DL (2001). A genetic model provides evidence that the receptor for atrial natriuretic peptide (guanylyl cyclase-A) inhibits cardiac ventricular myocyte hypertrophy. Pro Natl Acad Sci USA 98: 2703-2706.

Klopocki E, Kähler C, Foulds N, Shah H, Joseph B, Vogel H, Lüttgen S, Bald R, Besoke R, Held K, Mundlos S, Kurth I (2012). Deletions in *PITX1* cause a spectrum of lower-limb malformations including mirror-image polydactyly. Eur J Hum Genet 20: 705-708.

Klopocki E, Ott CE, Benatar N, Ullmann R, Mundlos S, Lehmann K (2008). A microduplication of the long range SHH limb regulator (ZRS) is associated with triphalangeal thumb-polysyndactyly syndrome. J Med Genet 45: 370-375.

Kokabu S, Gamer L, Cox K, Lowery J, Tsuji K, Raz R, Economides A, Katagiri T, Rosen V (2012). BMP3 suppresses osteoblast differentiation of bone marrow stromal cells via interaction with Acvr2b. Mol Endocrinol 26: 87-94.

Kondoh S, Sugawara H, Harada N, Matsumoto N, Ohashi H, Sato M, Kantaputra PN, Ogino T, Tomita H, Ohta T, Kishino T, Fukushima Y, Niikawa N, Yoshiura K (2002). A novel gene is disrupted at a 14q13 breakpoint of t(2;14) in a patient with mirror-image polydactyly of hands and feet. J Hum Genet 47: 136-139.

Kornak U, Mundlos S (2003). Genetic disorders of the skeleton: a developmental approach. Am J Hum Genet 73: 447-474.

Krawitz PM, Kamphans T (2012). GeneTalk: an expert exchange platform for assessing rare sequence variants in personal genomes. Bioinformatics 28: 2515-2516.

Kronenberg HM (2003). Developmental regulation of the growth plate. Nature 423: 332-336.

Kuratani S (2005). Craniofacial development and the evolution of the vertebrates: the old problems on a new background. Zoolog Sci 22: 1-9.

Kurban M, Wajid M, Petukhova L, Shimomura Y, Christiano AM (2011). A nonsense mutation in the *HOXD13* gene underlies synpolydactyly with incomplete penetrance. J Hum Genet 56: 701-706.

Kurth I, Klopocki E, Stricker S, van Oosterwijk J, Vanek S, Altmann J, Santos HG, van Harssel JJ, de Ravel T, Wilkie AO, Gal A, Mundlos S (2009). Duplications of noncoding elements 50 of SOX9 are associated with brachydactyly-anonychia. Nat Genet 41: 862-863.

Langenickel TH, Buttgereit J, Pagel-Langenickel I, Lindner M, Monti J, Beuerlein K, Al- Saadi N, Plehm R, Popova E, Tank J, Dietz R, Willenbrock R, Bader M (2006). Cardiac hypertrophy in transgenic rats expressing a dominant-negative mutant of the natriuretic peptide receptor B. Proc Natl Acad Sci USA 103:4735-4740.

Langer LO, Cervenka J, Camargo MA (1989). Severe autosomal recessive acromesomelic dysplasia, the Hunter-Thompson type, and comparison with the Grebe type. Hum Genet 81: 323-328.

Langille RM (1994). Differentiation of craniofacial mesenchyme. In: Differentiation and morphogenesis of bone, Hall BK (ed), vol 9, CRS press, Boca Raton, pp 1-63.

Le Goff C, Morice-Picard F, Dagoneau N, Wang LW, Perrot C, Crow YJ, Bauer F, Flori E, Prost-Squarcioni C, Krakow D, Ge G, Greenspan DS, Bonnet D, Le Merrer M, Munnich A, Apte SS, Cormier-Daire V (2008). *ADAMTSL2* mutations in geleophysic dysplasia demonstrate a role for ADAMTS-like proteins in TGF-beta bioavailability regulation. Nat Genet 40: 1119-1123.

Lefebvre V, Bhattaram P (2010). Vertebrate skeletogenesis. Curr Top Dev Biol 90: 291-317.

Lerch H (1948). Erbliche Synostosen der Ossa metacarpalia IV und V. Z Orthop 78: 13-16.

Lettice LA, Heaney SJH, Purdie LA, Li L, de Beer P, Oostra BA, Goode D, Elgar G, Hill RE, de Graaff E (2003). A long-range Shh enhancer regulates expression in the developing limb and fin and is associated with preaxial polydactyly. Hum Mol Genet 12: 1725-1735.

Lettice LA, Horikoshi T, Heaney SJ, van Baren MJ, van der Linde HC, Breedveld GJ, Joosse M, Akarsu N, Oostra BA, Endo N, Shibata M, Suzuki M, Takahashi E, Shinka T, Nakahori Y, Ayusawa D, Nakabayashi K, Scherer SW, Heutink P, Hill RE, Noji S (2002). Disruption of a long-range cis-acting regulator for Shh causes preaxial polydactyly. Proc Natl Acad Sci 99: 7548-7553.

Letunic I, Goodstadt L, Dickens NJ, Doerks T, Schultz J, Mott R, Ciccarelli F, Copley RR, Ponting CP, Bork P (2002). Recent improvements to the SMART domain-based sequence annotation resource. Nucleic Acids Res 30: 242-244.

Li H1, Durbin R (2009). Fast and accurate short read alignment with Burrows-Wheeler transform. Bioinformatics 25: 1754-1760.

Li HY, Ma HW, Wang HQ, Ma WH (2009) Molecular analysis of a novel cathepsin K gene mutation in a Chinese child with pycnodysostosis J Int Med Res 37: 264-269.

Li L, Krantz ID, Deng Y, Genin A, Banta AB, Collins CC, Qi M, Trask BJ, Kuo WL, Cochran J, Costa T, Pierpont ME, Rand EB, Piccoli DA, Hood L, Spinner NB (1997). Alagille syndrome is caused by mutations in human *Jagged1*, which encodes a ligand for Notch1. Nat Genet 16: 243-251.

Li X, Cao X (2006). BMP signaling and skeletogenesis. Ann N Y Acad Sci 1068: 26-40.

Li Y1, Pawlik B, Elcioglu N, Aglan M, Kayserili H, Yigit G, Percin F, Goodman F, Nürnberg G, Cenani A, Urquhart J, Chung BD, Ismail S, Amr K, Aslanger AD, Becker C, Netzer C, Scambler P, Eyaid W, Hamamy H, Clayton-Smith J, Hennekam R, Nürnberg P, Herz J, Temtamy SA, Wollnik B (2010). *LRP4* mutations alter Wnt/beta-catenin signaling and cause limb and kidney malformations in Cenani-Lenz syndrome. Am J Hum Genet 86: 696-706.

Lin K, Thomas JT, McBride OW, Luyten FP (1996). Assignment of a new TGF-beta superfamily member, human cartilage-derived morphogenetic protein-1, to chromosome 20q11.2. Genomics 34: 150-151.

Lupski JR, Reid JG, Gonzaga-Jauregui C, Rio Deiros D, Chen DC, Nazareth L, Bainbridge M, Dinh H, Jing C, Wheeler DA, McGuire AL, Zhang F, Stankiewicz P,Halperin JJ, Yang C, Gehman C, Guo D, Irikat RK, Tom W, Fantin NJ, Muzny DM, Gibbs RA (2010). Whole-genome sequencing in a patient with Charcot– Marie–Tooth neuropathy. N Engl J Med 362: 1181-1191.

Maes C, Kobayashi T, Selig MK, Torrekens S, Roth SI, Mackem S, Carmeliet G, Kronenberg HM (2010). Osteoblast precursors, but not mature osteoblasts, move into developing and fractured bones along with invading blood vessels. Dev Cell 19: 329-344.

Malik S (2012). Syndactyly: phenotypes, genetics and current classification. Eur J Hum Genet 20: 817-824.

Malik S, Abbasi AA, Ansar M, Ahmad W, Koch MC, Grzeschik KH (2006). Genetic heterogeneity of synpolydactyly: a novel locus SPD3 maps to chromosome 14q11.2-q12. Clin Genet 69: 518-524.

Malik S, Arshad M, Amin-Ud-Din M, Oeffner F, Dempfle A, Haque S, Koch MC, Ahmad W, Grzeschik KH (2004). A novel type of autosomal recessive syndactyly: clinical and molecular studies in a family of Pakistani origin. Am J Med Genet 126: 61-67.

Malik S, Percin FE, Ahmad W, Percin S, Akarsu NA, Koch MC, Grzeschik KH (2005). Autosomal recessive mesoaxial synostotic syndactyly with phalangeal reduction maps to chromosome 17p13.3. Am J Med Genet 134: 404-408.

Malik S, Ullah S, Afzal M, Lal K, Haque S (2014). Clinical and descriptive genetic study of polydactyly a Pakistani experience of 313 cases/families. Clin Genet 85: 482-486.

Mariani FV, Ahn CP, Martin GR (2008). Genetic evidence that FGFs have an instructive role in limb proximal-distal patterning. Nature 453: 401-405.

Mariani FV, Martin GR (2003). Deciphering skeletal patterning: clues from the limb. Nature 423: 319-325.

Marie PJ, Kaabeche K, Guenou H (2008). Roles of FGFR2 and twist in human craniosynostosis: insights from genetic mutations in cranial osteoblasts. Front Oral Biol 12: 144-159.

Martin GR (1998). The roles of FGFs in the early development of vertebrate limbs. Genes Dev 12: 1571-1586.

Martin RA, Jones MC, Jones KL (1993). Mirror hands and feet with a distinct nasal defect, an autosomal dominant condition. Am J Med Genet 46: 129-131.

Massague´ J, Attisano L, Wrens JL (1994). The TGF-b family and its composite receptors. Trends Cell Biol 4:173-178.

Matise TC, Chen F, Chen W, De La Vega FM, Hansen M, He C, Hyland FC, Kennedy GC, Kong X, Murray SS, Ziegle JS, Stewart WC, Buyske S (2007). A second-generation combined linkage physical map of the human genome. Genome Res 17: 1783-1786.

McDaniell R, Warthen DM, Sanchez-Lara PA, Pai A, Krantz ID, Piccoli DA, Spinner NB (2006). *NOTCH2* mutations cause Alagille syndrome, a heterogeneous disorder of the notch signaling pathway. Am J Hum Genet 79: 169-173.

McGrew MJ, Dale JK, Fraboulet S, Pourquié O (1998). The lunatic fringe gene is a target of the molecular clock linked to somite segmentation in avian embryos. Curr Biol 8: 979-982.

McKenna A, Hanna M, Banks E, Sivachenko A, Cibulskis K, Kernytsky A, Garimella K, Altshuler D, Gabriel S, Daly M, DePristo MA (2010). The Genome Analysis Toolkit: a Map Reduce framework for analyzing next-generation DNA sequencing data. Genome Res 20: 1297-1303.

Mellin GW (1963). The Frequency of Birth Defects. In: Birth Defects. Lippencott JB (ed), Philadelphia, pp 1-17.

Mendez-Ferrer S, Michurina TV, Ferraro F, Mazloom AR, Macarthur BD, Lira SA, Scadden DT, Ma'ayan A, Enikolopov GN, Frenette PS (2010). Mesenchymal and haematopoietic stem cells form a unique bone marrow niche. Nature 466: 829-834.

Merlo GR, Paleari L, Mantero S, Genova F, Beverdam A, Palmisano GL, Barbieri O, Levi G (2002). Mouse model of split hand/ foot malformation type I. Genesis 33: 97-101.

Mohan J (1969). Postaxial polydactyly in three Indian families. J Med Genet 6: 196-200.

Mollica F, Volti SL, Sorge G (1978). Autosomal recessive postaxial polydactyly type A in a Sicilian family. J Med Genet 15: 212-216.

Montagu MF (1953). A pedigree of syndactylism of the middle and ring fingers. Am J Hum Genet 5: 70-72.

Montenegro G, Powell E, Huang J, Speziani F, Edwards YJ, Beecham G, Hulme W, Siskind C, Vance J, Shy M, Züchner S (2011). Exome sequencing allows for rapid gene identification in a Charcot–Marie–Tooth family. Ann Neurol 69: 464-470.

Muragaki Y, Mundlos S, Upton J, Olsen BR (1996). Altered growth and branching patterns in synpolydactyly caused by mutations in *HOXD13*. Science 272: 548-551.

Nair SR, Varghese S, Kumar A, Jose RM (2001). A rare case of central polydactyly. Eur J Plast Surg 24: 264-265.

Nakashima K, Zhou X, Kunkel G, Zhang Z, Deng JM, Behringer RR, de Crombrugghe B (2002). The novel zinc finger-containing transcription factor osterix is required for osteoblast differentiation and bone formation. Cell 108: 17-29.

Naski MC, Wang Q, Xu J, Ornitz DM (1996). Graded activation of fibroblast growth factor receptor 3 by mutations causing achondroplasia and thanatophoric dysplasia. Nat Genet 13: 233-237.

Ng JK, Tamura K, Buscher D, Izpisua-Belmonte JC (1999). Molecular and cellular basis of pattern formation during vertebrate limb development. Curr Top Dev Biol 41: 37-66.

Niswander L (2003). Pattern formation: old models out on a limb. Nat Rev Genet 4: 133-143.

Niswander L, Tickle C, Vogel A, Booth I, Martin GR (1993). FGF-4 replaces the apical ectodermal ridge and directs outgrowth and patterning of the limb. Cell 75: 579-587.

Nunes ME, Schutt G, Kapur RP, Luthardt F, Kukolich M, Byers P, Evans JP (1995). A second autosomal split hand/split foot locus maps to chromosome 10q24-q25. Hum Mol Genet 4: 2165-2170.

Oda T, Elkahloun AG, Pike BL, Okajima K, Krantz ID, Genin A, Piccoli DA, Meltzer PS, Spinner NB, Collins FS, Chandrasekharappa SC (1997). Mutations in the human *Jagged1* gene are responsible for Alagille syndrome. Nat Genet 16:235-242.

Olney RC, Bükülmez H, Bartels CF, Prickett TC, Espiner EA, Potter LR, Warman ML (2006). Heterozygous mutations in natriuretic peptide receptor-B (*NPR2*) are associated with short stature. J Clin Endocrinol Metab 91: 1229-1232.

Olsen BR, Reginato AM, Wang W (2000). Bone development. Annu Rev Cell Dev Biol 16: 191-220.

Orel H (1928). Kleine Beitrage zur Vererbunswissenschaft. 1. Polydaktylie. Z Konstit-Lehre 13: 691-698.

Orioli IM, Castilla EE (1999). Thumb/hallux duplication and preaxial polydactyly type I. Am J Med Genet 82: 219-224.

Orioli IM, Castilla EE, Barbosa-Neto JG (1986). The birth prevalence rates for skeletal dysplasias. J Med Genet 23: 328-332.

Ornitz DM, Marie PJ (2002). FGF signaling pathways in endochondral and intramembranous bone development and human genetic disease. Genes Dev 16: 1446-1465.

Otto F, Thornell AP, Crompton T, Denzel A, Gilmour KC, Rosewell IR, Stamp GW, Beddington RS, Mundlos S, Olsen BR, Selby PB, Owen MJ (1997). Cbfa1, a candidate gene for cleidocranial dysplasia syndrome, is essential for osteoblast differentiation and bone development. Cell 89: 765-771.

Ozen RS, Baysal BE, Devlin B, Farr JE, Gorry M, Ehrlich GD, Richard CW (1999). Fine mapping of the split-hand/split-foot locus (SHFM3) at 10q24: Evidence for anticipation and segregation distortion. Am J Hum Genet 64: 1646-1654.

Pacheco M, Valencia M, Caparrós-Martín JA, Mulero F, Goodship JA, Ruiz-Perez VL (2012). EVC works in chondrocytes and osteoblasts to regulate multiple aspects of growth plate development in the appendicular skeleton and cranial base. Bone 50: 28-41.

Pagel-Langenickel I, Buttgereit J, Bader M, Langenickel TH (2007). Natriuretic peptide receptor B signaling in the cardiovascular system: protection from cardiac pertrophy. J Mol Med 85: 797-810.

Palmeirim I, Henrique D, Ish-Horowicz D, Pourquié O (1997). Avian hairy gene expression identifies a molecular clock linked to vertebrate segmentation and somitogenesis. Cell 91: 639-648.

Paznekas WA, Boyadjiev SA, Shapiro RE, Daniels O, Wollnik B, Keegan CE, Innis JW, Dinulos MB, Christian C, Hannibal MC, Jabs EW (2003). Connexin 43 (*GJA1*) mutations cause the pleiotropic phenotype of oculodentodigital dysplasia. Am J Hum Genet 72: 408-418.

Peifer M, Polakis P (2000). Wnt signaling in oncogenesis and embryogenesis—a look outside the nucleus. Science 287: 1606-1609.

Percin EF, Percin S, Egilmez H, Sezgin I, Ozbas F, Akarsu AN (1998). Mesoaxial complete syndactyly and synostosis with hypoplastic thumbs: an unusual combination or homozygous expression of syndactyly type I? J Med Genet 35: 868-874.

Parveen F, Rehman S (2012). Consanguineous marriages and their malformation in F1 generation. Asian J Pharm Hea Sci 2: 406-411.

Pfeifer A, Aszódi A, Seidler U, Ruth P, Hofmann F, Fässler R (1996). Intestinal secretory defects and dwarfism in mice lacking cGMP-dependent protein kinase II. Science 274: 2082-2086.

Pingault V, Ente D, Dastot-Le Moal F, Goossens M, Marlin S, Bondurand N (2010). Review and update of mutations causing Waardenburg syndrome. Hum Mut 31: 1-16.

Polinkovsky A, Robin NH, Thomas JT (1997). Mutations in *CDMP1* cause autosomal dominant brachydactyly type C. Nat Genet 17: 18-19.

Potter LR, Abbey-Hosch S, Dickey DM (2006). Natriuretic peptides, their receptors, and cyclic guanosine monophosphate-dependent signaling functions. Endocr Rev 27: 47-72.

Raas-Rothschild A, Manouvrier S, Gonzales M, Farriaux JP, Lyonnet S, Munnich A (1996). Refined mapping of a gene for split hand-split foot malformation (SHFM3) on chromosome 10q25. J Med Genet 33: 996-1001.

Radhakrishna U, Blouin J-L, Mehenni H, Patel UC, Patel MN, Solanki JV, Antonarakis SE (1997a). Mapping one form of autosomal dominant postaxial polydactyly type A to chromosome 7p15– q11.23 by linkage analysis. Am J Hum Genet 60: 597-604.

Radhakrishna U, Bornholdt D, Scott HS, Patel UC, Rossier C, Engel H, Bottani A, Chandal D, Blouin JL, Solanki JV, Grzeschik KH, Antonarakis SE (1999). The phenotypic spectrum of GLI3 morphopathies includes autosomal dominant preaxial polydactyly type-IV and postaxial polydactyly type-A/B; No phenotype prediction from the position of *GLI3* mutations. Am J Hum Genet 65: 645-655.

Radhakrishna U, Wild A, Grzeschik KH, Antonarakis SE (1997b). Mutation in *GLI3* in postaxial polydactyly type A. Nat Genet 17: 269-271.

Rehman AU, Santos-Cortez RL, Drummond MC, Shahzad M, Lee K, Morell RJ, Ansar M, Jan A, Wang X, Aziz A, Riazuddin S, Smith JD, Wang GT, Ahmed ZM, Gul K, Shearer AE, Smith RJ, Shendure J, Bamshad MJ, Nickerson DA; University of Washington Center for Mendelian Genomics, Hinnant J, Khan SN, Fisher RA, Ahmad W, Friderici KH, Riazuddin S, Friedman TB, Wilch ES, Leal SM. (2014) Challenges and solutions for gene identification in the presence of familial locus heterogeneity. Eur J Hum Genet 266: 1-9.

Riddle RD, Ensini M, Nelson C, Tsuchida T, Jessell TM, Tabin C (1995). Induction of the LIM homeobox gene *Lmx1* by *WNT7a* establishes dorsoventral pattern in the vertebrate limb. Cell 83: 631-640.

Robinow M, Johnson GF, Broock GJ (1982). Syndactyly type V. Am J Med Genet 11: 475-482.

Robledo RF, Rajan L, Li X, Lufkin T (2002). The *Dlx5* and *Dlx6* homeobox genes are essential for craniofacial, axial, and appendicular skeletal development. Genes Dev 16: 1089-1101.

Rodda SJ, McMahon AP (2006). Distinct roles for Hedgehog and canonical Wnt signaling in specification, differentiation and maintenance of osteoblast progenitors. Development 133: 3231-3244.

Rohmann E, Brunner HG, Kayserili H, Uyguner O, Nürnberg G, Lew ED, Dobbie A, Eswarakumar VP, Uzumcu A, Ulubil-Emeroglu M, Leroy JG, Li Y, Becker C, Lehnerdt K, Cremers CW, Yüksel-Apak M, Nürnberg P, Kubisch C,

Schlessinger J, van Bokhoven H, Wollnik B (2006). Mutations in different components of FGF signaling in LADD syndrome. Nat Genet 38: 414-417.

Rousseau F, Bonaventure J, Legeai-Mallet L, Pelet A, Rozet JM, Maroteaux P, Le Merrer M, Munnich A (1994). Mutations in the gene encoding fibroblast growth factor receptor-3 in achondroplasia. Nature 371: 252-254.

Rozen S, Skaletsky H (2000). Primer3 on the WWW for general users and for biologist programmers. Methods Mol Biol 132: 365-386.

Rudnicki JA, Brown AM (1997). Inhibition of chondrogenesis by Wnt gene expression in vivo and in vitro. Dev Biol 185: 104-118.

Ruiz-Perez VL, Blair HJ, Rodriguez-Andres ME, Blanco MJ, Wilson A, Liu YN, Miles C, Peters H, Goodship JA (2007). EVC is a positive mediator of Ihh-regulated bone growth that localises at the base of chondrocyte cilia. Development 134: 2903-2912.

Ruiz-Perez VL, Goodship JA (2009). Ellis-van Creveld syndrome and Weyers acrodental dysostosis are caused by cilia-mediated diminished response to hedgehog ligands. Am J Med Genet C Semin Med Genet 151C: 341-351.

Ruiz-Perez VL, Ide SE, Strom TM, Lorenz B, Wilson D, Woods K, King L, Francomano C, Freisinger P, Spranger S, Marino B, Dallapiccola B, Wright M, Meitinger T, Polymeropoulos MH, Goodship J (2000). Mutations in a new gene in Ellis–van Creveld syndrome and Weyers acrodental dysostosis. Nat Genet 24: 283-286.

Ruiz-Perez VL, Tompson SW, Blair HJ, Espinoza-Valdez C, Lapunzina P, Silva EO, Hamel B, Gibbs JL, Young ID, Wright MJ, Goodship JA (2003). Mutations in two nonhomologous genes in a head-to-head configuration cause Ellis–van Creveld syndrome. Am J Hum Genet 72: 728-732.

Sacchetti B, Funari A, Michienzi S, Di Cesare S, Piersanti S, Saggio I, Tagliafico E, Ferrari S, Robey PG, Riminucci M, Bianco P (2007). Self-renewing osteoprogenitors in bone marrow sinusoids can organize a hematopoietic microenvironment. Cell 131: 324-336.

Sambrook J, Fritschi EF, Maniatis T (1989). Molecular cloning: a laboratory manual, 2nd edtion. Cold Spring Harbor Laboratory Press, Cold Spring Harbor, New York, USA.

Sarfarazi M, Akarsu AN, Sayli BS (1995). Localization of the syndactyly type II (synpolydactyly) locus to 2q31 region and identification of tight linkage to HOXD8 intragenic marker. Hum Mol Genet 4:1453-1458.

Sarnat H, Amir E, Legum CP (1980). Developmental dental anomalies in Chondroectodermal dysplasia (Ellis-van Creveld syndrome). ASDC J Dent Child 47: 28-31.

Sato D, Liang D, Wu L, Pan Q, Xia K, Dai H, Wang H, Nishimura G, Yoshiura K, Xia J, Niikawa N (2007). A syndactyly type IV locus maps to 7q36. J Hum Genet 52: 561-564.

Scherer SW, Poorkaj P, Allen T, Kim J, Geshuri D, Nunes M, Soder S, Stephens K, Pagon RA, Patton MA (1994). Fine mapping of the autosomal dominant split hand/split foot locus on chromosome 7, band q21.3-q22.1. Am J Hum Genet 55: 12-20.

Schroeder TM, Jensen ED, Westendorf JJ (2005). Runx2: a master organizer of gene transcription in developing and maturing osteoblasts. Birth Defects Res C Embryo Today 75: 213-225.

Schultz J, Milpetz F, Bork P, Ponting CP (1998). SMART, a simple modular architecture research tool: identification of signaling domains. Proc Natl Acad Sci 95: 5857-5864.

Schulz S (2005). C-type natriuretic peptide and guanylyl cyclase B receptor. Peptides 26: 1024-1034.

Schwarz JM, Rödelsperger C, Schuelke M, Seelow D (2010). MutationTaster evaluates disease-causing potential of sequence alterations. Nat Methods 7: 575-576.

Seelow D, Schuelke M, Hildebrandt F, Nürnberg P (2009). HomozygosityMapper-an interactive approach to homozygosity mapping. Nucleic Acids Res 37: 593-599.

Serra R, Chang C (2003). TGF-beta signaling in human skeletal and patterning disorders.Birth Defects Res C Embryo Today 69: 333-351.

Shamseldin HE, Faden MA, Alashram W, Alkuraya FS (2011). Identification of a novel *DLX5* mutation in a family with autosomal recessive split hand and foot malformation. J Med Genet 49: 16-20.

Shiang R, Thompson LM, Zhu YZ, Church DM, Fielder TJ, Bocian M, Winokur ST, Wasmuth JJ (1994). Mutations in the transmembrane domain of *FGFR3* cause the most common genetic form of dwarfism, achondroplasia. Cell 78: 335-342.

Silberbach M, Roberts CJ (2001). Natriuretic peptide signalling: molecular and cellular pathways to growth regulation. Cell Signal 13: 221-231.

Silberstein M, Landon MR, Wang YE, Perl A, Vajda S (2006). Computational methods for functional site identification suggest a substrate access channel in transaldolase. Genome Inform 17: 13-22.

Sinha KM, Yasuda H, Coombes MM, Dent SY, de Crombrugghe B (2010). Regulation of the osteoblast-specific transcription factor Osterix by NO66, a Jumonji family histone demethylase. EMBO J 29: 68-79.

Smolenski A, Burkhardt AM, Eigenthaler M, Butt E, Gambaryan S, Lohmann SM, Walter U (1998). Functional analysis of cGMP-dependent protein kinases I and II as mediators of NO/cGMP effects. Naunyn Schmiedebergs Arch Pharmacol 358: 134-139.

Sparrow DB, Chapman G, Wouters MA, Whittock NV, Ellard S, Fatkin D, Turnpenny PD, Kusumi K, Sillence D, Dunwoodie SL (2006). Mutation of the LUNATIC FRINGE gene in humans causes spondylocostal dysostosis with a severe vertebral phenotype. Am JHum Genet 78: 28-37.

Sparrow DB, Guillen-Navarro E, Fatkin D, Dunwoodie SL (2008). Mutation of Hairy-and-Enhancer-of- Split-7 in humans causes spondylocostal dysostosis. Hum Mol Genet 17: 3761-3766.

Stelzer C, Winterpacht A, Spranger J, Zabel B (2003). Grebe dysplasia and the spectrum of *CDMP1* mutations. Pediatr Pathol Mol Med 22: 77-85.

Stevens JR, Miranda-Carboni GA, Singer MA, Brugger SM, Lyons KM, Lane TF (2010). Wnt10b deficiency results in age-dependent loss of bone mass and progressive reduction of mesenchymal progenitor cells. J Bone Miner Res 25: 2138-2147.

Stoll C, Dott B, Roth MP, Alembik Y (1989). Birth prevalence rates of skeletal dysplasias. Clin Genet 35: 88-92.

Storm EE, Huynh TV, Copeland NG, Jenkins NA, Kingsley DM, Lee SJ (1994). Limb alterations in brachypodism mice due to mutations in a new member of the TGF beta-superfamily. Nature 368: 639-643.

Sun M, Ma F, Zeng X, Liu Q, Zhao XL, Wu FX, Wu GP, Zhang ZF, Gu B, Zhao YF, Tian SH, Lin B, Kong XY, Zhang XL, Yang W, Lo W, Zhang X (2008). Triphalangeal thumb-polysyndactyly syndrome and syndactyly type IV are caused by genomic duplications involving the long-range, limb-specific SHH enhancer. J Med Genet 45: 589-595.

Swanson AB (1976). A classification for congenital limb malformations. J Hand Surg Am 1: 8-22.

Swanson AB, Brown KS (1962). Hereditary triphalangeal thumb. J Hered 53: 259-265.

Takeda S, Bonnamy JP, Owen MJ, Ducy P, Karsenty G (2001). Continuous expression of Cbfa1 in non hypertrophic chondrocytes uncovers its ability to induce hypertrophic chondrocyte differentiation and partially rescues Cbfa1-deficient mice. Genes Dev 15: 467-481.

Tamayo ML, Gelvez N, Rodriguez M, Flore S, Varon C, Medina D, Bernal JE (2008). Screening program for Waardenburg syndrome in Colombia: clinical definition and phenotypic variability. Am J Med Genet 146A: 1026-1031.

Tamura N, Doolittle LK, Hammer RE, Shelton JM, Richardson JA, Garbers DL (2004). Critical roles of the guanylyl cyclase B receptor in endochondral ossification and development of female reproductive organs. Proc Natl Acad Sci USA 101: 17300-17305.

Tamura N, Garbers DL (2003). Regulation of the guanylyl cyclase-B receptor by alternative splicing. J Biol Chem 278: 48880-48889.

Tassabehji M, Read AP, Newton VE, Harris R, Balling R, Gruss P, Strachan T (1992). Waardenburg's syndrome patients have mutations in the human homologue of the Pax-3 paired box gene. Nature 355: 635-636.

Tekin M, Bodurtha JN, Nance WE, Pandya A (2001). Waardenburg syndrome type 3 (Klein-Waardenburg syndrome) segregating with a heterozygous deletion in the paired box domain of PAX3: a simple variant or a true syndrome? Clin Genet 60: 301-304.

Temtamy SA (1990). Polydactyly, postaxial. In: Buyse ML (ed) Birth defects encyclopedia. Blackwell Scientific, Cambridge, pp 1397-1398.

Temtamy SA, McKusick VA (1978). Syndactyly. In: The Genetics of Hand Malformations. Alan R Liss (ed), New York, pp 301-322.

Temtamy SA, McKusick VA (1978). The genetics of hand malformations. Birth Defects Orig Artic Ser14 (3): i-xviii, 1-619.

Thomas JT, Kilpatrick MW, Lin K (1997). Disruption of human limb morphogenesis by a dominant negative mutation in *CDMP1*. Nat Genet 17: 58-64.

Thomas JT, Lin K, Nandedkar M, Camarqo M, Cervenka J, Luyten FP (1996). A human chondrodysplasia due to a mutation in TGF-β superfamily member. Nat Genet 12: 315-317.

Tickle C (2003). Patterning systems--from one end of the limb to the other. Dev Cell 4: 449-458.

Tompson SW, Ruiz-Perez VL, Blair HJ, Barton S, Navarro V, Robson JL, Wright MJ, Goodship JA (2007). Sequencing *EVC* and *EVC2* identifies mutations in two-thirds of Ellis-van Creveld syndrome patients. Hum Genet 120: 663-670.

Tsai LP, Liao HM, Chen YJ, Fang JS, Chen CH (2009). A novel microdeletion at chromosome 2q31.1-31.2 in a three-generation family presenting duplication of great toes with clinodactyly. Clin Genet 75: 449-456.

Tsukurov O, Boehmer A, Flynn J, Nicolai JP, Hamel BC, Traill S, Zaleske D, Mankin HJ, Yeon H, Ho C, Tabin C, Seidman JG, Seidman C (1994). A complex bilateral polysyndactyly disease locus maps to chromosome 7q36. Nat Genet 6: 282-286.

Tuan RS (2003). Cellular signaling in developmental chondrogenesis: N-cadherin, Wnts, and BMP-2. J Bone Joint Surg Am 2: 137-141.

Turnpenny PD, Alman B, Cornier AS, Giampietro PF, Offiah A, Tassy O, Pourquié O, Kusumi K, Dunwoodie S (2007). Abnormal vertebral segmentation and the notch signaling pathway in man. Dev Dyn 236: 1456-1474.

Ugur SA, Tolun A (2008). Homozygous *WNT10b* mutation and complex inheritance in split-hand/foot malformation. Hum Mol Genet 17: 2644-2653.

Ulucan H, Gul D, Sapp JC, Cockerham J, Johnston JJ, Biesecker LG (2008). Extending the spectrum of Ellis van Creveld syndrome: a large family with a mild mutation in the EVC gene. BMC Med Genet 9: 92.

Valencia M, Lapunzina P, Lim D, Zannolli R, Bartholdi D, Wollnik B, Al-Ajlouni O, Eid SS, Cox H, Buoni S, Hayek J, Martinez-Frias ML, Antonio PA, Temtamy S, Aglan M, Goodship JA, Ruiz-Perez VL (2009). Widening the mutation spectrum of EVC and EVC2: ectopic expression of Weyer variants in NIH 3T3 fibroblasts disrupts hedgehog signaling. Hum Mutat 30: 1667-1675.

Van Bokhoven H, Brunner HG (2002). Splitting *p63*. Am J Hum Genet 71: 1-13.

Vinay C, Reddy RS, Uloopi KS, Sekhar RC (2009). Clinical manifestations of Ellis-van Creveld syndrome. J Indian Soc Pedod Prev Dent 27: 256-259.

Wabg K, Li M, Kakonarson H (2010). ANNOVAR: functional annotation of genetic variants from high-trhoughput sequencing data. Nucleic Acids Research 38: e164.

Wagner T, Wirth J, Meyer J, Zabel B, Held M, Zimmer J, Pasantes J, Bricarelli FD, Keutel J, Hustert E, Wolf U, Tommerup N, Schempp W, Scherer G (1994). Autosomal sex reversal and campomelic dysplasia are caused by mutations in and around the SRY-related gene *SOX9*. Cell 79: 1111-1120.

Wang S, Haynes C, Barany F, Ott J (2009). Genome-wide autozygosity mapping in human populations. Genet Epidemiol 33: 172-180.

Wang ZQ, Tian SH, Shi YZ, Zhou PT, Wang ZY, Shu RZ, Hu L, Kong X (2007). A single C to T transition in intron 5 of *LMBR1* gene is associated with triphalangeal thumb polysyndactyly syndrome in a Chinese family. Biochem Biophys Res Commun 355: 312-317.

Warman ML, Cormier-Daire V, Hall C, Krakow D, Lachman R, LeMerrer M, Mortier G, Mundlos S, Nishimura G, Rimoin DL, Robertson S, Savarirayan R, Sillence D, Spranger J, Unger S, Zabel B, Superti-Furga A (2011). Nosology and classification of genetic skeletal disorders: 2010 revision. Am J Med Genet A155A: 943-968.

Wassel HD (1969). The results of surgery for polydactyly of the thumb. A review. Clin Orthop Relat Res 64: 175-193.

Weischenfeldt J, Lykke-Andersen J, Porse B (2005). Messenger RNA surveillance: neutralizing natural nonsense. Curr Biol 15: 559-562.

Whittock NV, Sparrow DB, Wouters MA, Sillence D, Ellard S, Dunwoodie SL, Turnpenny PD (2004). Mutated MESP2 causes spondylocostal dysostosis in humans. Am J Hum Genet 74: 1249-1254.

Wieczorek D, Pawlik B, Li Y, Akarsu NA, Caliebe A, May KJ, Schweiger B, Vargas FR, Balci S, Gillessen-Kaesbach G, Wollnik B (2010). A specific mutation in the distant sonic hedgehog (SHH) cis-regulator (ZRS) causes Werner mesomelic syndrome (WMS) while complete ZRS duplications underlie Haas type polysyndactyly and preaxial polydactyly (PPD) with or without triphalangeal thumb. Hum Mutat 31: 81-89.

Wieland I, Muschke P, Jakubiczka S, Volleth M, Freigang B, Wieacker PF (2004). Refinement of the deletion in 7q21.3 associated with split hand/foot malformation type 1 and Mondini dysplasia. J Med Genet 41: 54.

Wilkie AO (2005). Bad bones, absent smell, selfish testes: the pleiotropic consequences of human FGF receptor mutations. Cytokine Growth Factor Rev 16: 187-203.

Wilkie AO, Morriss-Kay GM (2001). Genetics of craniofacial development and malformation. Nat Rev Genet 2: 458-468.

Winter RM, Tickle C (1993). Syndactylies and polydactylies: embryological overview and suggested classification. Eur J Hum Genet 1: 96-104.

Witte F, Dokas J, Neuendorf F, Mundlos S, Stricker S (2009). Comprehensive expression analysis of all Wnt genes and their major secreted antagonists during mouse limb development and cartilage differentiation. Gene Expr Patterns 9: 215-223.

Wollnik B, Tukel T, Uyguner O, Ghanbari A, Kayserili H, Emiroglu M, Yuksel-Apak M (2003). Homozygous and heterozygous inheritance of *PAX3* mutations causes different types of Waardenburg syndrome. Am J Med Genet A 122A: 42-45.

Wood V (1970). Duplication of the index finger. J Bone Joint Surg Am 52: 569-573.

Wu L, Liang D, Niikawa N, Ma F, Sun M, Pan Q, Long Z, Zhou Z, Yoshiura K-I, Wang H, Sato D, Nishimura G, Dai H, Zhang X, Xia J (2009). A *ZRS* duplication causes syndactyly type IV with tibial hypoplasia. Am J Med Genet Part A 149A: 816-818.

Yang W, Cao L, Liu W, Jiang L, Sun M, Zhang D, Wang S, Lo HYW, Luo Y, Zhang X (2008). Novel point mutations in *GDF5* associated with two distinct limb malformations in Chinese: brachydactyly type C and proximal symphalangism. J Hum Genet 53: 368-374.

Yang X, Karsenty G (2004). ATF4, the osteoblast accumulation of which is determined post-translationally, can induce osteoblast-specific gene expression in non-osteoblastic cells. J Biol Chem 279: 47109-47114.

Yang Y (2003). Wnts and wing: Wnt signaling in vertebrate limb development and musculoskeletal morphogenesis. Birth Defects Res C Embryo Today 69: 305-317.

Zangwill KM, Boal DK, Ladda RL (1998). Dandy-Walker malformation in Ellis-van Creveld syndrome. Am J Med Genet 31: 123-129.

Zelzer E, Olsen BR (2003). The genetic basis for skeletal diseases. Nature 423: 343-348.

Zhao H, Tian Y, Breedveld G, Huang S, Zou Y, Y J, Chai J, Li H, Li M, Oostra BA, Lo WHY, Heutink P (2002). Postaxial polydactyly type A/B (PAP-A/B) is linked to chromosome 19p13.1–13.2 in a Chinese kindred. Eur J Hum Genet 10: 162-166.

Zhao X, Sun M, Zhao J, Leyva JA, Zhu H, Yang W, Zeng X, Ao Y, Liu Q, Liu G, Lo WH, Jabs EW, Amzel LM, Shan X, Zhang X (2007). Mutations in *HOXD13* underlie syndactyly type V and a novel brachydactyly-syndactyly syndrome. Am J Hum Genet 80: 361-371.

Zhou H, Mak W, Zheng Y, Dunstan CR, Seibel MJ (2008). Osteoblasts directly control lineage commitment of mesenchymal progenitor cells through Wnt signaling. J Biol Chem 283: 1936-1945.

Zuidam JM, Ananta M, Hovius SE (2008). Triplicated thumbs a rarity? J Plast Reconstr Aesthet Surg 61: 1078-1084.